STUDIES ON OPTICAL TECHNIQUES FOR PRECISE POSITION MEASUREMENT AND ALIGNMENT OF MACHINERY

By

RAVI DHAWAN

ENGG 01201304007

BHABHA ATOMIC RESEARCH CENTRE, MUMBAI-400085

A thesis submitted to the

Board of Studies in Engineering Sciences

In partial fulfillment of requirements

for the Degree of

DOCTOR OF PHILOSOPHY

of

HOMI BHABHA NATIONAL INSTITUTE

March, 2019

Homi Bhabha National Institute

Recommendations of the Viva Voce Committee

As members of the Viva Voce Committee, we certify that we have read the dissertation prepared by Ravi Dhawan entitled **"Studies on Optical Techniques for Precise Position Measurement and Alignment of Machinery"** and recommend that it may be accepted as fulfilling the thesis requirement for the award of Degree of Doctor of Philosophy.

Chairman – Dr. A. P. Tiwari	[signature]	Date: 19.3.19
Guide / Convener – Dr. B. Dikshit	B. Dikshit	Date: 19/3/19
Co-guide – (if any)		Date:
Examiner – Dr. Mukul Sarkar	[signature]	Date: 19/3/19.
Member 1- Dr. Anup Bhattacharjee	A Bhattacharjee	Date: 19/3/19
Member 2- Dr. V. H. Patankar	V.H. Patankar	Date: 19.03.2019
Member 3- Dr. S. Kar	SKar	Date: 19/3/19
Technology Advisor: Mr. Nitin Kawade	[signature]	Date: 19/03/19

Final approval and acceptance of this thesis is contingent upon the candidate's submission of the final copies of the thesis to HBNI.

I/We hereby certify that I/we have read this thesis prepared under my/our direction and recommend that it may be accepted as fulfilling the thesis requirement.

Date: 19/3/19

Place: Mumbai

B. Dikshit

Guide: Dr. B. Dikshit

STATEMENT BY AUTHOR

RAVI DHAWAN

DECLARATION

I, hereby declare that the investigation presented in the thesis has been carried out by me. The work is original and has not been submitted earlier as a whole or in part for a degree / diploma at this or any other Institution / University.

RAVI DHAWAN

List of Publications arising from the Thesis

Journal

1. "Design and development of linear optical fiber array based remote position sensor", **Ravi Dhawan**, Rushal Shah, Nitin Kawade and Biswaranjan Dikshit, *Optik-International Journal for Light and Electron Optics*, 2017, vol. 139, 355-365.
2. "Development of a two-dimensional fiber optic position sensor", **Ravi Dhawan,** Biswaranjan Dikshit and Nitin Kawade, *Optik-International Journal for Light and Electron Optics*, 2018, vol. 169, 376-381
3. "Design and Performance of a Laser-Based Compact Position Sensor for Long Standoff Distance," **Ravi Dhawan**, Nitin Kawade and Biswaranjan Dikshit, *IEEE Sensors Journal*, 2018, vol. 18(16), pp. 6557-6562.
4. "Laser based two-dimensional position measurement of a cylindrical object for precision alignment", **Ravi Dhawan**, Biswaranjan Dikshit and Nitin Kawade, *Optical Engineering,* 2018, vol. 57(8),084102.

Conferences

1. "Laser triangulation based position and vibration sensor", **Ravi Dhawan**, Nitin Kawade, Biswaranjan Dikshit, International Conference on Advances in Optics and Photonics, ICAOP-2017, 23-26 Nov, 2017. ISBN-978-93-84871-109, OP-97.
2. "Design Optimization of Optical Triangulation Based Displacement Sensor for Different Target Surfaces", **Ravi Dhawan**, Ronie A Ghosh, Nitin O Kawade, Kallol Roy, National Laser Symposium, NLS-24, RRCAT, Indore, 2-5 Dec, 2015. ISBN-978-81-903321-6-3, Article CP-11.7.
3. "Study of Spot Size Variation and Change in its Center of Intensity at the Detector in Laser Triangulation based Displacement Sensors", **Ravi Dhawan**, Nitin O Kawade, Kallol Roy, National Laser Symposium, NLS-23, S.V University, Tirupati, 3-6 Dec, 2014. ISBN-9788190332156, Article CP-11.2.

4. “Algorithm for Displacement Measurement in Fiber Array Based Laser Triangulation Sensor”, Piyush Ahuja, **Ravi Dhawan**, Nitin O Kawade, Joe Peter K., P. Nagabhushana, National Laser Symposium (NLS-26), BARC, Mumbai, 20-23 Dec, 2017.Article CP-11.08.
5. “Modified Fiber based Fabry Perot Interferometer for Vibration Sensing using Quadrature Phase signals”, Anisha Acharya, Rushal Shah, **Ravi Dhawan**, Nitin Kawade, National Laser Symposium (NLS-25), KIIT, Bhubneshwar, 20-23 Dec, 2016.
6. “Development of Laser Triangulation Based Vibration Measurement Sensor”, Aseem Singh Rawat, **Ravi Dhawan**, Nitin O Kawade, National Laser Symposium, NLS-24, RRCAT, Indore, 2-5 Dec, 2015. ISBN-978-81-903321-6-3, Article CP-11.5.
7. “Depth Measurement Using 2D Image of Small Objects and Surface Mapping Using Laser Triangulation Technique”, Nitin O Kawade, Pooja Bai, **Ravi Dhawan**, National Laser Symposium, NLS-24, RRCAT, Indore, 2-5 Dec, 2015. ISBN-978-81-903321-6-3, Article CP-11.4.

RAVI DHAWAN

Dedicated

To

My Parents

ACKNOWLEDGEMENTS

I would like to express my deep sense of gratitude towards my guide Dr. Biswaranjan Dikshit and my technical advisor Mr. Nitin Kawade for their valuable guidance, keen interest and encouragement during the course of this work. I thank Dr. Kallol Roy, who helped and motivated me during my thesis work. I am extremely grateful to my doctoral committee members Dr. A. P. Tiwari, Dr. Anup Bhattacharjee, Dr. V. H. Patankar and Dr. S. Kar for their constant encouragement and fruitful discussions during this work.

I am indebted to Mr. Aseem Singh Rawat, Dr. Vinod Singh Rawat and Mr. Mandar Joshi for their support and discussions on various aspects of the process. My sincere thanks to my colleagues in lab Mr. Rushal Shah, Ms. Anisha Acharya, Mr. Piyush Ahuja, Ms. Pooja Chakraborty, Mr. Sanjay Patil and Mr. Ram Gangurde for their valuable suggestions and co-operation during the experiments. I would like to extend my thanks to the personals of workshop of L&PTD.

Last but not the least; I would like to thank my parents and all the family members for being supportive in my endeavor and extending encouragement throughout the work.

CONTENTS

SYNOPSIS

Presently, industries are moving towards better accuracy and faster inspection time to determine whether a given part conforms to the accepted quality characteristics. For proper working condition of the machines, all the components of the machines should be precisely positioned and aligned. Precise measurement of position and alignment involves finding accurate location of a target with respect to a reference object. If the components are not properly positioned and aligned, then during the operation it might lead to the unwanted vibrations resulting in the failure of machines. Position measurement and alignment are required in industrial applications such as in production engineering, positioning of tool to the command position on work-piece in CNC machines, assembly of pin to the target hole using robotics arm, differential gear alignment and wheels positioning in vehicles, alignment of fueling machines in nuclear reactors, shaft alignment, satellite antenna alignment, roller alignment in paper and steel industries etc. All these position measurement and alignment activities are now increasingly being carried out by different optical techniques as these are non-contact, fast, accurate, remotely monitored, and immune to electromagnetic interference (EMI) and can be implemented in hazardous environment.

In the past two decades, rapid development of laser, optics, fiber optics and detector technology have taken place. Different optical measuring methods are now available for a variety of measuring and inspection tasks. Their applicability and benefits are demonstrated successfully for offline and online measurements of various physical and chemical quantities. Laser beams, due to its special characteristics such as high intensity and directionality, are generally used in optical sensors. In general, laser used in optical sensor can be He-Ne laser or diode laser. The beam is guided either directly in air or through the optical fiber to the target. The reflected or transmitted beam is guided back to the detector to measure the required characteristics of the physical parameter.

This thesis contributes towards the mathematical model, design and development of the intensity based-fiber optic sensors, confocal based sensors and laser triangulation sensors for both one and two-dimensional position measurements. By varying the parameters of these sensors as indicated in mathematical model, desired range and resolution could be achieved as per requirements of different applications. For example, due to the space constraints, a non-contact probe type position sensor or a laser triangulation sensor with long standoff distance are required. Therefore, to ensure reliable measurement under these conditions, a confocal optical fiber based axial position sensor was investigated. Then, a laser triangulation sensor with 1000 mm standoff distance was designed and tested. The prime challenge in this case was to keep the optical assembly compact without losing sensitivity. Since some applications located in hazardous environments containing radioactivity or electromagnetic noise demand remote measurement, we have also used linear optical fiber array combined with CCD camera as detector for the laser triangulation technique. The cylindrical objects (such as shafts, pipes etc.) play an important role in industries. The change in position and alignment of these from a particular co-ordinate system or from its aligning counterpart needs to be measured accurately to prolong life of machinery and to avoid accidents. Two-dimensional position measurement of cylindrical target using two optical sensors is not available in literature. So, we have developed a mathematical model for above configuration taking curvature of surface into account and experimentally verified using the two-optical fiber array based laser triangulation sensors. These sensors can be used for fuel channel alignments in Nuclear reactors. Another improvement in the optical sensing method was for the 2-D position measurement of planar targets. Although measurement of lateral position in one-dimension is reported in literature by use of light coupling between single fiber to linear fiber array, we have modified the technique by simultaneously measuring both axial and lateral position. Axial position was inferred from change in peak intensity and lateral position from change in centroid at CCD camera. As the measurement accuracy may be affected by intensity variation due to differing roughness of target surface, we have tested all the above-mentioned sensors with targets of known (standard) roughness values.

The thesis is organized into eight chapters. Chapter 1, which forms the introduction to the thesis, provides the requirement and challenges of position measurement and alignment in machines. Some of the industrial position and alignment problems such as shaft alignment, airframe assembly alignment, and fueling channel alignment of Pressurized Heavy Water Reactor (PHWR) is described. Brief introduction of contact and non-contact techniques for position measurement is given along with the need of optical techniques for measurement.

Chapter 2 provides the comprehensive literature survey on different optical techniques for position and alignment monitoring. This chapter provides the working principle, mathematical model, range and resolution of the techniques such as intensity based fiber optic sensors, time of flight sensors, interferometers, confocal sensors and laser triangulation sensors. The advantages and disadvantages of these techniques are also described.

In chapter 3, a non-contact intensity based axial position measurement system using a single optical fiber is designed, developed and demonstrated. The system comprises of Y optical fiber coupler and lens which together acts as a single probe for simultaneously transmitting and receiving signal for position change measurement. Lens confocally collects the backscattered light from the target and sends the imaged light back to the detector. At the focus point of the spot, the maximum intensity is received at the detector and the intensity decreases on the either side of standoff target position. Thus, the intensity variation is indicative of the axial position change of the target. The slope of the linear curve on the either side of the intensity profile represents the positive and negative direction of position change. The standard target surfaces of different known roughness values were used and effect of surface roughness on the output was investigated. Overall, we could achieve a sensor resolution of 100 μm for targets with different roughness in a measurement range from 1000 μm.

Chapter 4 provides the design and performance of laser based position sensor for long standoff distance of the target. In the literature, most of the laser triangulation based position sensors are used for small standoff distances of the target. Sometimes it becomes difficult to place the sensor near the target to make the measurements. In this chapter, laser triangulation based long standoff distance position sensor is designed and to make the sensor compact, beam-folding technique was used in the path of the converging light from lens which ultimately falls on the position-sensing detector (PSD). Position resolution of 1 mm at a standoff distance of ~1000 mm between target and light collecting lens was achieved for the developed sensor. The calibration of sensor was done based on the output voltage obtained at PSD with near and far displaced position of the target. The sensor output was found to be linearly varying with target position. The sensor performance was tested for different target roughness and different target tilts (maximum upto ± 10°). The effect of temperature on the output of developed sensor was also studied and the error in measurement was found to be within the sensor resolution. The developed sensor has many potential applications in industrial environment where the position has to be measured at long standoff distance of targets having different surface roughness and variable ambient temperature.

Chapter 5 describes the development of linear optical fiber array based non-contact remote position sensor that uses oblique laser triangulation technique. Oblique triangulation method was selected as it has better resolution. In all the optical triangulation techniques reported in literature, scattered or reflected light from the target is collected by the lens and is directly focused onto the CCD or PSD without use of optical fibers, and so these methods are not meant for remote measurement and thus cannot be used in the hazardous environments. In our case, the backscattered light from the target surface is collected by the lens and is focused to the individual fiber of the linear fiber array and the other end of fiber array is connected to the CCD Camera. The centroid of the image spot at CCD camera is measured, thus giving the position information. The given sensor was tested for different target roughness samples. The resolution achieved in our system for position measurement was 1 mm at a standoff distance of ~100 mm between target and light collecting lens. It was seen that the error was minimum for target surface with 0.025 μm roughness and it was maximum for surfaces with roughness between 0.4 and 1.6 μm. This might be due to the fact that the wavelength of laser (0.638 μm) being much larger than the roughness 0.025 μm eliminates the possibility of diffraction effects changing the intensity pattern. For surfaces with roughness between 0.4 to 1.6 μm, wavelength of laser (0.638 μm) becomes comparable to it leading to diffraction and consequent change in intensity pattern. However, the roughness-induced uncertainty in all the cases was found to be less than the resolution ~1%, which was acceptable.

Chapter 6 presents a method for online measurement of position of cylindrical objects in a two-dimensional (2-D) plane using two linear optical fiber array based laser triangulation sensors placed in the perpendicular configuration. In industries, during the assembly of the cylindrical objects (shafts, pipes etc.) in heavy machines, change in position and alignment of these from a particular co-ordinate system or from its aligning counterpart needs to be measured accurately to prolong life of machinery and to avoid large-scale accidents. By measuring the two-dimensional positions at two different planes perpendicular to the axis of shaft, the alignment/tilt of the cylindrical shaft can be inferred. At first, a mathematical model was developed in order to deduce the 2-D position of target axis using two perpendicularly placed sensors taking into account the curvature of target surface on measurements. Then, using the derived formulae and our recorded experimental data, the measurement of change in 2-D position of cylindrical object with both sensors placed remotely at 100mm standoff distance was done. The cylindrical target of 75 mm radius was displaced in all the four quadrants of XY plane using a two-dimensional micrometer stage and the outputs of both the sensors were monitored. Micrometer was given incremental displacement of ± 1 mm along both the axes. The outputs of both the sensors give the displacement of the image spot across the fiber at CCD in terms of pixel values. These pixels values were utilized in our derived formulae to estimate the 2-D displacement of target. The maximum error seen in the measurement was ~5%. The sensor can be helpful in determining the wobble effects in cylinders. Further, the given technique can be extremely useful for fuel channel alignment in Nuclear Reactors where one has to monitor the alignment remotely.

In Chapter 7, instead of using 2 different sensors as explained in Chapter 6, transmission based two-dimensional (2-D) fiber optic position sensor is designed that utilizes the simultaneous measurement of the change in intensity and centroid of image on CCD camera. Jason et al used transmission configuration sensor only to determine lateral position in one-dimension by use of light intensity coupling between single fiber to linear fiber array. However, we have modified the technique by simultaneously measuring both axial and lateral position change of the target. Axial position change was inferred by the change in peak intensity at the CCD camera and lateral position change was measured by the change in centroid of image spot at CCD camera. The measurement data for two-dimensional position produced by our optical sensor were found to be reasonably matching with the values measured by the micrometer. The position resolution of the sensor was ~50 µm along both the dimensions. The maximum error was ~6% in our measurement range. In this measurement technique, the pitch of the fiber array determines the resolution of lateral position and the sensitivity of axial position is decided by the diameter of optical fiber. This system can be used for position measurement and alignment monitoring in a 2-D plane for structural health monitoring, alignment monitoring of shafts etc. where the non-contact measurement is needed.

Thus, this thesis contributes to the design, development and application of optical sensors for measurement of one dimensional and two-dimensional position changes of the planar and cylindrical targets. The optical sensors for measurement of position and alignment described in the thesis include intensity based fiber optic confocal sensor, laser triangulation sensor for long standoff distance, optical fiber array based laser triangulation sensor, 2-D position sensor for cylindrical target and 2-D position sensor for planar target. As industrial environment may be hazardous, hot or affected by EMI, suitable optical sensors need to be selected. This thesis gives the scope and choice to the user for a specific optical sensor to be selected depending upon requirement and industrial environment.

LIST OF FIGURES

LIST OF TABLES

ABBREVIATIONS

CCD: Charge Couple Devices

CMOS: Complementary Metal Oxide Semi-conductors

CNC: Computer Numerical Control

NA: Numerical Aperture

PSD: Position Sensing Detectors

PHWR: Pressurised Heavy Water Reactor

NOMENCLATURE

φ: Scheimpflug angle

λ: wavelength of laser

δ: image position change at detector

θ: angle of emission of light from fiber

Δ: target position change

θ: Angle of incidence of laser

d_o: target distance or standoff distance

d_i: image distance

f: focal length of lens

m: magnification of lens

n_1: refractive index of core

n_2: refractive index of cladding

CHAPTER 1: INTRODUCTION

1.1 REQUIREMENT & CHALLENGES FOR POSITION MEASUREMENT AND ALIGNMENT IN INDUSTRIES

Today, as manufacturing industries are growing and becoming very competitive, requirements for the production of precise and accurate mechanical assemblies or parts are in demand. Firstly, quality checks are the essential part of production industries to ensure precise dimensions and tolerances of product. Secondly, to ensure continuous production, periodic inspection of machine as part of preventive maintenance is necessary. Some inspection tasks are complex, time consuming and are difficult for human personnel due to hazardous environmental conditions, so there is a need for developing automated inspection systems and sensors, which can operate with high accuracy, without the intervention of humans and give the direct output. Continuous new development is going on to refine available sensors and design the new sensors to meet the measurement requirements. To cope up with the industrial demands, the scientific community is putting a large amount of efforts to evolve new futuristic technology, which can support production industries precisely and accurately.

Precise position sensing and alignment monitoring is a rapid developing technology which is applied in many different machines and instruments. Position measurement is defined as the accurate measurement of the location of the target (machine or mechanical components) with respect to some reference point or to a particular co-ordinate system. Alignment means adjusting the target in a specific line or plane by continuously monitoring the position of the target. During the installation, maintenance and calibration of industrial equipment or during alignment of machines, there are some basic requirements, which are to be monitored such as straightness, flatness, angle or its distance from a specific position. If the components in machines are not properly positioned and aligned initially during the machine set-up, then during its operation, it might lead to the unwanted vibrations finally leading to the failure of machines. These failures of machines lead to the stoppage of production leading to the increase in the cost of production. Therefore, applications of precise position measurement and alignment are mostly needed in industrial environments such as manufacturing and production industries. Few examples where the accurate position and alignment needs to be measured are positioning of tool to the command position on work-piece in Computer Numerical Control (CNC) machines, assembly of pin to the target using robotics arm, differential gear alignment and wheels positioning in vehicles, alignment of fueling channels in nuclear reactors, shaft alignment, satellite antenna alignment, roller alignment in paper and steel industries etc. Mechanical engineers also benefit from a wide range of technologies and methods to accomplish their measurement and alignment needs. Some of the industrial applications for position measurement and alignment are described in detail in the following sections.

1.1.1 Shaft Positioning and Alignment

A shaft is an essential part of the rotating machine and is used to transmit power and motion from the driving shaft to the driven shaft. They can be divided into two categories as transmission shafts or machine shafts. A common problem associated within rotating machinery is shaft misalignment [1]. Shaft misalignment occurs when the center lines of rotation of two or more machinery shafts are not in line with each other [2]. In general, shaft misalignments are of three types:

(1) Offset: When the centerline of two shafts is parallel but is on separate lines as shown in Figure 1.1 (a).

(2) Angular: When both the shafts are on same axis but are at the angle to each other as shown in Figure 1.1 (b).

(3) Combined offset and angular misalignment: In reality, shaft misalignment would be a combination of both of these effects as shown in Figure 1.1 (c).

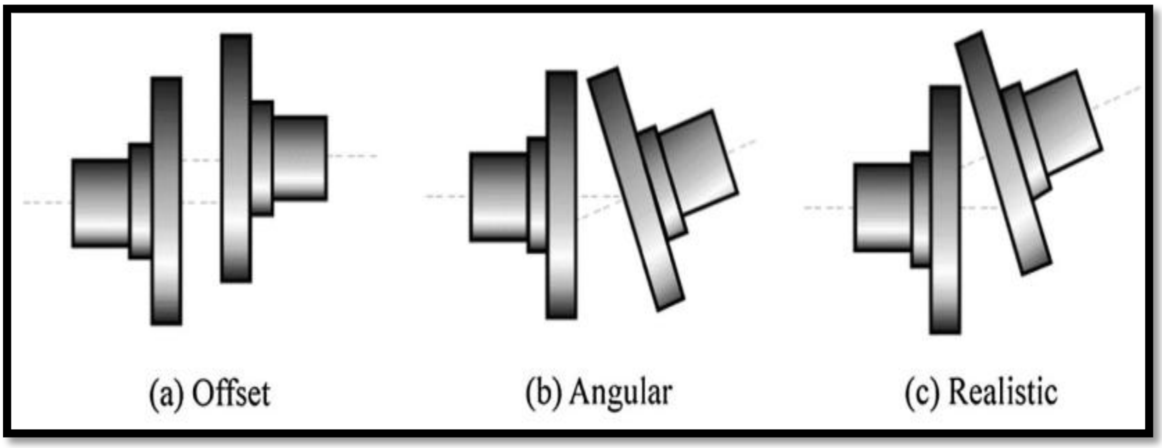

Figure 1.1: Types of Shaft Misalignment [2]

Different types of misalignments of shafts have different effects at the output for e.g. power consumption in offset misalignment is more as compared to the angular misalignments. The process of shaft alignment is the positioning of the shaft center lines of the driving shafts and driven shafts to create collinear shafts, where the rotational center lines of the coupled shafts are parallel. In general, to measure the amount of shaft misalignment, the following methods are commonly used:

(1) Straight edge: The straight edge is usually the first stage of inspection which is used to get an approximate reading before moving onto the more accurate methods. Figure 1.2 (a) gives the basic straight edge measurement technique. This

is a contact measurement technique and is based on the operator measurement skill.

(2) Dial indicator: This is also a contact measurement technique using mechanical based reverse indicator method shown in Figure 1.2 (b).

(3) Laser indicator: Recently, dial indicators have been replaced by laser based misalignment measurement methods, which are more accurate and can be automated to calculate the amount of shaft misalignment automatically. The measurement technique is shown in Figure 1.2 (c). High resolution (~10 microns) is achieved based on this technique, but the main disadvantage is that the given technique cannot be used in the EMI and radioactive environments as the electronic components get affected under these circumstances. Moreover, the components have to be fixed on the driving and driven shafts that add an extra weight.

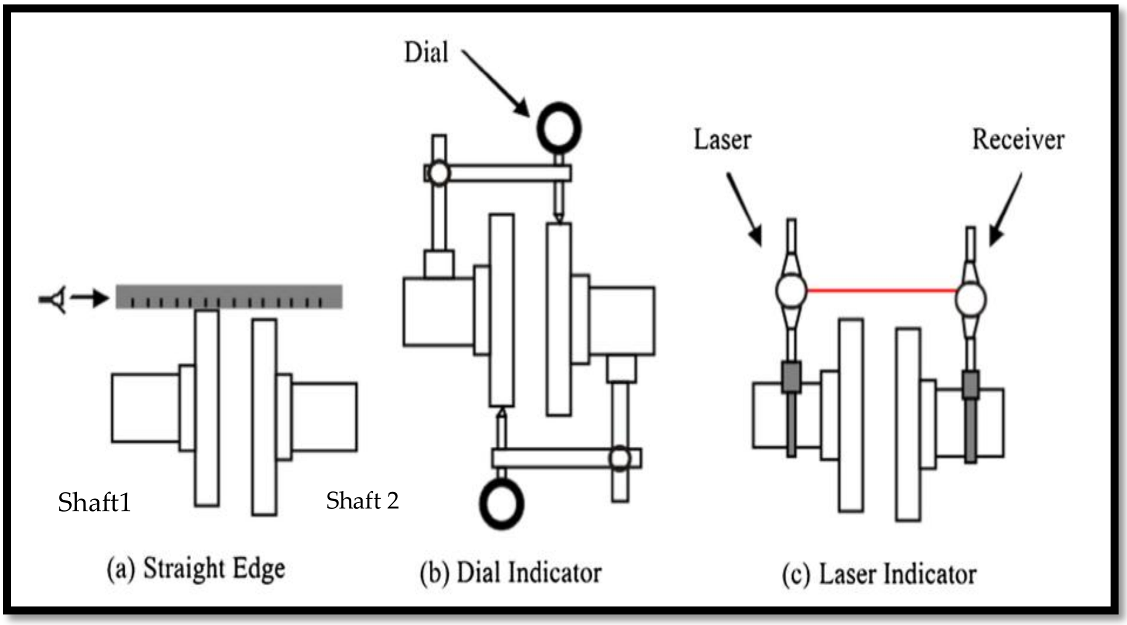

Figure 1.2: Measuring Techniques of Shaft Misalignments [2]

Thus a non-contact optical measurement technique is required which not only helps in measuring the change in position but also gives the accurate and precise results.

1.1.2 Positioning and Aligning of Parts in Airframe Assembly

The process of positioning, mating and joining large airframe sub-assemblies are generally accomplished by using multiple mechanical actuators that are attached to the airframe structures. These mechanical actuators are driven by pneumatic motors to provide the motion to the desired assembly or part. Since each mechanical actuator in this conventional system is an independent device, factory personnel have to work in coordination with these actuators to move the individual parts to form an assembly. This is accomplished by moving a single actuator while communicating with others. Since the personnel cannot coordinate the movement of multiple actuators effectively and the part's movement may be along a complex path, the movement and assembly of parts can be inaccurate and unpredictable. Moreover, actuators used can potentially counteract each other, thus imparting unwanted forces to the airframe structure, adding stresses to the structures. This might lead to the internal cracks of the structures thus reducing the lifetime of the assembly.

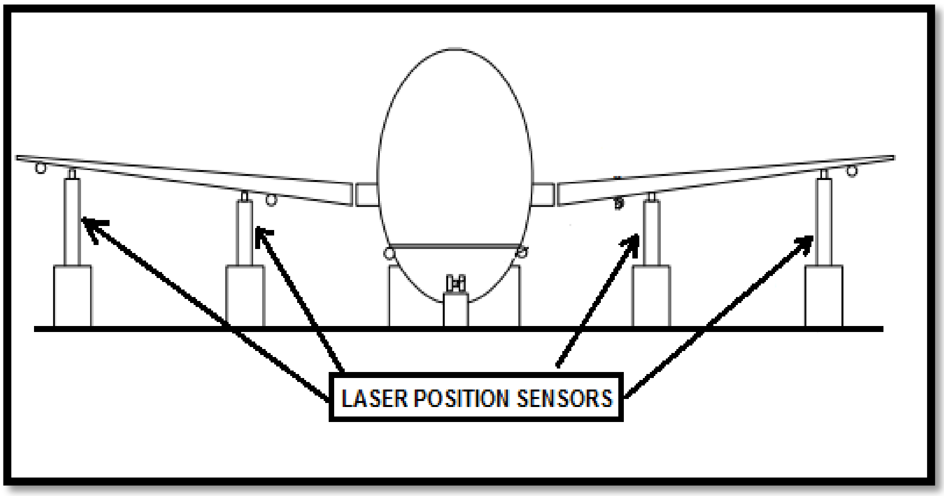

Figure 1.3: Schematic for the use of laser based position sensor and alignment for aircraft assemblies

Unlike the conventional process, automated positioning relies on a control system to coordinate the motion of multiple mechanical actuators to manipulate aircraft parts in a known fashion [3]. For the above automated positioning measurement, as shown in Figure 1.3, a non-contact optical measurement technique is required that can give feedback signals during the positioning and aligning of the airframe structures and also does not add weight over them that might lead to the bending and adding stress which might lead to the crashing of air craft.

1.1.3 Machine Tool Alignment

The increase in the number of the complex application of the CNC machines in manufacturing industry has emphasized the need of positioning accuracy of the tool/cutter. In order to meet the quality requirements of the manufactured products and to minimize the waste, positioning and alignment of tools is essential. To precisely guide the tool/cutter to a desired location or along the desired path highly accurate position measurements in real time within the working space with the automatic tool tracking ability is needed [4]. Therefore, a non-contact based position sensor is extremely important, as it does not intervene in the ongoing process.

1.1.4 Fuel Channel Alignment in Pressurized Heavy Water Reactor (PHWR)

In the nuclear industry, the alignment among the various components plays an important role considering the criticality of the job involved. Refueling operation is common to all the reactors for their continuous operation over their extensive lifetime. Refueling involves inserting new fuel bundles into the reactor and collecting the spent fuel bundles from the reactor. A specifically designed Fueling machine based on the reactor type performs these operations. The alignment between the Fueling Machine and the reactor core is critical to ensure the safety of the new fuel bundles and the spent fuel bundles while they are being transferred from the Fueling Machine to the reactor or vice-versa. On-Power refueling feature of the Indian PHWR reactors further adds to the importance of the alignment between the Fueling machine and the coolant channels to ensure the safety of the reactor and to prevent any radioactivity leakage.

The Fueling Machine must be precisely aligned with the End-fitting of the coolant channel before its head is clamped on to it. Nowadays, this alignment is generally measured using the Potentiometers (detail of working principle is explained in section 1.2.1) or Linear Variable Differential Transformers (LVDT) sensors (detail of working principle is explained in section 1.2.2). However, a non-contact type sensing mechanism is preferred as it does not disturb the End-fitting and gives a better result.

Some of the other industrial applications where the position measurement and alignment monitoring is needed are: steam turbine position and alignment, hinge position and alignment, bore position and alignment, guide rail alignment, periscope alignment, antenna alignment, propeller shaft alignment etc.

1.2 DIFFERENT TYPES OF POSITION AND ALIGNMENT MONITORING SENSORS WITH THEIR COMPARISON

For measuring the position and alignment, a number of techniques have been developed to make these measurements. However, many of them result in inaccuracies so high that proper operation of the equipment involved is compromised or seriously endangered. The sensing techniques used for measurement can be classified as contact and non-contact types [5-7]. As the name indicates, contact type sensors measure the position of a target by directly contacting it. Different types of contact and non-contact type position sensors are described below.

1.2.1 Potentiometer or Variable Resistance Position Sensors

The potentiometer is the electrical sensor, which works on the principle of change of resistance of the wire with its length. As the resistance of wire is directly proportional to the length of wire, therefore variation in resistance of wire gives the variation in length. The typical potentiometer is shown in the Figure 1.4. The point *C* is the slider, which is connected to the target whose position is to be measured. Here, the voltage V_s is applied across the two points of the wire *A* and *B*. As the length of wire *AC* changes, the voltage V_o also changes.

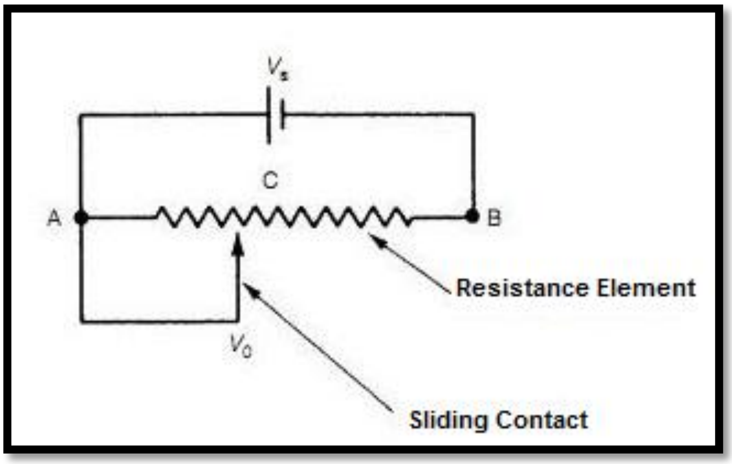

Figure 1.4: Schematic of working principle of potentiometer

The Position change can be easily determined by measuring the voltage V_o between points A and C. These sensors are cheap and highly efficient. However, major disadvantage is that there is wear and tear due to the movement of slider thus reducing their life [6, 7].

The sensitivity of potentiometer depends upon the smallest change in potential that can be measured in response to the displacement. This can be done by increasing the length of the potentiometer wire or by decreasing the current in the wire (when the length of wire is fixed). The resolution is of the order of 0.1 mm. However, potentiometer technique being a contact type measurement, it may not be suitable in all applications.

1.2.2 Linear Variable Differential Transformer

Linear Variable Differential Transformers (LVDT's) are the common type of electro-mechanical transducers that convert rectilinear motion of target to which they are coupled mechanically into the electrical signal. It consists of primary winding centered between pair of identically wound secondary windings. A rod shaped magnetic core is placed centrally inside the coil assembly that provides the medium for linking the magnetic flux across the primary and secondary windings.

The LVDT's primary winding P is energized by a constant amplitude AC source. The core to the adjacent secondary windings S_1 and S_2 couples the magnetic flux developed due to the primary winding. If the core is located midway between S_1 and S_2, equal flux is coupled to each secondary. So, the voltages E_1 and E_2 induced in windings S_1 and S_2 respectively are equal. At this reference midway core position, known as the null point, the differential voltage output $(E_1 - E_2)$ is essentially zero. As shown in Figure 1.5, if the core is moved closer to S_1 than to S_2, more flux is coupled to S_1 and less to S_2.So, the induced voltage E_1 is increased while E_2 is decreased, resulting in the differential voltage $(E_1 - E_2)$. Conversely, if the core is moved closer to S_2, more flux is coupled to S_2 and less to S_1 resulting in the differential voltage $(E_2 - E_1)$ [6, 7].

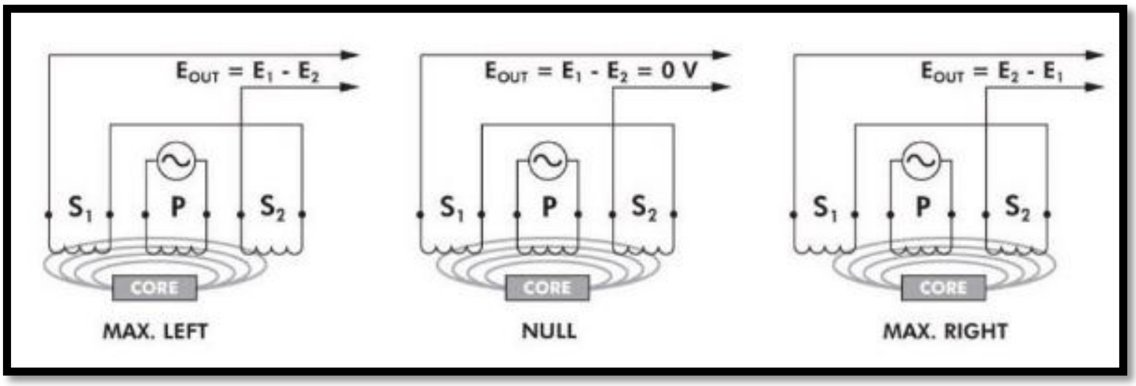

Figure 1.5: Working principle of LVDT

Demerits of the contact type sensors are: they cannot be used for delicate target surfaces, components having high temperature and with the radioactive targets.

Moreover, these sensors need to be installed before the commissioning of the machinery. Therefore, to avoid such problems non-contact sensors are preferred.

Among the non-contact sensors, different types of sensors are available for position measurement based on capacitive, electromagnetic, ultrasonic and optical techniques as shown in Figure 1.6 [5, 6].

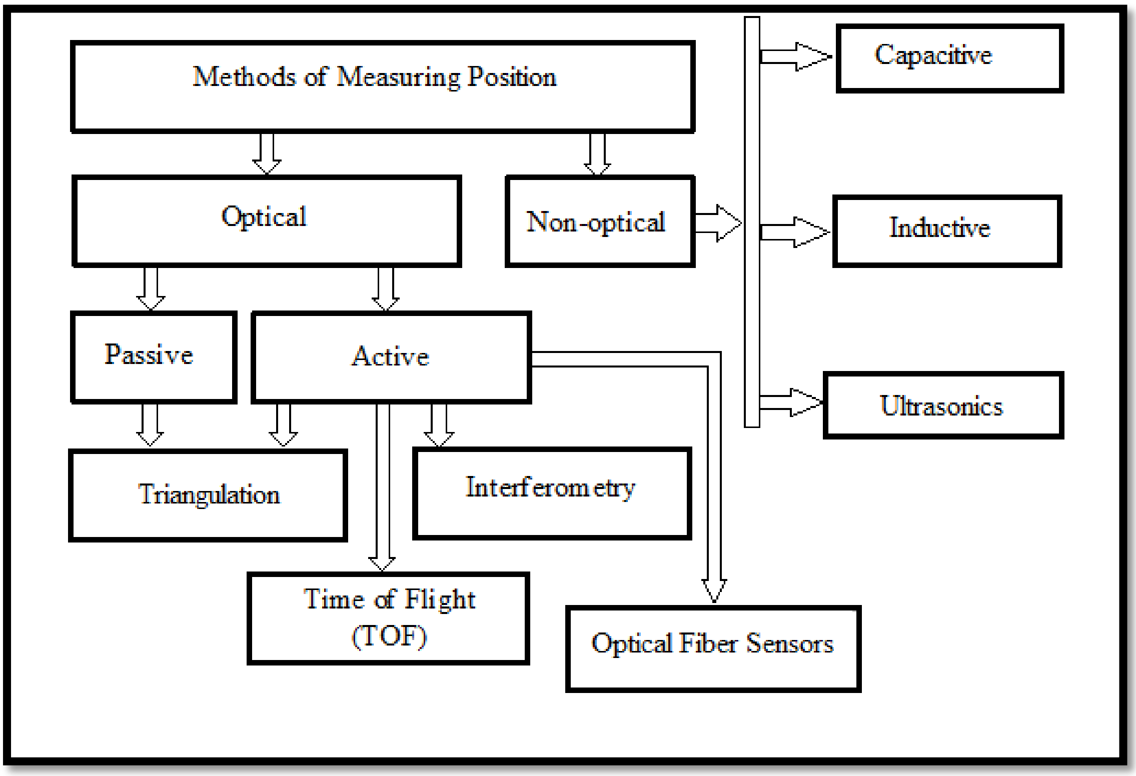

Figure 1.6: Non-contact Position Measurement Techniques

1.2.3 Capacitive Sensors

The capacitive sensors are non-contact sensors that work by measuring changes in capacitance. In typical capacitive sensing applications, the sensor is one of the conductive objects and the target whose position is to be measured is the other. The sizes of the sensor and the target are assumed to be constant as is the material between them. Therefore, any change in capacitance is a result of a change in the distance between the probe and the target. The capacitance C is given as:

$$C = \frac{Dielectric \times Area}{Distance} \tag{1.1}$$

Thus, capacitance increases when the distance decreases from which information about change in position is inferred. Although the sensitivity of the capacitive sensors is high, they are highly dependent on the surrounding parameters such as temperature, dirt, moisture etc [6].

1.2.4 Inductive Sensors

An inductive sensor is non-contact sensor that detects the metallic targets approaching the sensor. Their operating principle is based on a coil and oscillator that creates an electromagnetic field in the close surroundings of the sensing surface. The main components used in these are coil, oscillators, detectors and output circuit. The presence of a metallic object in the operating area causes a dampening of the oscillation amplitude. A threshold circuit that changes the output of the sensor identifies the rise or fall of such oscillation. The operating distance of the sensor depends on the actuator's shape and size and is strictly linked to the nature of the material. These sensors are accurate, have high switching rate and can work in harsh environments but have limited operating range and can detect only metallic targets [6].

1.2.5 Ultrasonic Sensors

Ultrasonic generally refers to a high pitch sound that is inaudible to humans having frequency greater than 20 kHz. Ultrasonic sensors measure the distance by using ultrasonic waves. The sensor head emits an ultrasonic wave and receives the wave reflected back from the target. They measure the distance to the target by measuring the time elapsed between the emission and reception. So, detection in these sensors is unaffected by the target material and surface properties. Of course, since rough surfaces reflect the acoustic energy in multiple directions (diffuse); this can decrease the detection range of the sensor.

1.2.6 Optical Sensors

An optical sensor converts the modulation in light rays into electronic signal. Optical Sensors are used for non-contact detection, counting or positioning of mechanical parts. Optical position sensors can be classified into optical fiber sensors, interferometers, time of flight sensors, confocal sensors and triangulation sensors. These types of sensors provide a “positional” feedback. One method of determining a position is to use either “distance”, which could be the distance between two points such as the distance travelled or moved away from some fixed point, or by “rotation” (angular movement). Details of different optical techniques used for position sensing and alignment monitoring are discussed in Chapter 2. Table 1.1 gives different non-contact position measurement techniques.

Table 1.1: Different non-contact position sensing technologies

Technology	**Sensing Range**	**Applications**	**Target Materials to be aligned**
Inductive	4-40 mm	Any close-range detection for ferrous materials	Iron, steel
Capacitive	3-60 mm	Close range detection of non-ferrous materials	Liquid, wood, plastic, glass etc.
Optical/Laser based	10 µm – 100 m	Long range, small range, high resolution	Any kind of targets, silicon,

			paper, metals
Ultrasonics	2 cm – 10 m	Long range detection of targets with complex surface properties	Glass, liquid, metal

1.3 WHY DO WE NEED OPTICAL OR LASER BASED SENSORS?

From Table 1.1, one can observe that optical/ laser based sensors can be directly used as the measurement tool as they have maximum sensing range, high resolution and are suitable in hazardous/EMI affected environments. During the measurement, it is important that the measurement taken is both accurate and precise. Accuracy represents how close the measurement is to its true value whereas precision represents how close the series of measurements of the same parameter are to each other. Laser- based instruments are both accurate and precise. Lasers combining with optical fibers form a new sensing mechanism known as optical fiber sensors. Optical fibers can be used for transmitting the information of the measured parameters sensed or can be directly used as the sensors. Optical fiber sensors have received considerable research efforts due to its potential sensitivity, detection speed and abilities to be used in hazardous environments. Other advantages of optical fiber sensors are compactness, low cost fabrication process and the compatibility with other optical components. Thus, the application of these sensors for position monitoring and alignment purpose is most suitable.

In laser-based sensors, as light travels in straight line, it can produce precise measurements that cannot be achieved by manual or mechanical methods. Level lines can be established over large distances so accurately that every point is exactly perpendicular to the line of gravity. Right angles using them can be produced quickly and precisely with auxiliary components as mirrors and prisms. Moreover, the presence of electronic detector for various wavelengths have increased the applications of laser based instruments in the different types of applications. Not only the direct laser light but also the reflected and backscattered light from any target surfaces can be used for measurement [9]. The backscattered light from the target surface is spread over a large solid angle and so, a lens is used for focusing it on a detector. Thus, angular variation of the intensity or noise is averaged out.

1.4 THESIS OUTLINE

The thesis consists of following parts

Chapter 1 gives the introduction to the thesis, provides the requirement and challenges of position measurement and alignment in machines. Some of the industrial position and alignment problems such as shaft alignment, airframe assembly alignment, and fueling channel alignment of PHWR are described. Brief introduction of contact and non-contact techniques for position measurement along with the need of optical techniques for measurement is presented.

Chapter 2 gives the literature survey and comparative assessment of different optical techniques for position and alignment monitoring. The working principle of intensity based fiber optic sensors; time of flight, interferometers, confocal based sensors and laser triangulation sensors is described along with their working range and applications in different fields.

Chapter 3 describes the axial position measurement of the target using single optical fiber and lens. The system comprises of an optical fiber coupler and lens which together acts as a single probe for simultaneously transmitting and receiving signal for position change measurement.

Chapter 4 gives a design and performance study of a laser triangulation based compact position sensor for long standoff distance (~1000 mm) using beam folding technique. The system is designed for the back scattered diffused light collection. The given sensor was tested for the different target roughness samples and the output was found to be independent of it. The effect of temperature on the output of developed sensor was also studied and the error in measurement was found to be within the sensor resolution.

Chapter 5 gives the design and development of modified laser triangulation sensor. Here instead of directly using the detector, the light is transmitted through the linear optical array. The change in position of the image spot through the fiber array helps in determining the position change of the target. Thus, the given sensor system can be used for remote position measurement.

Chapter 6 gives the mathematical model and experiment results for the measurement of the position of circular target in a two-dimensional plane using the in-house developed two linear fiber array based laser triangulation sensor.

Chapter 7 describes the sensing principle of fiber optic transmission based position sensing in a two-dimensional plane by using the light coupling between the single fiber and linear fiber array. This technique directly measures the two-dimensional position change by sensing change of centroid and intensity distribution of image at CCD camera.

Chapter 8 gives the conclusion and future scope for the thesis.

CHAPTER 2: LITERATURE SURVEY

With the advancement of lasers, optical fibers and optoelectronics in recent years, various types of optical and laser-based sensors have been developed for position measurement and alignment monitoring. Being non-contact in nature, these sensors have gained importance in various industries like automobiles, military, nuclear, power etc [5, 6, 8, 9]. For position measurement and alignment monitoring from a distance different kinds of optical sensors are available such as intensity based optical fiber sensors, interferometers, time of flight sensors, confocal based sensors and laser triangulation sensors [8, 9]. This chapter gives the comprehensive study of above-mentioned techniques for the position measurement, mathematics and physics behind their working, their range of operation and the factors causing the uncertainty in measurement in these techniques.

2.1 INTENSITY BASED OPTICAL FIBER SENSORS

An optical fiber is a light waveguide that takes the form of a long cylindrical structure consisting of three layers viz. core, the cladding and the protective jacket. Both the core and cladding are made from either glass or plastic and the external jacket provides protection against the physical damage. The optical fibers can be of single mode (core diameter up to 10 µm) or multimode (core diameter from 50 µm to 1000 µm) [10-14]. The capability of fibers for collecting or receiving the light is governed by the Numerical Aperture (NA) that is defined as the sine of angle of acceptance or emission cone.

$$NA = \sin\theta = \sqrt{(n_1^2 - n_2^2)} \tag{2.1}$$

Where, n_1 is refractive index of core and n_2 is refractive index of cladding and ($n_1 > n_2$).

Depending on the physical dimensions of the core/cladding, refractive index and wavelength, anything from one to thousands of modes can be supported within a single optical fiber. The two most commonly manufactured variants of optical fibers are single mode fiber (which supports a single guided mode) and multimode fiber (which supports a large number of guided modes). In multimode fibers, the spatial profile of light exiting the fiber core depends on the launch conditions, which determine the distribution of power among the spatial modes. In these fibers lower-order modes tend to confine light spatially in the core of the fiber; higher-order modes, on the other hand, tend to confine light spatially near the core/cladding interface.

The number of modes propagating through the fiber is governed by the V-number. V-number is a dimensionless quantity is proportional to the free space optical frequency but is normalized to guiding properties of an optical fiber.

The V-number is defined as:

$$V = \frac{2\pi(\frac{d}{2})}{\lambda} \times NA$$

Where, V is the normalized frequency (V-number), d/2 is the fiber core radius, and λ is the free space wavelength.

If V-number is less than 2.405 then the fiber is single mode but if V is greater than 2.405 then fiber is multimode.

V number is also related with the number of modes is the fiber as:

For step index fiber no. of modes $N = V^2/2$.

For Number of modes graded index fiber is $N = V^2/4$.

For a multimode fiber, which accepts light over a wide NA, the condition of the light (e.g., source type, beam diameter, NA) coupled into the fiber, can have a significant effect on performance. An under-filled launch condition occurs when the beam diameter and NA of light at the coupling interface are smaller than the core diameter and NA of the fiber. Under-filled launches tend to concentrate light spatially in the center of the fiber, filling lower-order modes preferentially over higher-order modes. As a result, they are less sensitive to macro-bend losses and do not have cladding modes. The measured insertion loss for an under-filled launch tends to be lower than typical, with a higher power density in the core of the fiber.

Overfilled launches are defined by situations where the beam diameter and NA at the coupling interface are larger than the core diameter and NA of the fiber. An overfilled launch completely exposes the fiber core and some of the cladding to light, enabling the filling of lower and higher-order modes equally. This increased percentage of higher-order modes means that overfilled fibers are more sensitive to bending loss. The measured insertion loss for an overfilled launch tends to be higher than typical, but results in an overall higher output power compared to an under-filled fiber launch.

A larger acceptance angle of the fiber simplifies the launching of light, e.g. from a semi-conductor source. In addition, a high NA reduces the losses associated with fiber bending. Due to the effects of bending, the propagation direction of each individual ray is changed relative to the axis of the fiber. In the case of multi-mode fibers, a part of the rays is always extracted because the rays exceed the angle of total reflection at the interface between core and cladding. For fibers with a large NA, the effect of a change in angle for a certain amount of bending is not so significant so that the bending losses diminish.

The choice of a type of a light source for a certain optical fiber sensor application is very much dependent on the stability of the source and the power loss that occurs through the coupling of the light to the fiber. Light Emitting Diodes (LED's incoherent light sources) and laser sources (coherent light sources) are widely used based on the type of application required [10].

The intensity-based optical fiber sensors are the earliest and most widely used technology to date because of its low cost, easy installation and high sensitivity. The sensors that directly transform the measurands to the variation of light intensity on the receiving fiber are intensity-based optical fiber sensors. They can be classified as intrinsic or extrinsic type sensors [15]. In the intrinsic sensor, the measurand modulates the transmission properties of the sensing fiber whereas in extrinsic sensors modulation takes place outside the fiber. Extrinsic intensity-based optical fiber sensors generally have two configurations: transmission and reflective based sensors. In the transmission-based sensors, two fibers face each other at a certain distance while in the reflection-based sensors; one or more fiber transmits the light to a reflecting target while the other collects the light reflected from the target based on different configurations. In both the above-mentioned sensing techniques, optical fibers connected with the light source and detector is known as transmitting and receiving fiber respectively. Intensity based optical fiber sensors are widely employed for the measurement of deflection [16], pressure [17], liquid refractive index [18] and vibration [19-21] etc. They inherit two primary advantages; which include accurate and non-contact sensing and flexibility in incorporating the optical sensors into compact and composite structures without affecting the process. As the thesis is concentrated on position sensing applications, the detailed mathematical descriptions of transmission and reflection type intensity-based position sensors are described in following sections.

2.1.1 Transmission Type Optical Fiber Position Sensors

In general, most of the transmission or coupling based optical fiber position sensors utilize the single fiber-to-fiber light coupling, where the light is transmitted from one optical fiber to other with a known gap between them and output of receiving fiber is coupled to the detector [19-22]. This position is considered as the reference position where the maximum intensity is achieved at the detector. As the position of receiving fiber changes (laterally or axially), the variation of intensity at the detector takes place which is finally interpreted to infer the position change along one-dimension.

The optical fiber position sensor structure is shown in Figure 2.1. In this case geometrical model is considered, the light emitted from the fiber core is assumed to be circular. Let P_e be the optical power of light emitted from the transmitting fiber and P_r is the optical power received by the receiving fiber. Considering that the fibers have the same diameter d having θ as the emission angle related to the half-light cone and the distance between both fiber be x. The collected light depends on the optical power at the tip of receiving fiber that in turn depends on the distance between both fiber tips x and on the NA of transmitting and receiving fiber.

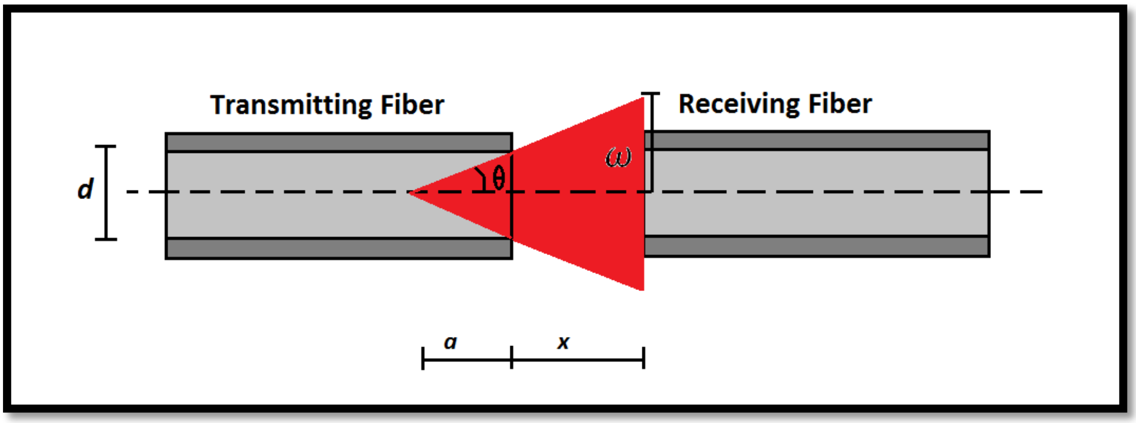

Figure 2.1: Schematic of the optical sensor arranged in transmission mode

Let ω is the radius of the circular cross section corresponding to the light cone at the receiving fiber. Then,

$$\omega = (a + x) \times \tan\theta \tag{2.2}$$

$$\omega = (a + x) \times \tan(\sin^{-1}(NA)) \tag{2.3}$$

Considering that the illumination I is constant over the entire surface of the receiving fiber, the power collected by the receiving fiber can be obtained by multiplying the corresponding illuminated area S of receiving fiber and the illumination value evaluated at the fiber tip. So,

$$P_r(x) = S \times I(x) \tag{2.4}$$

Where, $S = \pi\left(\frac{d}{2}\right)^2$. Therefore,

$$P_r(x) = \pi\left(\frac{d}{2}\right)^2 \times \frac{P_e}{\pi\omega^2} \tag{2.5}$$

$$P_r(x) = \frac{\left(\frac{d}{2}\right)^2 \times P_e}{\left((a + x) \times \tan\theta\right)^2} \tag{2.6}$$

As in Figure 2.1,

$$a = \frac{\left(\frac{d}{2}\right)}{\tan\theta} \tag{2.7}$$

From Eq.(2.6),when x=0, received power is equal to transmitted power.

The sensitivity of the sensor with the change in position is given by,

$$\frac{dP_r}{dx} = \frac{2\left(\frac{d}{2}\right)^2 \times P_e}{(\tan\theta)^2 \times (a + x)^3} \tag{2.8}$$

The above Eq. (2.6) is applied to study a sensor in transmission structure composed of two fibers with core diameter *d* = 1 mm and NA = 0.5 mm. Figure 2.2 gives the simulated result of normalized output (the ratio between the received power and the input power) vs. axial position change.

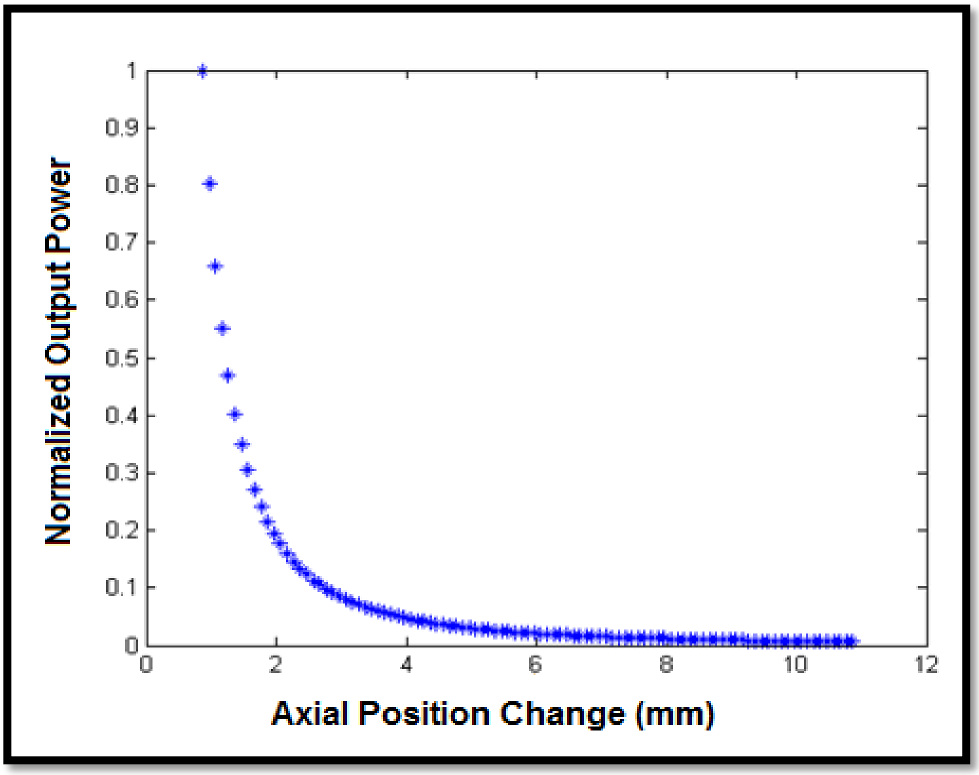

Figure 2.2: Normalized output vs. the axial position change (mm)

From Eq. (2.8), position sensitivity is inversely proportional to the cube of distance between the fibers and directly proportional to the square of diameter of fiber. Therefore, transmitting and receiving fiber should be placed as close as possible and cross-sectional diameter of the fibers should be more. From the Eq. (2.6), we conclude that when the fiber tips are in contact, the received power is equal to the transmitted power. Otherwise, when there is a gap between the fiber tips, the ratio Pr/Pe (normalized output power) decreases as the inverse of the square of the distance. The relationship between the distance and the optical power collected by the receiving fiber helps in determining the axial position. Being intensity dependent, the light source used in the given sensing mechanisms should be stable.

Different researchers have modified these kinds of sensing systems to enhance the sensitivity of these sensors. As the light source intensity variation affects the output; Libo et al [23] have used the compensation mechanism based on light intensity distribution coming from the output fiber and the twin receiving fiber does the compensation. This is done by finding the ratio of the output of pair of detecting fiber that is independent of light source intensity and losses in optical fibers.

Jason et al [24, 25] have proposed a different intensity based sensor concept to determine the lateral position measurement by the by the use of light intensity coupling between single fiber to linear fiber array with CCD camera as a readout. They have simulated the system and experimentally demonstrated the lateral position change of transmitting fiber by calculating the centroid of the image spot received at the CCD camera.

Abdullah et al [26] also used the lateral displacement measurement by the light coupling between two optical fibers. They demonstrated the lateral sensing with different diameter of optical fibers and the output profile for all the fibers was Gaussian. The separate measurement of lateral and axial measurement was done and it was found that sensitivity of lateral sensor is seven times higher corresponding to a core diameter and has three times better performance than the conventional axial type displacement sensor.

2.1.2 Reflective Configuration based Optical Fiber Position Sensors

The reflective configuration based fiber optic sensors is one of the most widely used intensity modulated sensors and are used as displacement sensors, vibration sensors, proximity sensors in robotics and automation control, pressure sensor etc. The basic configuration of these kinds of sensors has two parallel fibers and a reflecting target [27-29]. A light source is connected to the one fiber called as transmitting fiber and the receiving fiber coupled with detector collects the reflected light from the target. Single-fiber sensors are arranged in an anti-parallel geometry as shown in Figure 2.3.

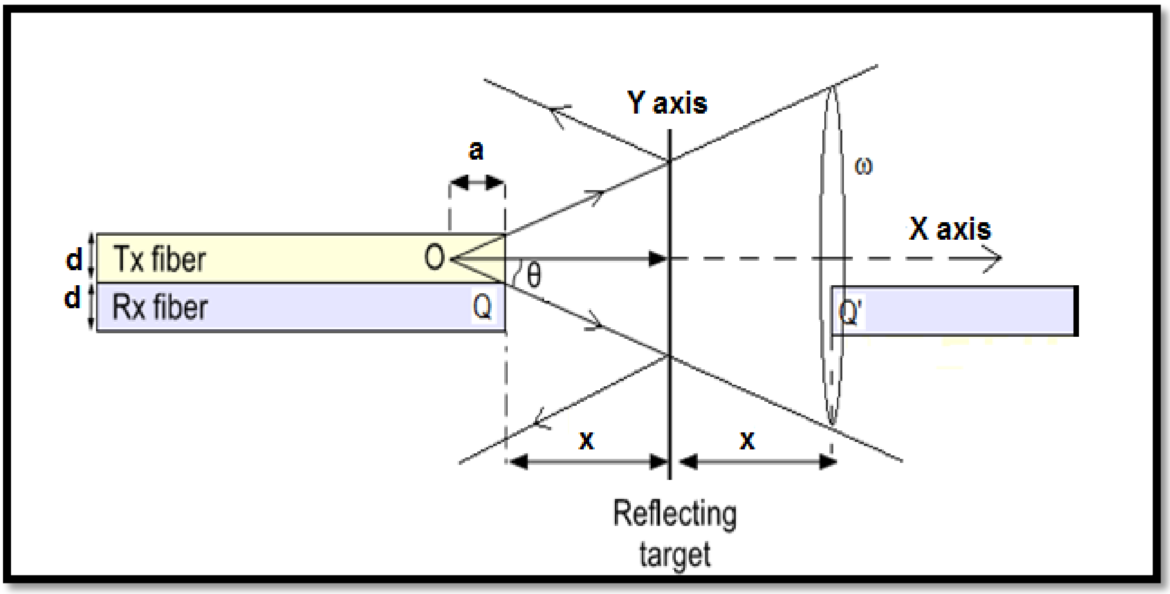

Figure 2.3: Basic Configuration of reflective configuration based fiber optic sensor

Considering that, both the fibers are circular having cross-section of area *S* and diameter *d* and there is no space left between both fibers as shown in Figure 2.3. The light leaving the transmitting fiber (Tx) is represented by perfectly symmetrical cone with the divergence angle θ and vertex *O* located at a distance a inside the transmitting fiber. Co-ordinates of point Q' i.e. the reflected image of receiving fiber (Rx) is given as (*X*= a + *2x*, *Y*= d). Considering the geometrical approach, with the assumption is considered that intensity of light remains constant inside the cone throughout the x-axis and the intensity of light remains zero outside the cone.

For $x > a$

Intensity of light inside the cone is given as:

$$I(x) = \frac{P_e}{\pi\omega^2} \tag{2.9}$$

Intensity outside the cone:

$$I(x) = 0 \tag{2.10}$$

Where, *Pe* is the light transmitted by transmitting fiber, ω is the radius of circular cross-section of the cone of current co-ordinate x. So,

$$\omega = (a + 2x) \times tan\,\theta = (a + 2x) \times \frac{\left(\frac{\mathrm{d}}{2}\right)}{a} \tag{2.11}$$

For $x < a$, no overlap of reflected cone and receiving fiber core is observed. Hence, total received light intensity at the detector is zero. This range is called as blind region.

For $x > a$, two conditions arise:

(a) Partial overlap condition of light at receiving fiber

This condition arises when during the position change; the reflected light intensity covers the part of the receiving fiber. This condition is shown in Figure 2.4 (a). Here $Q'P$ = d/2 i.e. radius of image of receiving fiber. $OP = \omega$, i.e. the radius of light cone at the face of image of receiving fiber.

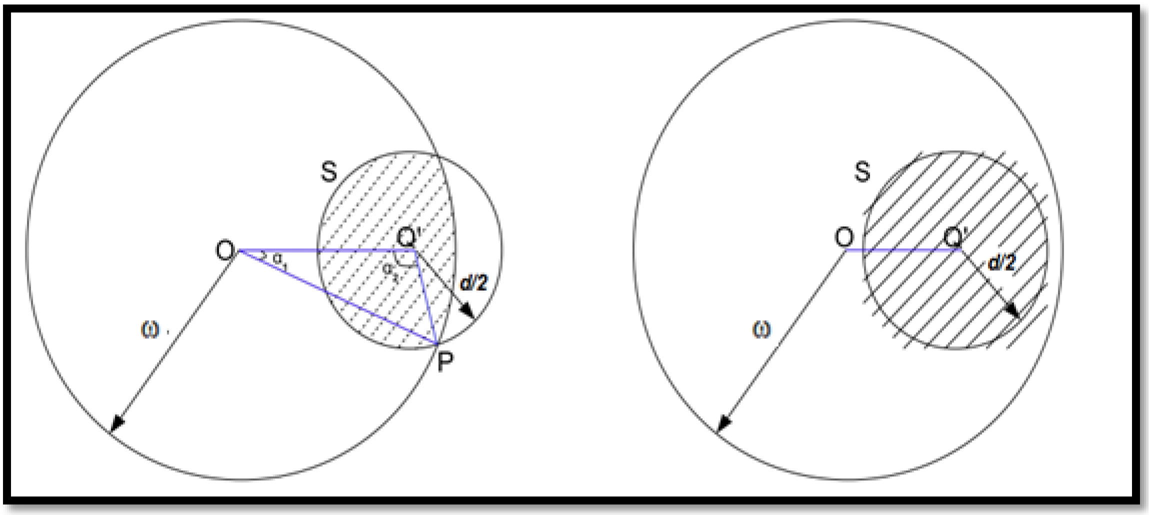

Figure 2.4: (a) Partial overlap (b) Complete Overlap

Calculation of overlap area:

'S' is divided into 2 regimes of S_1 and S_2. For overall consideration,

$$S = 2(S_1 + S_2) \tag{2.12}$$

Where, S_1: Semi-area of segment of circle 'ω' and angle α_1, S_2: Semi-area of segment of circle 'd/2' and angle α_2.

Both the areas can be calculated by applying the concept of area of sector and area of triangle.

S_1 = Area of circular sector (ω, α_1) – Area of triangle

$$S_1 = \tfrac{1}{2}\alpha_1\omega^2 - \tfrac{1}{2}x_a y_a \tag{2.13}$$

S_2 = Area of circular sector ($d/2$, α_2) + Area of triangle

$$S_2 = \frac{1}{2}\alpha_2\left(\frac{\mathrm{d}}{2}\right)^2 - \frac{1}{2}x_a(y_a - 2\left(\frac{\mathrm{d}}{2}\right)) \tag{2.14}$$

Where, P is the point of intersection of two circles having coordinates (x_a, y_a).

$$x_a = \omega\sin\alpha_1 = \left(\frac{\mathrm{d}}{2}\right)\sin\alpha_2 = \sqrt{\omega^2 - y_a^2} \tag{2.15}$$

$$y_a = \frac{1}{4\left(\frac{\mathrm{d}}{2}\right)}\left(\omega^2 + 3\left(\frac{\mathrm{d}}{2}\right)\right) \tag{2.16}$$

The y_a equation is achieved by applying the distance formula in above Figure 2.4.

Now substituting the values of S_1 and S_2 in $S = 2\,(S_1 + S_2)$ we get,

$$S = \alpha_1\omega^2 + \left(\frac{\mathrm{d}}{2}\right)^2\left[\alpha_2 - \frac{x_a}{\left(\frac{\mathrm{d}}{2}\right)}\right] - x_a\left(\frac{\mathrm{d}}{2}\right) \tag{2.17}$$

Eliminating x_a in the above equation, we get,

$$S = \alpha_1\omega^2 + \left(\frac{\mathrm{d}}{2}\right)^2[\alpha_2 - \sin\alpha_2] - \omega\left(\frac{\mathrm{d}}{2}\right)\sin\alpha_1 \tag{2.18}$$

The optical power $P(x)$ collected by the receiving fiber is now obtained by multiplying the illuminated area in S by the light irradiance $I(x)$.

$$P(x) = \int I(x)ds \tag{2.19}$$

$$P(x) = \frac{P_e}{\pi\omega^2} . S \tag{2.20}$$

(b)Complete overlap condition

For x ≥ a; considering Figure 2.4 (b)

$$P(x) = P_e \frac{\left(\frac{d}{2}\right)^2}{\omega^2} \tag{2.21}$$

An intensity-based sensor will have a response similar to the one shown in Figure 2.5 [9]. When the reflective target is very close to the transmitting fiber, no light is coupled to the receiving fiber. As the distance x increases, the reflective light from the target starts coupling to the receiving fiber and the power starts increasing. After complete overlap of light cone at the receiving fiber, the power starts decreasing as *x* increases, the increase of effective collecting area *S*, at receiving fiber tip increases thus decreasing the surface irradiance.

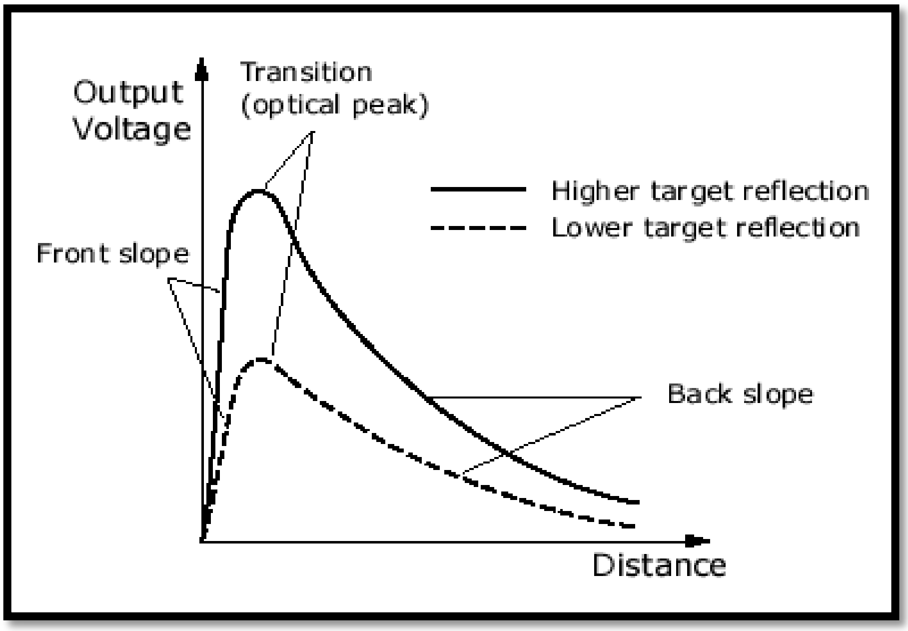

Figure 2.5: Output response of reflective configuration based fiber optic sensors

The signal response of Figure 2.5 presents two opportunities for distance sensing, namely, the near and the far sides of the peak, designated, as the "front slope" and the "back slope" respectively. The front slope usually exhibits higher sensitivity and lower dynamic range than the back slope. In order to use the sensor for measuring the absolute position to an object, the response curve must be known in advance; i.e., a calibration curve such as Figure 2.5 must first be obtained by using the specific object itself. Although different objects may exhibit calibration curves of similar shape, the signal amplitude at a certain distance is object dependent i.e. absolute reflectance and the diffusivity of the specific object.

Faria et al [27] has given the detailed analysis of geometrical and Gaussian beam approach for bifurcated fiber based position sensors. These sensors may use either single fibers or fiber bundles for illumination and detection. If an optical fiber bundle is used, then the transmitting and receiving fibers may be arranged in numerous ways as hemi-circular, concentric, or random [27-34]. The distance that yields the peak intensity, depends on the fiber diameters, numerical apertures (NAs) and the distance between both fibers and the geometrical distribution of illumination and detection fibers.

Different researchers have modified the given configuration by varying the distance between the fibers, or by varying the core diameters of the transmitting and receiving fibers, or by varying the reflective target surfaces etc. Based on the applications one can select the type of the configurations needed for the measurements. Comparison among these is given in Table 2.1.

Table 2.1: Sensitivities and linear range of different configuration.

Sensor Probe Configuration	**Reflective targets**	**Sensitivity**	**Linear range**	**Ref**
50:50 coupler based fiber optic displacement sensors	Mirror	0.0001 mV/µm	1500 µm	Yasin et al[29]
50:50 coupler based fiber optic displacement sensors	Aluminium	1.7 mV/µm	1500 µm	Yang et al [35]
Two symmetric parallel fiber optic displacement sensors	Mirror	1.9890 mV/µm	0.294mm	Lim et al [45]
Two asymmetric parallel fiber optic displacement sensors	Mirror	1.7615 mV/µm	0.580mm	Rahman et al [46]
One SMF, One MMF based fiber optic displacement sensors	Mirror	1.04m/W	240 µm	Golnabi et al [28]
Three Fibers: 1 transmitting, 2 receiving, based fiber optic displacement sensors	Mirror	0.06 mV/mm	900 µm	Harun et al [47]
Two symmetric inclined fiber optic displacement sensors	Mirror	10.5mV/ µm	800 µm	Sakamoto et al [34]
Two asymmetric inclined fiber optic displacement sensors	Mirror	0.726mV/ µm	1000 µm	Buchade et al [36]

Different parameters of the optical fiber used for the development of sensor affect the range and sensitivity of the sensor [29]. Table 2.2gives the parameters affecting the range and sensitivity on sensor.

Table 2.2: Effect of range and sensitivity on the optical fiber parameters

Parameters		**Sensitivity**	**Linear Range**
Transmitting Fiber	Diameter	No effect	No effect
	Numerical Aperture (NA)	NA increases, Sensitivity increases	NA increases, Linear Range Decreases
Receiving Fiber	Diameter	Diameter Increases, Sensitivity Increases.	Diameter Increases, Linear range decreases.
	Position of Receiving fiber w.r.t. transmitting fiber	Increases	Decreases

Other literatures [30-36] have reported that the performances of fiber optic displacement sensors can be improved by using different kinds of fiber bundle structures and different inclination angles. The relationship between the blind region and peak position, inclination angle and gap spacing between the transmitting core and receiving core have also been investigated and reported in literatures [36-47].

Some studies as discussed above are concentrated on the high resolution while others are oriented towards the long dynamic range. Based on the requirement user selects the type of the configuration needed, for measurement. Although easy and simple in operation, there are some disadvantages of these sensors, such as: pre-calibration for all target objects is necessary, since the distance is derived from the measured signal intensity and any change in the signal intensity will be interpreted as a distance change. Thus, illumination intensity variations, optical connection losses, variations of the target reflectivity, dust, dirt, etc. will be interpreted by default as a distance or position changes.

2.2 TIME OF FLIGHT SENSORS (LASER RANGE-FINDER)

The Time-of-Flight sensor works on the principle of measuring the time interval between the emission of a signal and its return to the detector after being reflected by an object. The signal travels at constant velocity that allows the calculation of the distance [8]. Light is preferred over sound because it travels in straight line at high speed. The speed of light in vacuum (c_o) is the universal constant $3\times 10^8 ms^{-1}$[48]. In a medium, light propagates at the lower speed (v) due to the high refractive index of the medium (n) as compared to the speed in vacuum (c_o). Let D is the distance between the target and the start point, and t_d is the time taken by light for the round trip as measured by the detector, then

$$D = \frac{c_o}{2n} \times t_d \tag{2.22}$$

The uncertainty δD in the measured distance is primarily due to the uncertainty δt_d of the measured time t and is given as:

$$\delta D = \frac{c_o}{2n} \times \delta t_d \tag{2.23}$$

This uncertainty in distance generally takes place due to the time jitter in the photodetectors, variations in rise times, and electrical noise in the pulses.

Most of the laser-based time-of-flight sensors operate by transmitting a nanosecond duration light pulse to the targets. These sensors require complex electronics for the detectors since measured distance is related to time delay that is of the order of nanoseconds. For example, total flight time of light from a target at 1 m away is about 6.7 ns. Figure 2.6 shows the schematic of working principle of time of fight sensor.

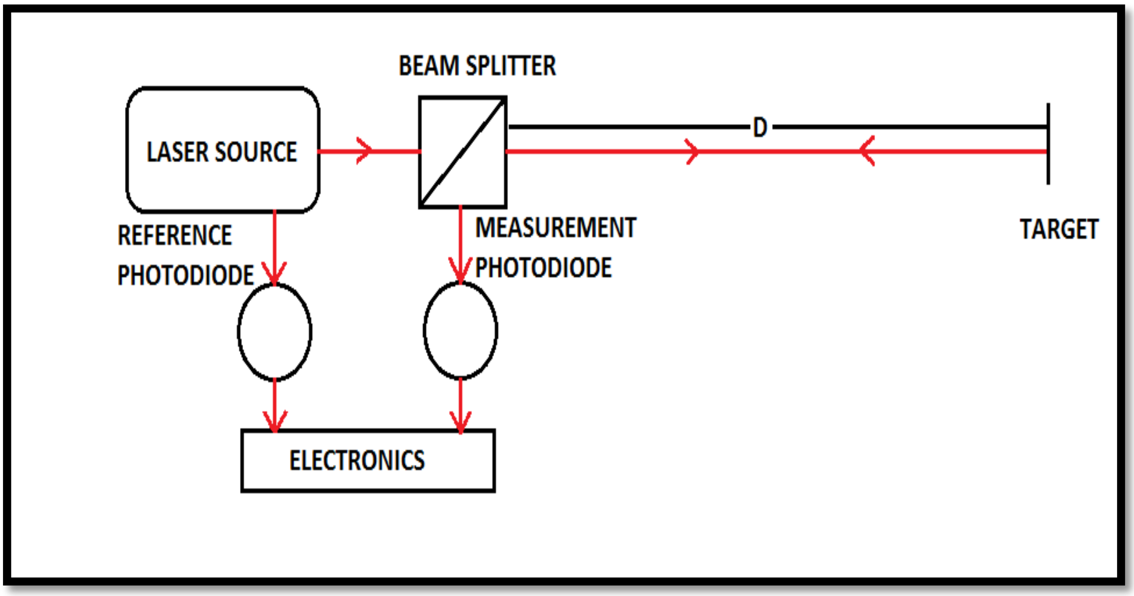

Figure 2.6: Schematic of time of flight measurement

An alternative approach to the pulse illumination is to use amplitude modulated continuous light. In this case, a phase shift ($\Delta\varphi$) in the modulation signal is measured between the launched and the returned light, and the time-of-flight is determined by dividing the phase shift by the modulation frequency (*fm*). The time of flight is given by:

$$t_d = \frac{\Delta\varphi}{2\pi fm} \tag{2.24}$$

The uncertainty δt_d in the measured time is primarily due to the uncertainty $\delta\Delta\varphi$ of measured phase difference between emitted and received waves and is given as:

$$\delta t_d = \frac{\delta\Delta\varphi}{2\pi fm} \tag{2.25}$$

The true phase shift is the measured residual phase shift with an integral number of full cycles (2π phase shifts). This ambiguity can be eliminated by measuring the true phase shift at an additional non-harmonic frequency. This approach is most practical for measuring distances in the intermediate region from a few meters up to 50 m (times of flight a few times larger than typical short pulses), but more difficult for distances shorter than 1 m, as the required modulation rate approaches the gigahertz range [4, 9].

Time-of-flight sensing is used for many civilian applications of range sensing, such as mapping and surveying. In these applications, resolution and accuracy generally depend on the accuracy of the electronics. The applicable maximum range distance will depend on the laser power, the detector sensitivity, the reflectivity and visibility of the target object, and the signal/noise ratio consequently obtained. A comparison table for different commercially available time of flight sensors is given in Table 2.3.

Table 2.3: Comparison between different readily available time-of-flight sensors

Name	Modulation	Meas. Range	Accuracy	Meas. Time
Laser Tech. Impulse 100LR	Pulse	0-575 m	3 cm @ 50 m, white target	0.3 - 0.7 s
Riegl FG21-HA	Pulse	2-600 m	± 5 cm	0.1-1 s
Riegl LD90-3100VHS-FLP	Pulse	2-200 m	± 2.5 cm	0.5 ms
Laser Optronix LDM500 MIL	Pulse	0-999 m	± 1 m	
Lecia DISTO pro	Sine wave	0.3-100 m	± 3 mm	0.5 - 4 s
Laser Optronix PH 30	Sine wave	0-30 m	± 5 mm	

2.3 LASER INTERFEROMETERS

There exist many and varied reports in the literature of interferometric techniques for position and displacement measurements. General concept of interferometer is that a laser beam passes through a beam splitter and splits single beam into two beams (I_1 and I_2) as shown in Figure 2.7.

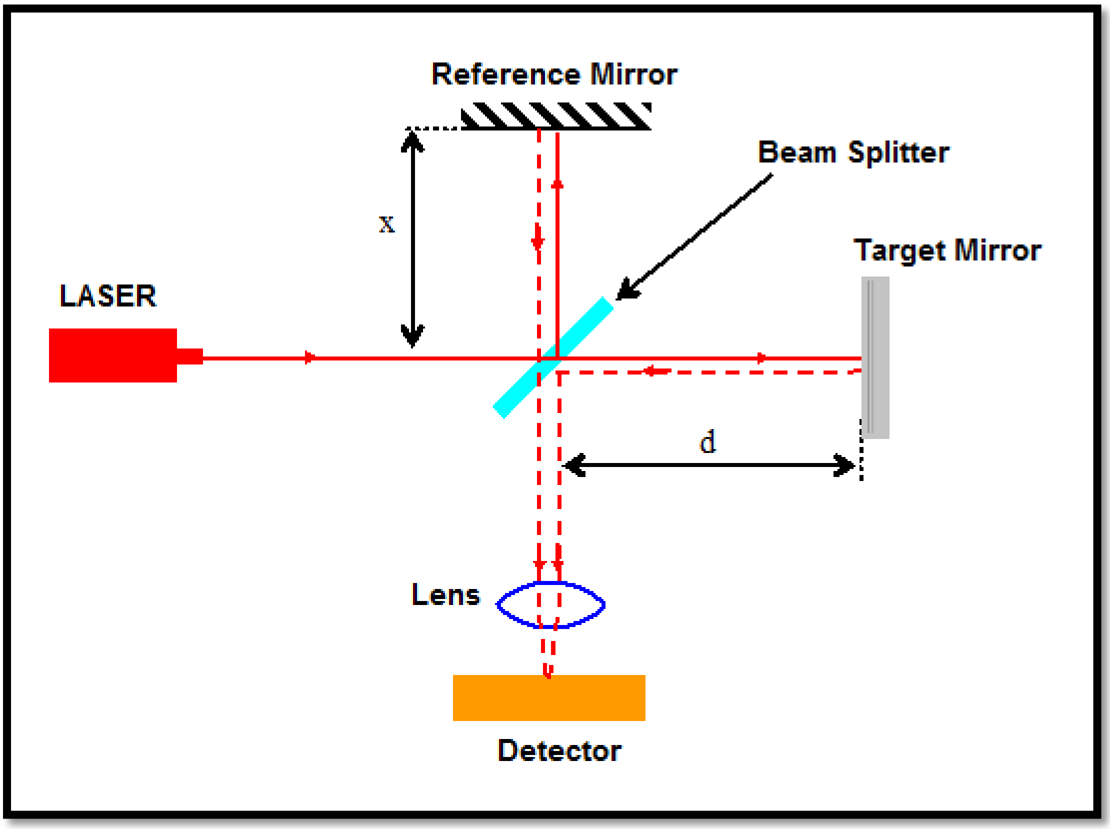

Figure 2.7: Schematic of Michelson Interferometer

Let, I_1 is the intensity of the reference beam (from the reference mirror), and I_2 is the intensity of the beam from the target. One beam passes straight while other is reflected at 90˚, each beam then travels around the arm of interferometer and at the end of each arm a mirror reflects back the beam to the beam splitter where the two beams merge back to the single beam. On merging, the two beams interfere leading to the formation of bright and dark fringes.

$$I = I_1 + I_2 + 2\sqrt{I_1 I_2}\cos\frac{4\pi(d-x)}{\lambda} \qquad (2.26)$$

Eq. (2.26) assumes that the light is spatially and temporally coherent and that the interfering beams have not acquired a net phase shift due to reflections. Assuming for the sake of simplicity $I_1 = I_2$, Eq. (2.26) shows that the combined intensity I varies from 0 to $4I_1$ depending on the value of d-x.

If $(d\text{-}x) = n\lambda/2$ (n = 0,1,2...), a constructive interference occurs and the combined intensity is $4I_1$.

For $(d\text{-}x) = (n+1/2)\,\lambda/2$, a destructive interference occurs and $I = 0$.

Suppose that the location x of the reference mirror is such that the photodetector registers a maximum when the target is at location d. If the target now moves either away or towards the beam splitter, the photodetector will register a minimum and a maximum each time the target moves through a point that is $(n+1/2)\lambda/2$ and $n\lambda/2$, respectively away from the starting point. When both the mirrors are parallel and are at equal distance, the circular fringes are formed. If the reference mirror is inclined at a particular angle then shape of the fringes becomes linear. These spatial fringes are converted into temporal form using photodetectors. As the target mirror is moved, the fringe is shifted at the detector.

Calculation for displacement using interferometer is represented as:

$$D = N \times \frac{\lambda}{2} \qquad (2.27)$$

Where, N is no. of fringes, λ is the wavelength of light used; D is the displacement of target.

As open-air setup requires much more space, and alignment of components takes much more time, researchers have moved towards the fiber optic interferometers. The advantages of fiber optic sensors include insensitivity to electrical and magnetic noise (due to optical coupling), safe operation in explosive, high-temperature; hazardous environments and high sensitivity. With inherent electrical isolation and immunity to electromagnetic interference, fiber-optic sensors (FOS) offer position measurements in highly localized parts of machinery. In these sensors, mechanical loading and wear problems do not exist because fiber optic position sensors have stationary sensor heads hence enabling position monitoring using compact and portable packages [49-50]. Various kinds of Interferometers used in fiber-optic sensing configuration are Mach-Zehnder, Michelson, Sagnac, and Fabry-Perot (FP) Interferometers [15]. In the Mach-Zehnder, Michelson and Sagnac Interferometers, light is divided into two arms, one reference and another measuring arm. Light from the measuring arm is back reflected from the vibrating object and then interferes with signal from the reference arm. This gives a modulated wave with interference fringes.

In a fiber based Fabry-Perot Interferometer, both sensing and reference signal travel in the same fiber. This reduces the number of optical components as well as the cost unlike other fiber optic interferometers. Other advantages of Fiber based Fabry Perot Interferometer includes better sensitivity, frequency bandwidth and precision. Interference in Fabry-Perot Interferometer can be modeled as multiple beam interference model or two beam interference model.

2.3.1 Multiple Beam Interference Model

In Fabry-Perot Interferometer, a cavity is formed between the fiber tip and an external reflector resulting in a transmitted and a reflected interference pattern [51]. This is shown in Figure 2.8.

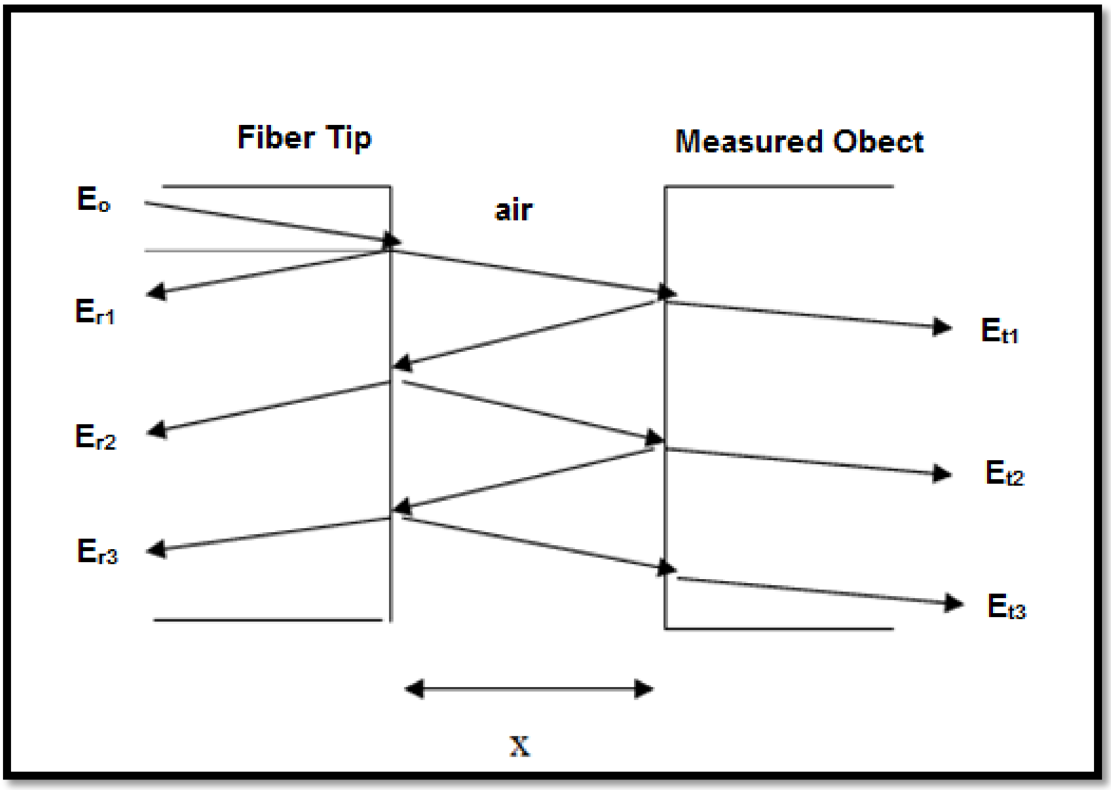

Figure 2.8: Multiple reflections in Fabry-Perot cavity

If light is incident at the fiber tip with an intensity of I_o and an angle of α with the normal plane of the reflecting surface of fiber tip, then a phase difference is introduced due to path difference between the reflected light from the fiber tip and reflecting surface. The optical phase difference introduced due to this one round trip in the air cavity in-between is given by φ.

$$\varphi = \frac{4\pi n x \cos\alpha}{\lambda} \tag{2.28}$$

Where λ is the wavelength of Laser, n is the refractive index of the cavity and x is the gap between the two surfaces.

For air, n=1 and for perpendicular incidence α=0.Therefore the Eq. (2.28) reduces to

$$\varphi = \frac{4\pi x}{\lambda} \tag{2.29}$$

Figure 2.9 shows the reflection of the light diverging from the fiber tip from the reflecting mirror surface of the etalon. The intensity of the light coupled back to the fiber tip is a function of the gap in the etalon which is derived below.

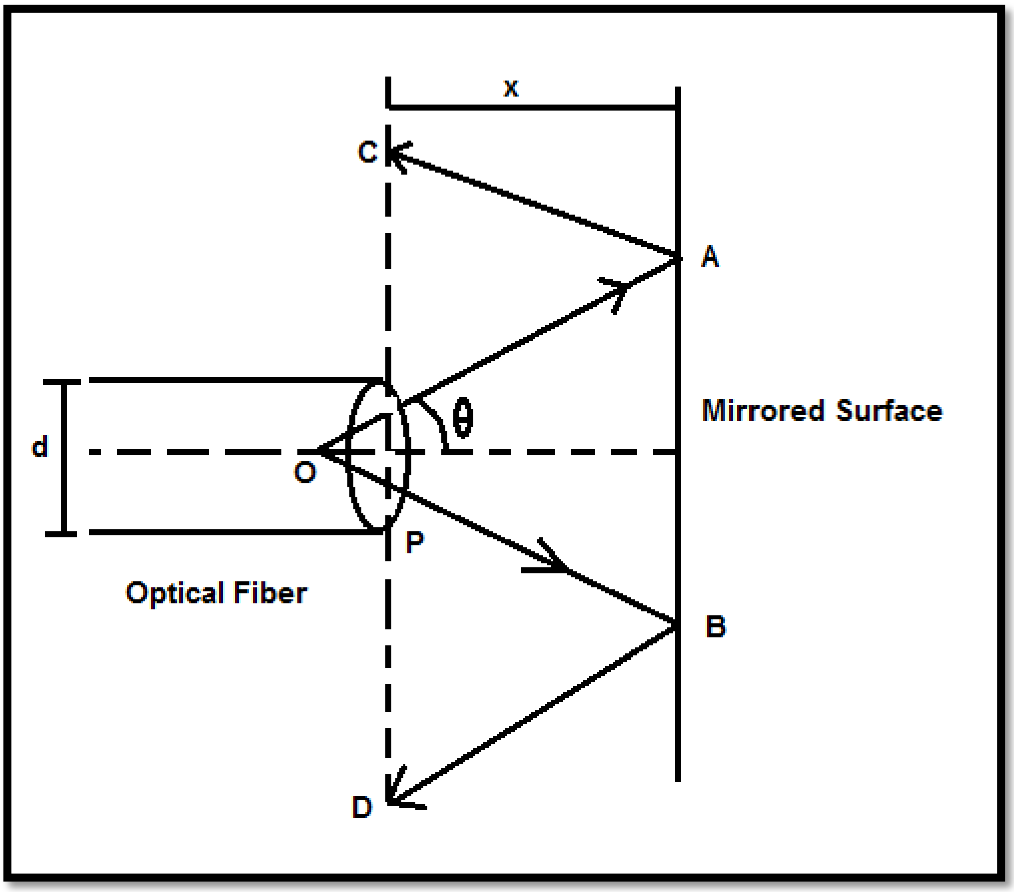

Figure 2.9: Equivalent Reflectivity of mirrored target

Let the intensity at fiber tip P be I_o. (Refer Figure 2.9) If NA is the numerical aperture of the fiber then assuming light diverges from O we have,

$$OP = \frac{\left(\frac{d}{2}\right)}{\tan\left(\sin^{-1} NA\right)} \tag{2.30}$$

Where, d is the fiber core diameter.

The distance travelled by the beam before re-entering the fiber tip is given by the equation:

$$OX + 2x = \frac{\left(\frac{\mathrm{d}}{2}\right)}{\tan\left(\sin^{-1} NA\right)} + 2x \tag{2.31}$$

Where x is the etalon gap.

If I_r is the Intensity of light after one reflection at the fiber tip, then by Inverse square law,

$$\frac{I_o}{(OX + 2x)^2} = \frac{I_r}{OX^2} \tag{2.32}$$

If the reflectivity of the mirror is R, the intensity I_r can be thus written as

$$I_r = \left\{\frac{\left(\frac{\mathrm{d}}{2}\right)}{\left(\frac{\mathrm{d}}{2}\right) + 2xtan[\sin^{-1}(NA)]}\right\}^2 .R.I_0 \tag{2.33}$$

The above equation can be written as

$$I_r = R_2 I_o$$

Where R_2 is the equivalent reflectivity of the mirror and can be written as

$$R_2 = \left\{\frac{\left(\frac{\mathrm{d}}{2}\right)}{\left(\frac{\mathrm{d}}{2}\right) + 2xtan[\sin^{-1}(NA)]}\right\}^2 .R \tag{2.34}$$

Therefore, only a part of the transmitted light re-enters the fiber after reflection. R_2 is the equivalent reflectivity of the 2^{nd} Interface and is a function of distance between fiber tip and the reflecting surface. Power reflectivity R_1 at fiber tip is 4% for the interface between air and glass (Fresnel Reflection).

Therefore, for power reflectivity R_1 and R_2 for fiber tip and reflective surface respectively, the normalized power reflection ratio is given by

$$\frac{I_r}{I_o} = \frac{R_1 + R_2 - 2\sqrt{R_1 R_2}\cos\varphi}{1 + R_1 R_2 - 2\sqrt{R_1 R_2}\cos\varphi} \tag{2.35}$$

2.3.2 Two Beam Interference Model

If the area of one of the parallel reflecting surface is very small, one can assume the interference occurring is two-beam interference. The beams interfering would be Fresnel reflected beam and the reflected beam from the target-reflecting surface, if the optical phase difference due to this one round trip in the air cavity in-between is given by φ. The resulting intensity is as per two beam interference would be

$$I_r = I_1 + I_2 + 2\sqrt{I_1 I_2}\cos\varphi \tag{2.36}$$

Where, $I_1$is the intensity of back reflected beam from the fiber tip,I_2 is the intensity of the light reflected from the target surface and φ is the phase difference between the two reflected beams.

The standard resolution of interferometer system is $\frac{\lambda}{2}$. This resolution of system depends upon the wavelength of light used for the measurement. For 633 nm wavelength, the position resolution achieved is 316.5 nm. The resolution of the interferometers can be improved by the signal processing techniques; Pullteap et al [52] have claimed the resolution of $\frac{\lambda}{8}$. The coherence length of the utilized laser light principally limits the measuring range of interferometric measurements. The uncertainty of measurement in interferometers is determined by wavelength stability of the laser, mechanical and thermal stability of the complete mechanical structure, resolution of the electronics, which evaluates the detector signals and by knowledge, constancy of the refractive index of the ambient air and temperature.

2.4 CONFOCAL SENSORS

Another type of optical sensor, generally applicable for accurate measurements of position change in distances of millimeters, is the confocal sensors. In these sensors, the light source is focused by the objective lens on the target and the back reflected light is collected by the very same lens and is deflected by a beam splitter towards a detector. The aperture present in front of detector defines the detector area. Aperture area is set in a way that when the target is exactly in-focus, all of the back scattered light from the target reaches the detector. As the target position changes, de-focusing of the image spot takes place leading to the distribution of light energy in a large area around the detector that corresponds to a small detector signal as shown in Figure 2.10. Thus, one can measure the position change using this configuration.

Confocal sensors can further be classified as monochromatic confocal sensors [53, 54] and polychromatic confocal sensors [55-57]. Monochromatic confocal sensor generally used in closed loop, employing a feedback mechanism to ensure that the sensor is positioned to receive the maximum signal from the target. As the position of target changes, the defocusing of the spot takes place at the target and correspondingly intensity changes at the detector [59-61]. Common applications for such a sensor are minute position change measurements by feedback mechanism.

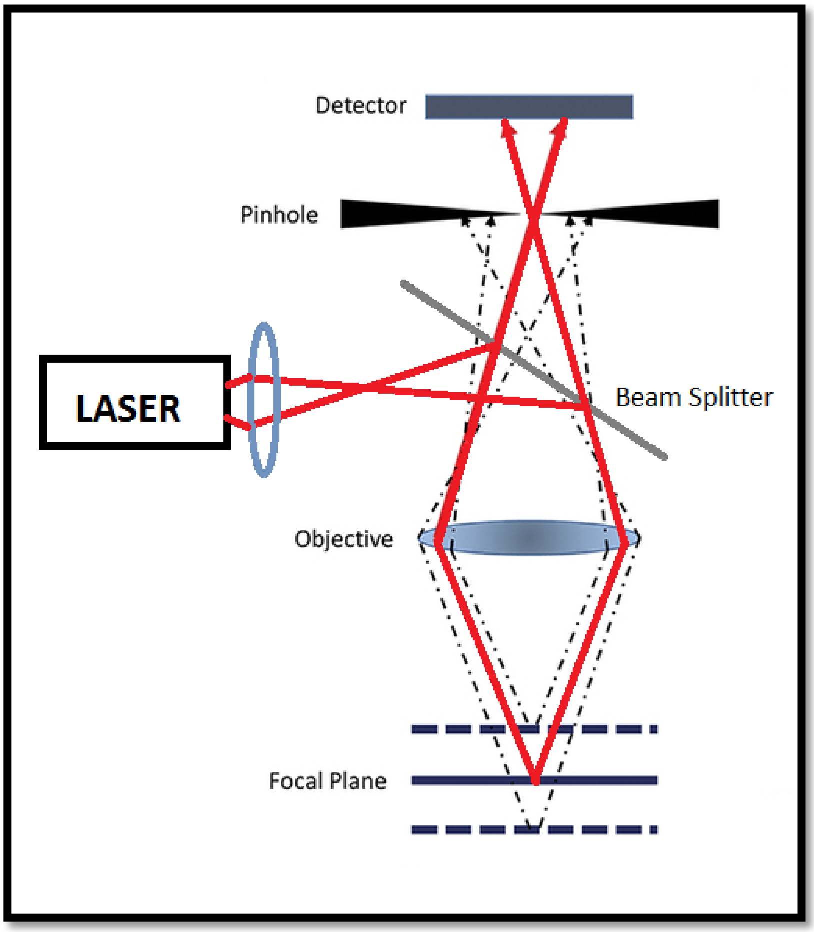

Figure 2.10: Schematic of confocal based measurement technique.

In another configuration as shown in Figure 2.11, a Y optical fiber coupler is used for transmitting the light from one arm, a lens focuses the light emerging from the tip of an optical fiber to the target, the same lens collects light back reflected or scattered from the object back into the fiber. The other end of a Y coupler collects the light and is connected to the detector that is camera. This process is most efficient when the target is located precisely at the image plane. As the target, gets displaced the intensity of light captured by the camera decreases in either direction, from the image plane. The resolution of these sensors depends on the core diameter of fiber, NA of fiber, diameter of lens used and the optical magnification.

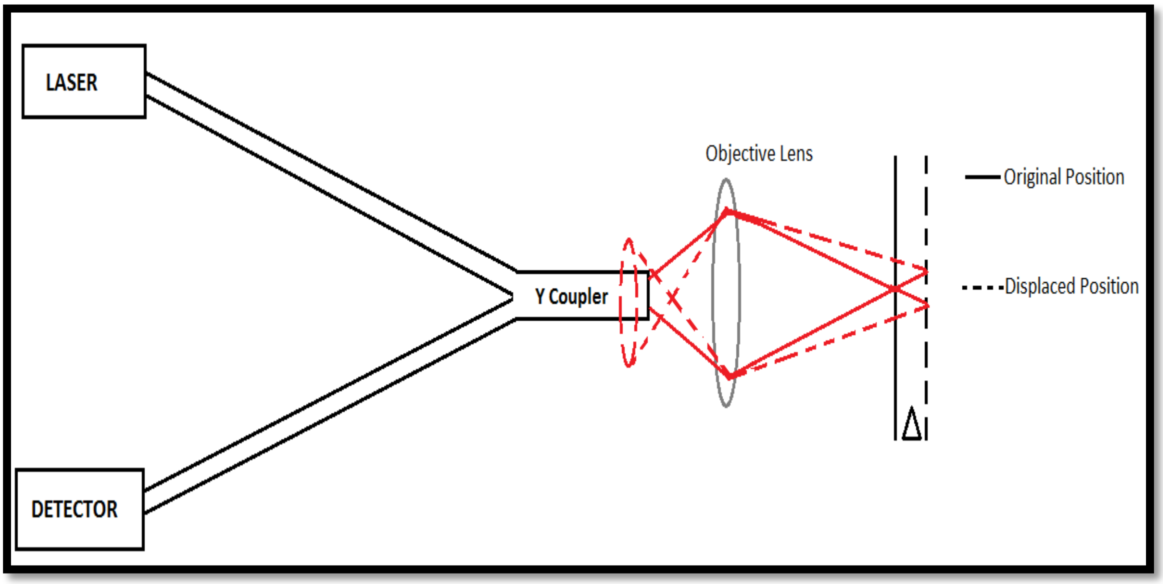

Figure 2.11:Schematic of fiber optics based confocal position sensor

In polychromatic confocal sensor, broadband source or multiple wavelength [58, 60] is used and the chromatic dispersion of lens leads to the different wavelength components is being imaged at different longitudinal points along the optical axis. Thus in the region of the image plane, each point along the optical axis is the image point of a specific wavelength. This wavelength will be the dominant wavelength in the light backscattered confocally to the detector by an object at this point. Consequently, spectral measurement of the backscattered light can be translated very accurately to object position. However, this configuration requires costly components then the monochromatic confocal sensors.

2.5 LASER TRIANGULATION SENSORS

Triangulation refers to a distance or position measurement technique from considerations based on the geometries of similar triangles. For determining, the position via triangulation, the source and detector angles as well as the distance between them is used. In general, a source is used to illuminate the target whose position is to be measured. The back-scattered or reflected light from the target is captured by the lens and is imaged to the detector. As the target changes its position, there is the change in position of image spot at the detector. Thus, one can measure the change in the position of the target. As these sensors are based on the geometry, therefore there is limit on the minimum and maximum distance one can measure. Since the laser spot is imaged on the linear detector array, the nearest and farthest detector pixel locations, combined with the optical magnification, impose these limits.

Ji et al [62] have described the design analysis of optical triangulation sensors based on Scheimpflug principle. Zhuang et al [63] has given the laser triangulation measurement principle using the two detectors for the measurement range of ± 2 mm. Song et al[64] described the design and analysis of laser triangulation sensors using PSDs, they compared PSD's with CCD devices and claimed that PSD's have high sensitivity, high response and has continuous sensing surface. Park et al [65] has developed an optical system that can measure the target displacement and vibration using the oblique ray method, by employing a single convex lens. Jung et al [66] studied on intensity control of triangulation based PSD sensor independent of object color variation. Dong et al [67] presented a study on the non-linearity of laser triangulation probes. The structure parameters of the probe, which influence the variables on non-linearity, were studied by response surface methodology, and the significant factors were identified. The laser triangulation technique gives the abundant information such as position, distance, vibration, thickness, shape [68], surface profile [69] etc. Most of the studies [70-76] on laser triangulation are done to improve the performance for small range of operation and small standoff distances.

In general, laser triangulation sensor can be specular-reflection based or diffused reflection based. This is dependent on the type of the surface under consideration for measurement. The following section will give the detail mathematical model for the both the configurations.

2.5.1 Specular-Reflection based Laser Triangulation Sensor

In this technique, when the laser light is made to fall on a target at an angle, due to the target roughness, along with specular-reflected light that follows the Snell's law and some of the diffused light is scattered in all directions as shown in Figure 2.12. The intensity of light reflected or scattered depends upon the type of surface i.e. the material of the target, roughness of the target, gloss of the target etc. If the surface is highly reflective then, most of light gets specularly reflected and very low light is scattered across the other directions.

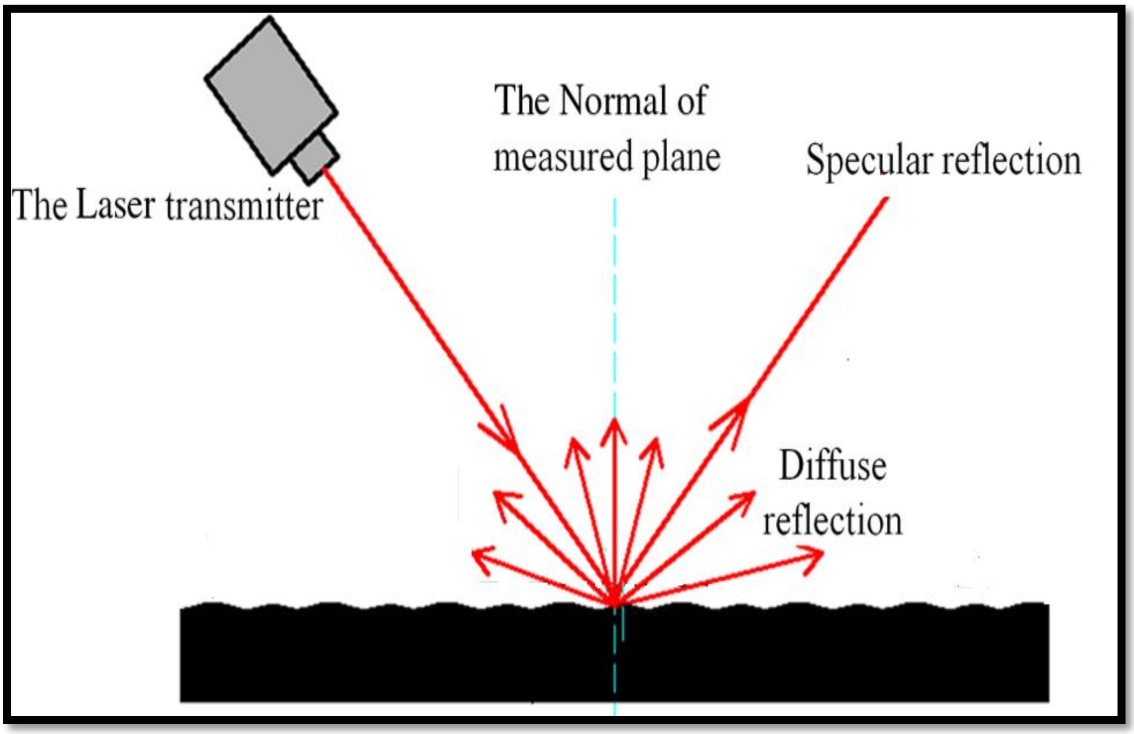

Figure 2.12: Schematic of diffuse and specular reflection from the target surface

Consider that laser is focused on the target surface at an angle θ. The lens collects the specular-reflected light and is focused to the detector. As the position of target changes normally, the reflected light is collected by the lens changes its position at detector. The schematic of the measurement system is as shown inFigure 2.13.

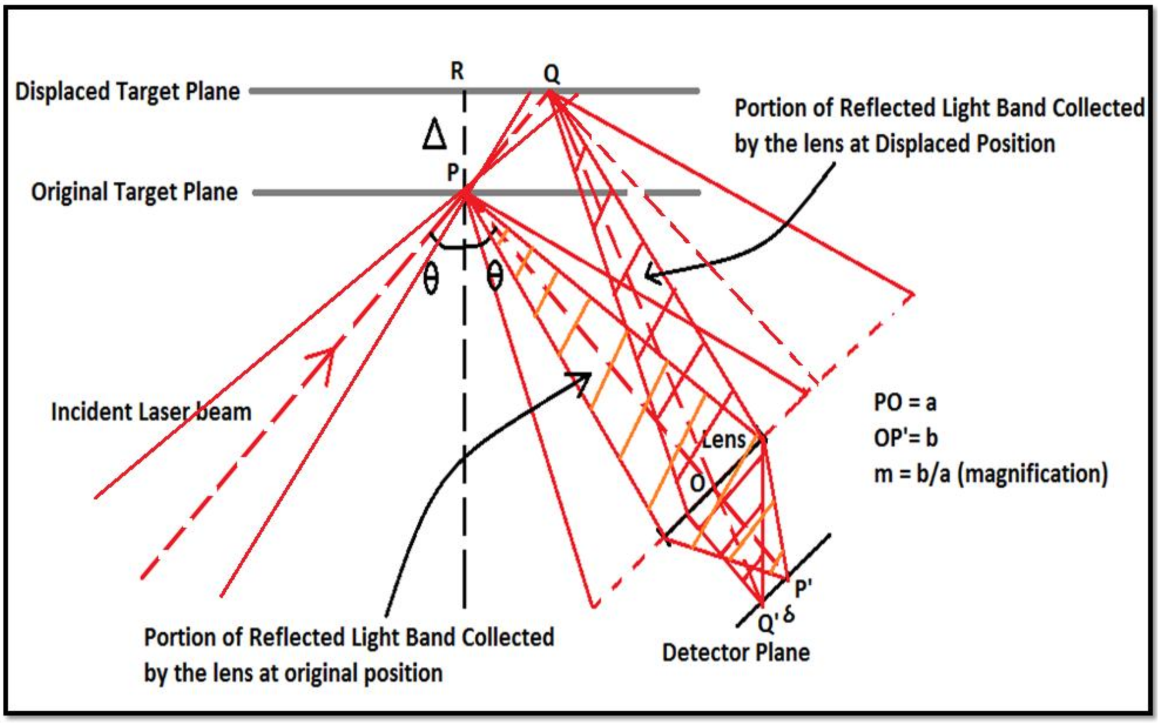

Figure 2.13: Schematic of specular-reflection based position measurement

As shown in Figure 2.13, let the converging laser beam is incident at the target surface at point P. As the target moves vertically from P to R, the laser beam hits the object at point Q. Applying trigonometric relationship and concept of similar triangle; one can obtain an expression for transforming the position change of the image spot into displacements of the target. Figure 2.13, Δ is the target position change and $\boldsymbol{\delta}$ is the image position change.

Consider triangle PQR,

$$\tan\theta = \frac{QR}{PR} = \frac{QR}{\Delta} \tag{2.37}$$

$$\cos\theta = \frac{PR}{PQ} = \frac{\Delta}{PQ} \tag{2.38}$$

As triangle POQ and triangle P′OQ′ are similar. Therefore,

$$\frac{PQ}{PO} = \frac{P'Q'}{O'P'} \tag{2.39}$$

Thus,

$$\delta = \frac{\Delta}{\cos\theta} \times \frac{b}{a} \tag{2.40}$$

As, magnification of lens m = b/a, so,

$$\delta = \frac{\Delta}{\cos\theta} \times m \tag{2.41}$$

$$\Delta = \frac{\delta \times \cos\theta}{m} \tag{2.42}$$

Thus, from above equation, we can conclude that actual target displacement is directly proportional to the image displacement at the detector and is inversely proportional to the magnification of the lens of the system.

2.5.2 Diffused-Reflection based Laser Triangulation Sensor

In this type of measurement technique, instead of collecting the reflected light from the target, a diffused light intensity is collected from the target and is focused to the detector. As these sensors works on the diffused light collection, hence extremely suitable for variety of industrial surfaces. Moreover there is less chances of the detector being saturated used during the measurement. Diffused-reflection based laser triangulation can further be divided into two categories:

(a) Direct Laser Triangulation

In direct laser triangulation, the focused laser is vertically incident on the target surface. The scattered light from the surface is captured by the focusing lens and then by the detector. In the Figure 2.14, d_o is the object distance, d_i is image distance, Δ is the displacement of the measured object surface from A to B, θ is the angle between the incident light axis and imaging optical axis, φ is the angle between photo detector sensitive surfaces and imaging lens optical axis (Scheimpflug condition), δ is image displacement.

Since triangle *BCO* is similar to triangle *B′C′O*,

$$\frac{\Delta \sin\theta}{d_o - \Delta\cos\theta} = \frac{\delta\sin\varphi}{d_i + \delta\cos\varphi} \tag{2.43}$$

$$\Delta\sin\theta\,(d_i + \delta\cos\varphi) = \delta\sin\varphi\,(d_o - \Delta\cos\theta) \tag{2.44}$$

$$\Delta(d_i\sin\theta + \delta\sin\theta\cos\varphi + \delta\sin\varphi\cos\theta) = d_o\delta\sin\varphi \tag{2.45}$$

$$\Delta = \frac{d_o\delta\sin\varphi}{d_i\sin\theta + \delta\sin(\theta+\varphi)} \tag{2.46}$$

When the detector is kept parallel to the lens i.e. φ = 90°, the displacement at the detector is represented as,

$$\varDelta = \frac{d_o \delta}{d_i \sin\theta + \delta\cos\theta} \tag{2.52}$$

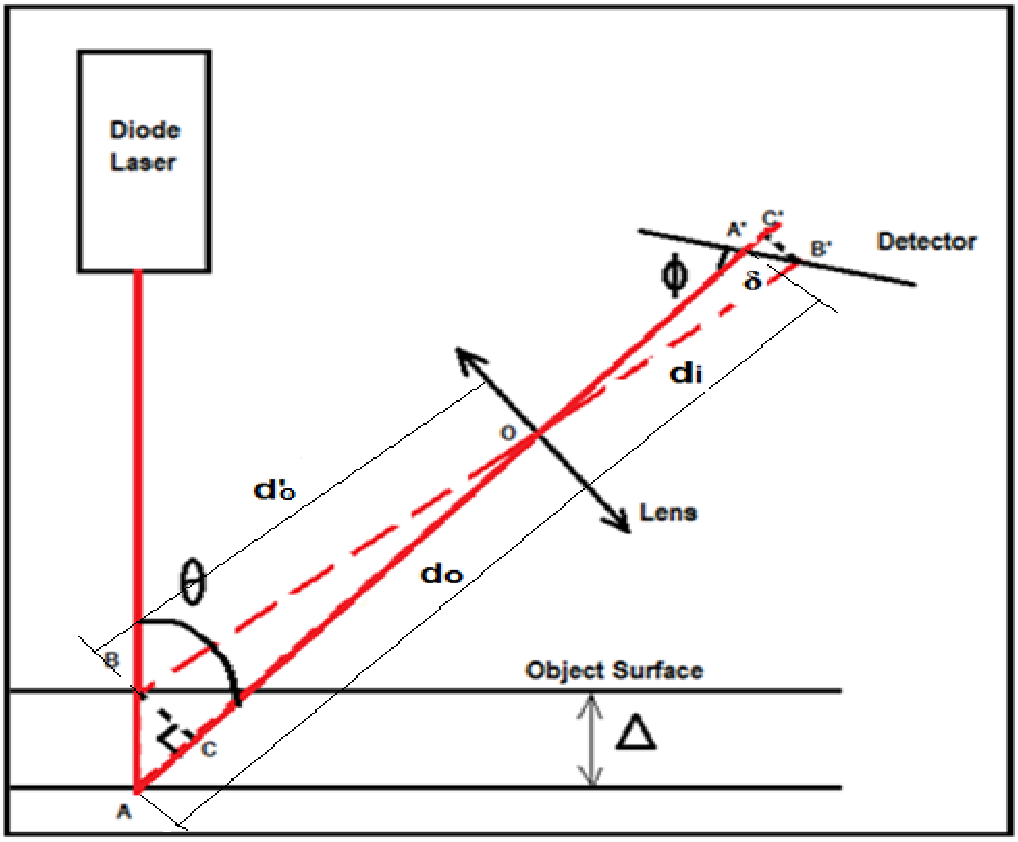

Figure 2.14: Direct Configuration based Laser Triangulation

Therefore, the actual target displacement $\varDelta$ can be measured by the displacement of laser image spot δ at the detector.

(b) Oblique Laser Triangulation

In oblique laser triangulation, the focused laser is incident on the target surface at an angle. The scattered light from the surface is captured by the focusing lens and then to detector. In the Figure 2.15, d_o is the object distance, d_i is image distance, $\varDelta$ is the displacement of the measured object surface A to C, θ is the angle between the incident light axis and imaging optical axis, φ is the angle between photo detector sensitive surfaces and imaging lens optical axis (Scheimpflug condition), δ is image displacement.

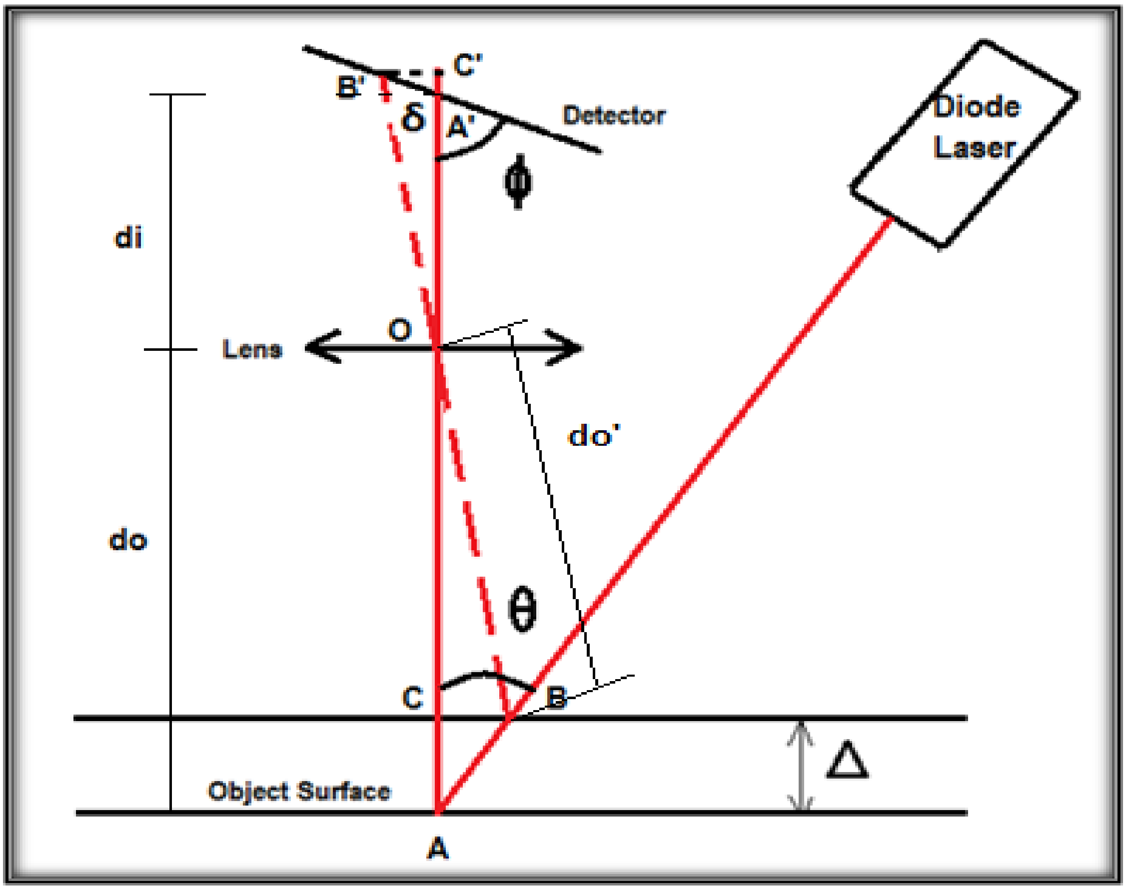

Figure 2.15: Oblique Configuration based Laser Triangulation

Triangle BCO is similar to triangle $B'C'O$

$$\frac{\Delta \tan\theta}{d_o - \Delta} = \frac{\delta \sin\varphi}{d_i + \delta\cos\varphi} \tag{2.47}$$

$$\Delta = \frac{d_o \delta \sin\varphi}{d_i \tan\theta + \delta\cos\varphi\tan\theta + \delta\sin\varphi} \tag{2.48}$$

When the detector is kept parallel to the lens i.e φ = 90°, the displacement at the detector is represented as,

$$\Delta = \frac{d_o \delta}{d_i \tan\theta + \delta} \tag{2.49}$$

Therefore, the actual target displacement Δ can be measured by the displacement of laser image spot δ at the detector.

Again in Figure 2.15,

$$\tan\theta = \frac{BC}{AC} \tag{2.50}$$

$$BC = \Delta \tan\theta \tag{2.51}$$

BC is the shift in point of striking of laser on the target when the target has moved from its reference position to the new displaced position. This acts as a disadvantage in the configuration, as the surface contact point with the laser changes.

So, in this configuration, minimum target width is required for the measurement of target displacement.

(c) Comparison of the sensitivity of Direct and Oblique Triangulation Technique

The displacement at detector δ_{direct} for direct triangulation technique is given as,

$$\delta_{direct} = \frac{\Delta d_i \sin\theta}{d_o - \Delta \cos\theta} \tag{2.52}$$

Similarly, the displacement at detector $\delta_{oblique}$ for oblique triangulation is given as,

$$\delta_{oblique} = \frac{\Delta d_i \tan\theta}{d_o - \Delta} \tag{2.53}$$

So, simulation was done in order to study the sensitiveness of the both the techniques. The angle θ is varied from 5° to 45° and other parameters were taken as, focal length of lens d_i= 25 mm, d_o = 100 mm and $\Delta = 5\ mm$. Plots of displacement of image at the detector for direct and oblique triangulation techniques are shown in Figure 2.16.

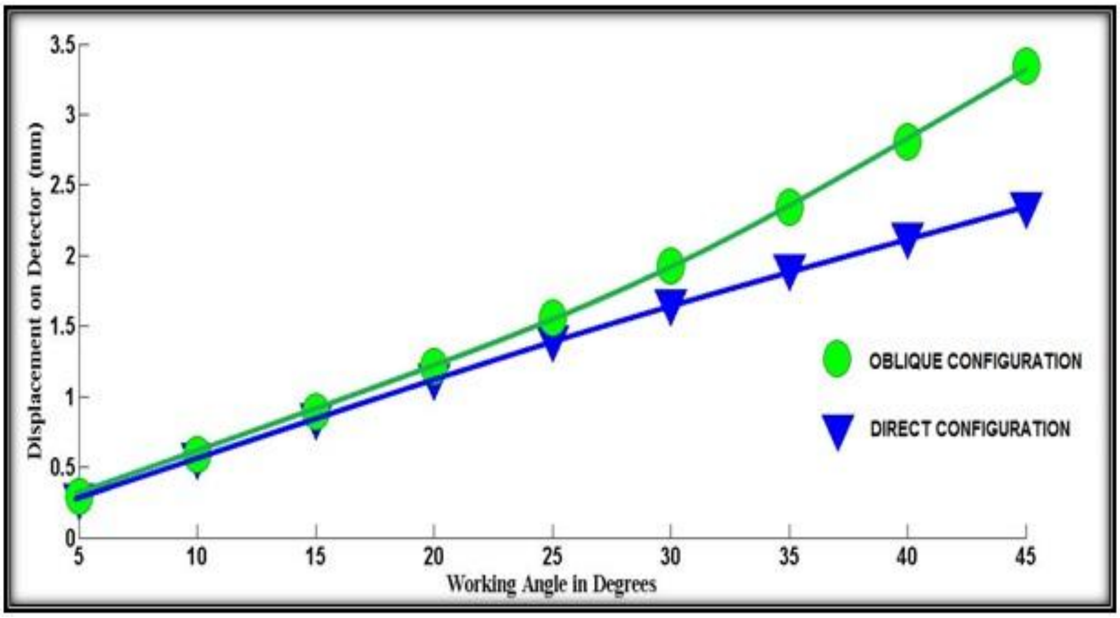

Figure 2.16: Displacement on Detector (mm) vs. working angle in (degrees)

It is found that the image displacement in oblique case is more sensitive i.e. $\delta_{oblique} > \delta_{direct}$ for the same displacement Δ of the target plane. Thus, higher resolution can be achieved in oblique triangulation as compared to the direct technique.

Based on the requirement of the range and resolution one can select the type of configuration for measurement.

Summary

This chapter gives the literature survey of different optical sensors used for position measurement and alignment. The sensor includes intensity based fiber optic sensors, time of flight sensors, interferometers, confocal sensors and laser triangulation sensors.Intensity based fiber optic sensors are generally used for measurement of axial displacement and vibration sensors. This is because, these sensors have small range of measurement in mm and resolution is in tens of microns. Time of flight sensors are generally used for long distance measurement applications such as in satellite positioning, missile tracking because they have measurement ranges in meters (1-1000 m) and generally have the resolution in cm. Laser interferometric techniques are extremely precise and accurate for position measurements in nanometer range as it depends upon the wavelength of laser used. However, its range is limited due to coherence length of laser. So, it is generally used in diaphragm type pressure sensors, wobbling of machines, vibrometers, nanotechnology etc. Monochromatic confocal sensors offer micrometer distance resolution over a range of several millimeters. The working range typically may be from 1 mm up to several tens of millimeters which depends on the focal length of the optics. Owing to the requirement of tight focusing, longer working distances become impractical. So, these are used for short range measurements such as precise positioning of tools in CNC machines, height measurement of fuel rods in nuclear reactors, surface roughness measurement and small contours of mechanical parts. Laser triangulation sensors have sensitivity of ~0.1 mm with operating range varying from 1 mm to 100 mm. So, these are generally used in applications such as robotics, rail road alignment system, rotating shaft alignment, online thickness measurement and fuel channel alignment in nuclear reactors.

CHAPTER 3: OPTICAL FIBER BASED AXIAL POSITION MEASUREMENT SENSOR

After discussing different techniques for position measurement in Chapter 2, in this chapter, intensity based axial position measurement sensor using a single optical fiber is designed, developed and demonstrated. In these kinds of sensors**,** standoff distances and measurement ranges are in general larger than those used in profilometry applications. The sensor comprises of a Y optical fiber coupler and lens which together acts as a single probe for simultaneously transmitting and receiving signal from target to determine the change in its position. The lens collects the light reflected and scattered from the target surface and sends it back into the fiber and then to the detector. At the focus point of the light spot at the target, the maximum intensity is achieved at the detector and the intensity decreases on the either side of standoff target position. Thus, the variation in intensity profile is identified as the position change measurement. This variation in intensity is symmetric about the standoff or mean position of the target. The slope of the linear curve on the either side of the intensity profile represents the direction of change in position of target. The position resolution of 100 μm (with standard deviation~20 μm) was achieved using the sensing configuration given in this chapter. The sensor was calibrated using the micrometer having resolution of 10 μm. The standard target surfaces of different known roughness values were studied and effect of surface roughness at the output is investigated.

3.1 PRINCIPLE OF OPERATION

A lens focuses the light emerging from optical fiber tip of a Y optical fiber coupler to the target surface which acts as a single probe as shown in Figure 3.1. The same lens collects light reflected or back- scattered from the target back into the same fiber tip and then to the detector. When the target is located at the focused point of light, the back reflected light has the maximum intensity received by the fiber tip due to the focusing of back scattered light at fiber tip and is transmitted to the detector. The output at detector decreases when the position of the target varies from the focused position in either direction. The intensity of back reflected light to the fiber therefore acts as a function of the change in position of the target. The Numerical Aperture (NA) of fiber defines the light divergence. The placement of lens is done at a position where all the diverged light from the fiber is collected by the lens. The fiber is placed behind the focal point of lens so that the light is focused to the target.

From Figure 3.1, diverging light (geometric consideration) from the fiber tip is focused to the target using a lens. As the target is displaced to the new position away from the lens ($v+\Delta$), the light spot at the target increases in diameter ($2y$) due to the defocusing of the light spot. As the lens also captures the backscattered light from the target and it focuses before the fiber tip leading to increase in diameter of the image spot ($2y'$). Similar process happens when the target is moved towards the lens.

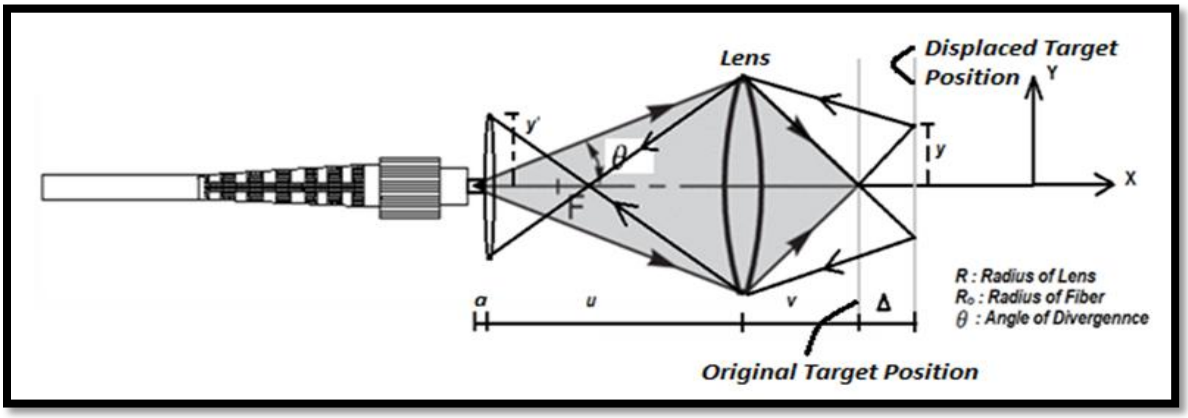

Figure 3.1: Schematic of probe for position measurement

The Numerical Aperture (NA) of the emission cone of fiber is given as

$$\mathrm{NA} = \sin\theta \tag{3.1}$$

Let R_f be the radius of the optical fiber. So from the Figure 3.1,

$$\tan\theta = \tan\left(\sin^{-1}(NA)\right) = \frac{R_f}{a} \tag{3.2}$$

Let R_l be the radius of the lens, the light received by the lens from the optical fiber is given by

$$\tan\theta = \tan\left(\sin^{-1}(NA)\right) = \frac{R_l}{u + a} \tag{3.3}$$

For the given focal length of the lens f, applying the lens formula,

$$\frac{1}{f} = \frac{1}{u} + \frac{1}{v} \tag{3.4}$$

From the Figure 3.1,

$$\frac{R_l}{v} = \frac{y}{\Delta} \tag{3.5}$$

$$y = \frac{R_l \times \Delta}{v} \tag{3.6}$$

Where, y is the height of image spot at the target from the optical axis of lens.

As the fiber tip is at a fixed distance from the lens u and as the position of target is varying as $v \pm \Delta$, therefore,

$$\frac{y}{v \pm \Delta} = \frac{y^{'}}{u} \tag{3.7}$$

$$y = \frac{y^{'} \times (v \pm \Delta)}{u} \tag{3.8}$$

Now equating Eq.(3.6) and Eq. (3.8) we get y',

$$y^{'} = \frac{R_l \times \Delta \times u}{v \times (v \pm \Delta)} \tag{3.9}$$

Where, y' is the height of the backscattered light captured by the fiber tip from the optical axis, $'+'$ is for positive position change and $'-'$ is for negative position change.

Area of fiber tip A_f capturing the backscattered light from the target is given as

$$A_f = \pi \times R_f^2 \tag{3.10}$$

Area of light cone A_l formed at the fiber tip after the target is displaced is given as

$$A_l = \pi \times (y^{'})^2 \tag{3.11}$$

$$A_l = \pi \times \left(\frac{R_l \times \Delta \times u}{v \times (v \pm \Delta)}\right)^2 \tag{3.12}$$

As, power P is proportional to the area considering the power is constant throughout the illumination received at the tip of fiber. Therefore, the ratio of area of fiber tip and area of light cone formed at the fiber tip gives the power variation for the position change given as

$$P = \frac{A_f}{A_l} \tag{3.13}$$

$$P = \frac{\pi \times R_f^2}{\pi \times \left(\frac{R_l \times \Delta \times u}{v \times (v \pm \Delta)}\right)^2} \tag{3.14}$$

$$P = \frac{R_f^2}{\left(\frac{R_l \times \Delta \times u}{v \times (v \pm \Delta)}\right)^2} \tag{3.15}$$

Thus, for the known parameters, R_f, R_l, u and v, one can find the relation between the power received at the detector P to the change in target position Δ.

The standoff distance of target is governed by Eq. (3.3) and Eq. (3.4), such that all the light transmitted by the fiber is collected by the lens and is focused to the target. As the target is displaced by Δ away from the lens, light starts diverging, due to the fixed focal length of the system, the diameter of light cone received at the fiber tip also starts increasing as shown in Figure 3.1. This leads to the decrease in the intensity captured by the fiber.

3.2 METHODOLOGY

The schematic for experimental setup is shown in Figure 3.2. The sensor setup consists of a light source, a Y optical fiber coupler, an aspheric lens and standard target surfaces of stainless steel of known roughness values. A Y optical fiber coupler having core diameter of 400 µm, cladding diameter 440 µm and NA 0.22 is used. The 400 µm fiber was selected, in order to see the variation in power clearly at the detector with respect to the change in position of the target. If the diameter of fiber core is large, then the sensitivity will be low as light being collected over a large area will lead to small variation in total light falling on detector in response to change in target position. On the other hand, if the fiber core diameter is very small, it will lead to poor signal to noise ratio at detector as less power is received at the fiber tip. So, the choice of choice of 400 µm fiber core was made so that good sensitivity can be at reasonable signal to noise ratio. An aspheric lens of F# 1 is used (focal length 25 mm, diameter 25 mm) for focusing the light to the target. Substituting the values of core radius, lens radius and NA in Eq. (3.2) and Eq. (3.3), we get the value of $u = 54.45$ mm. By lens equation [Eq. (3.4)], the value of $v = 46.36$ mm. The light source is He-Ne laser with wavelength of 633 nm and is continuous. So, although PORT 1 of optical fiber contains both incoming and outgoing light, the PORT 3 which is connected to detector contains only outgoing (or reflected) light. Thus, the outgoing light from the laser source is distinguished from the incoming light at the detector.

A THORLAB power-meter with Si photo-diode (S-120C) is used as the detection unit. This detector provides a high-speed detection with the optical response of 400-1100 nm, making it compatible with wide range of applications. The sensor of power meter has resolution of 1nW with uncertainty in measurement of ± 3% for the wavelength range of 440-980 nm. He-Ne laser light is coupled to the PORT 1 of the Y coupler. The output of light diverges from the PORT 2 due to the NA of fiber. The backscattered and reflected light from the target is confocally collected by the lens and is focused back to the PORT 2. The light collected by PORT 2 is transmitted to photodiode via PORT 3. Thus, the power is measured for the corresponding change in the target position through micrometer stage. The output power is determined by the power-meter.

The fiber tip, the lens and target were aligned with each other in a way that their centre axis lays on a same line. The target was displaced by mounting it on the micrometer translation stage, which is fixed on the vibration isolation table in order to reduce the effect of vibrations.

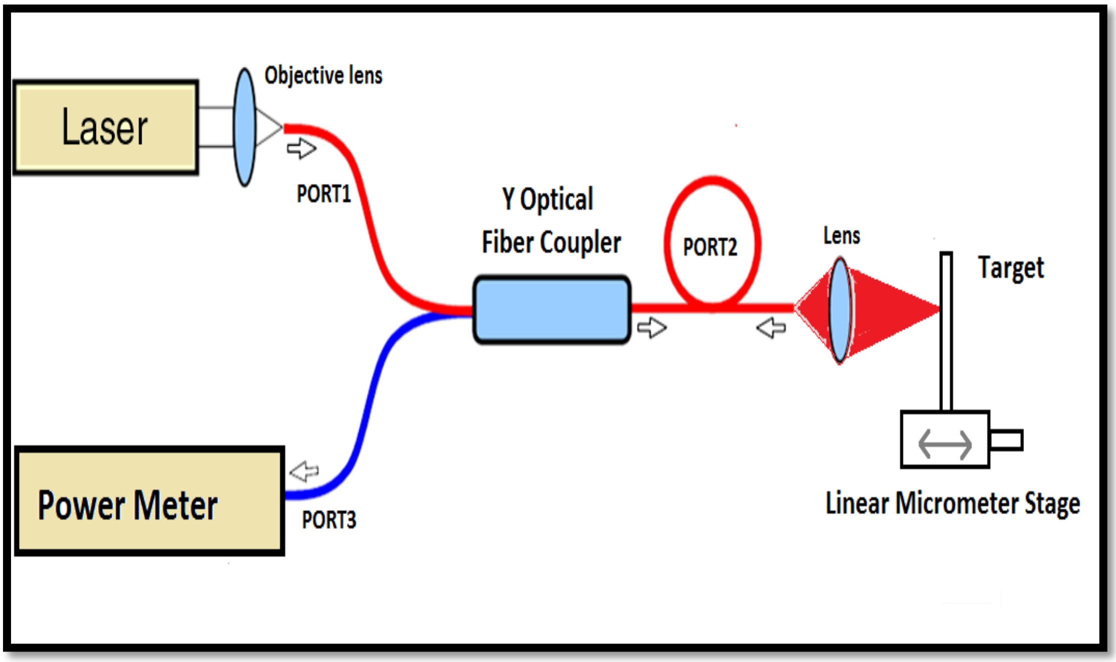

Figure 3.2: Schematic of experimental setup

The experiments were performed in both dark and ambient light conditions for the target surfaces having different roughness values (0.025 µm Ra, 0.05 µm Ra, 1.6 µm Ra and 3.2 µm Ra) and the effect of output power with respect to the surface roughness was studied.

3.3 RESULT AND DISCUSSION

The variation of the output power against position change of different target surfaces from the focus point is shown in Figure 3.3. Thus, the power variation is indicative of the axial position change of the target. This can be easily understood as the peak power was measured when the target was at the focus points and then decreases symmetrically on both the positive and negative side.

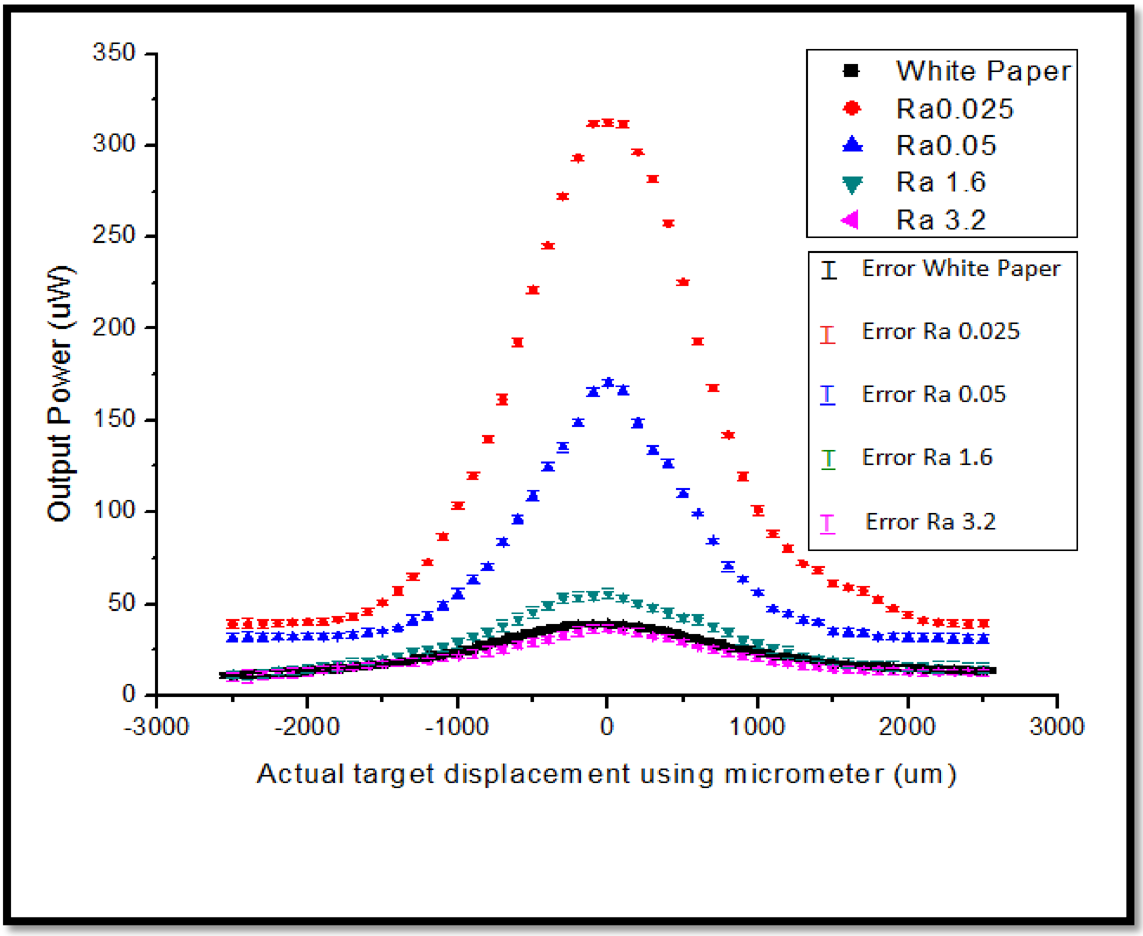

Figure 3.3: Output for the position change for target surfaces of different roughness with the error bars.

From the Figure 3.3 we can see that two linear slopes can be extracted from the sensor output, near linear slope (+ve) and far linear slope (-ve). Near linear slope corresponds to the target position change when it has moved towards the lens (i.e. negative direction) and far linear slope corresponds to the target position change when it has moved away (i.e. positive direction).

Again, from the Figure 3.3, one can see that when the target has low roughness values (for Ra 0.025 µm), the intensity received at the detector is high and as the roughness of target increases, the intensity received at the detector decreases.

This is because as the roughness of the surface starts decreasing, specular reflection of light from the surface increases. This leads to larger reflection in case of less rough surface. Thus, the sensor needs to be calibrated for different target surfaces for measurement. Different target roughness corresponds to the different linear ranges. Figure 3.4 gives the sensitivity plot for different target roughness samples. Sensitivity is found to be more for smooth surface of the target.

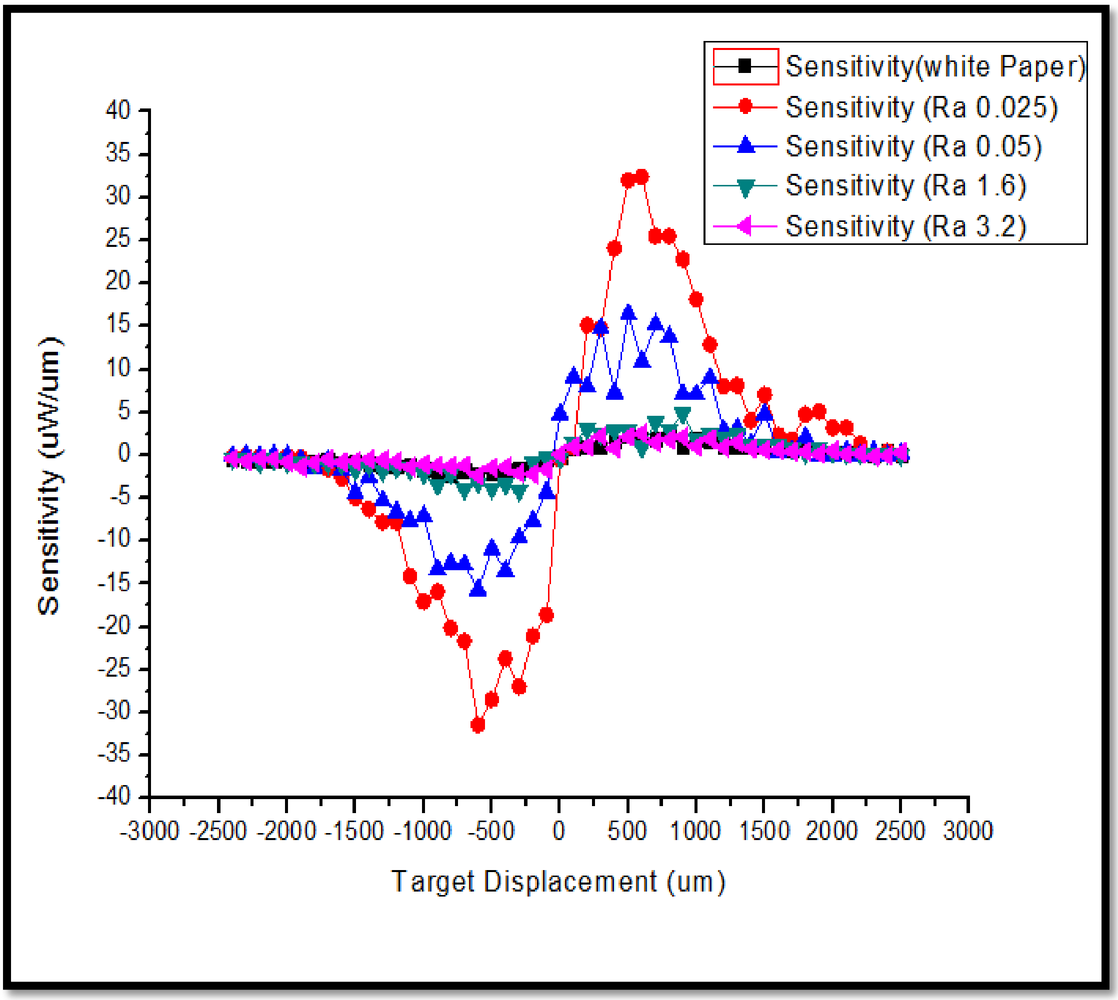

Figure 3.4: Sensitivity vs. Target Displacement plot.

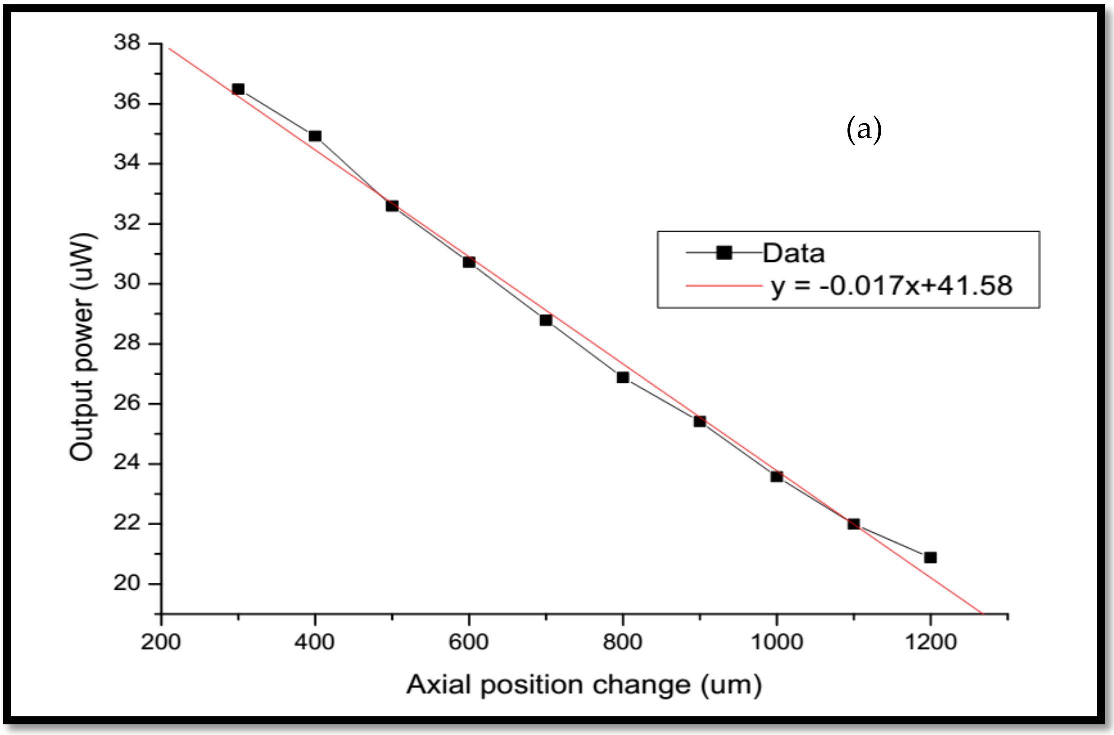

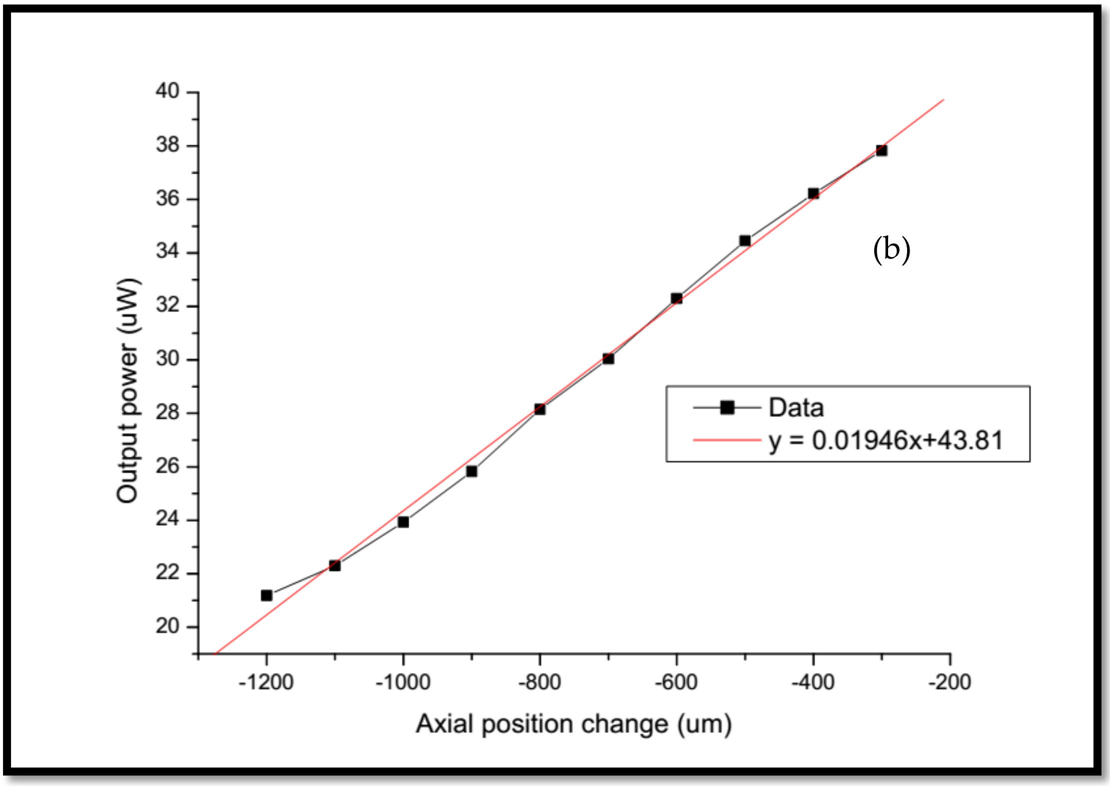

Figure 3.5: Output power vs. axial position change for white paper as target

(a) far linear region (b) near linear region

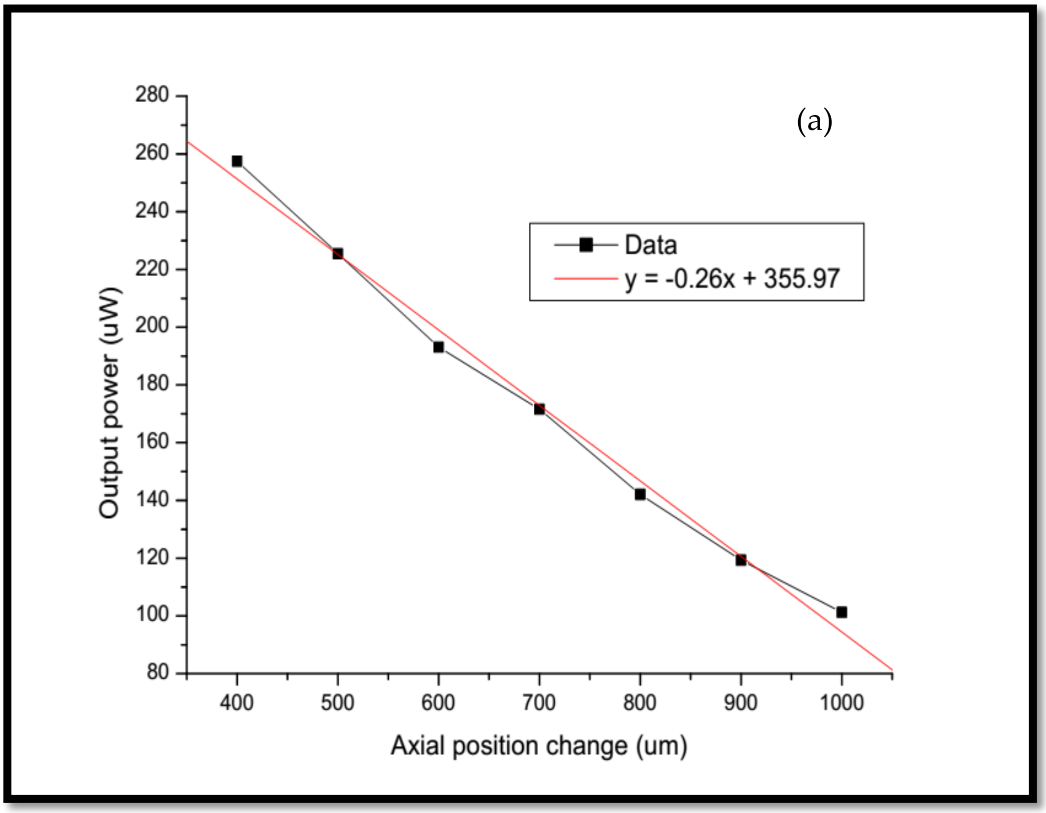

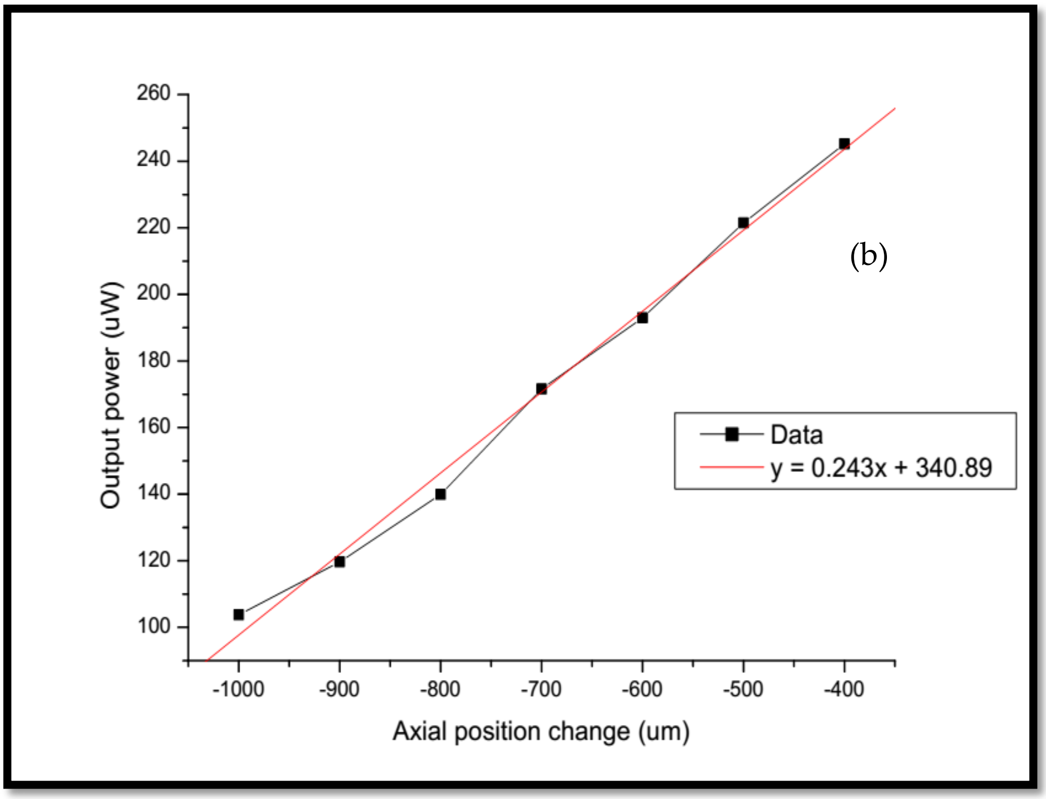

Figure 3.6: Output power vs. axial position change for target of roughness Ra 0.025

(a) far linear region (b) near linear region

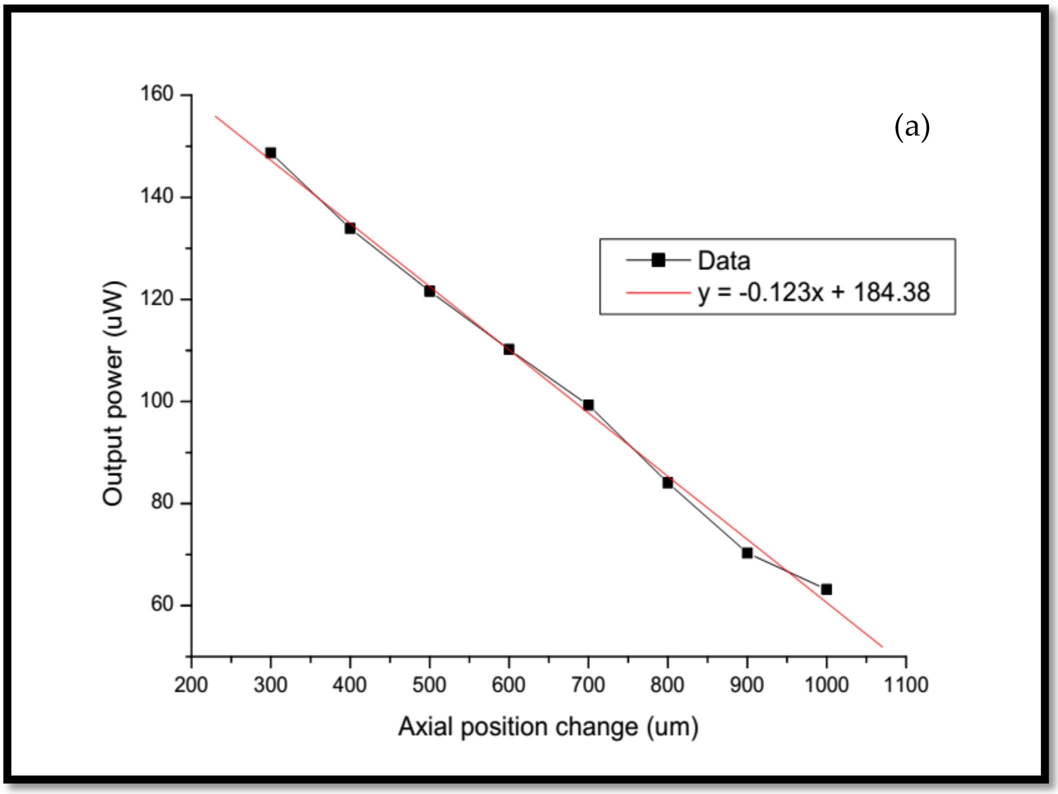

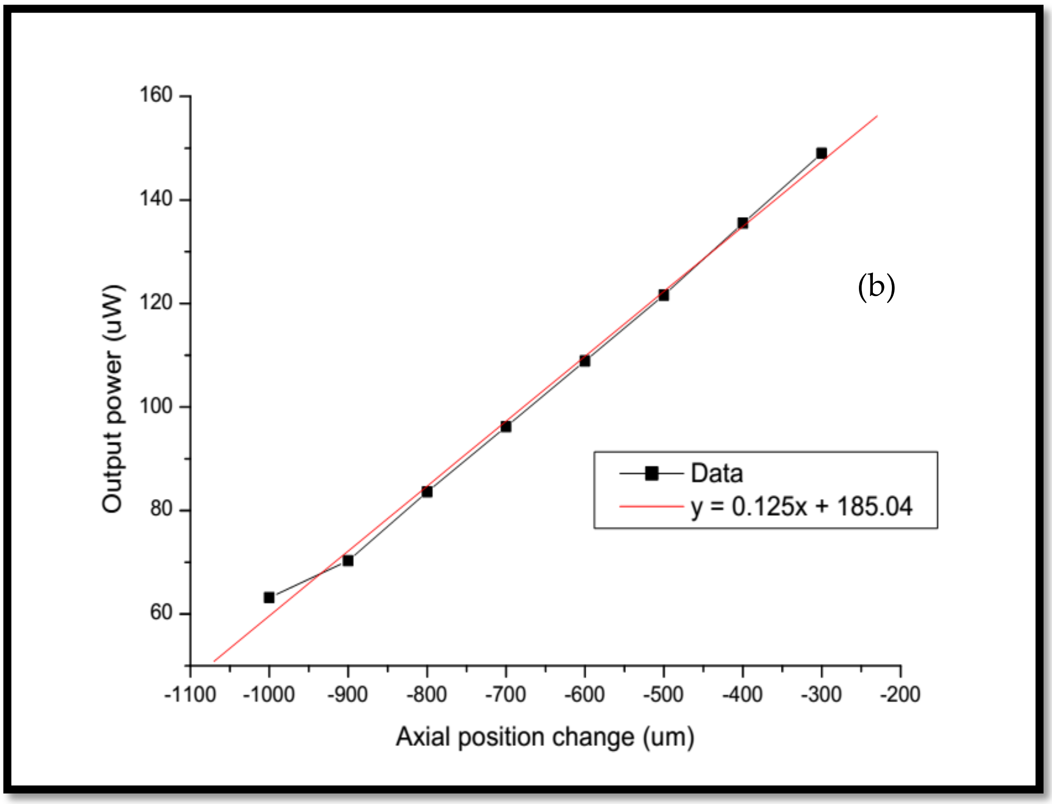

Figure 3.7: Output power vs. axial position change for target of roughness Ra 0.05

(a) far linear region (b) near linear region

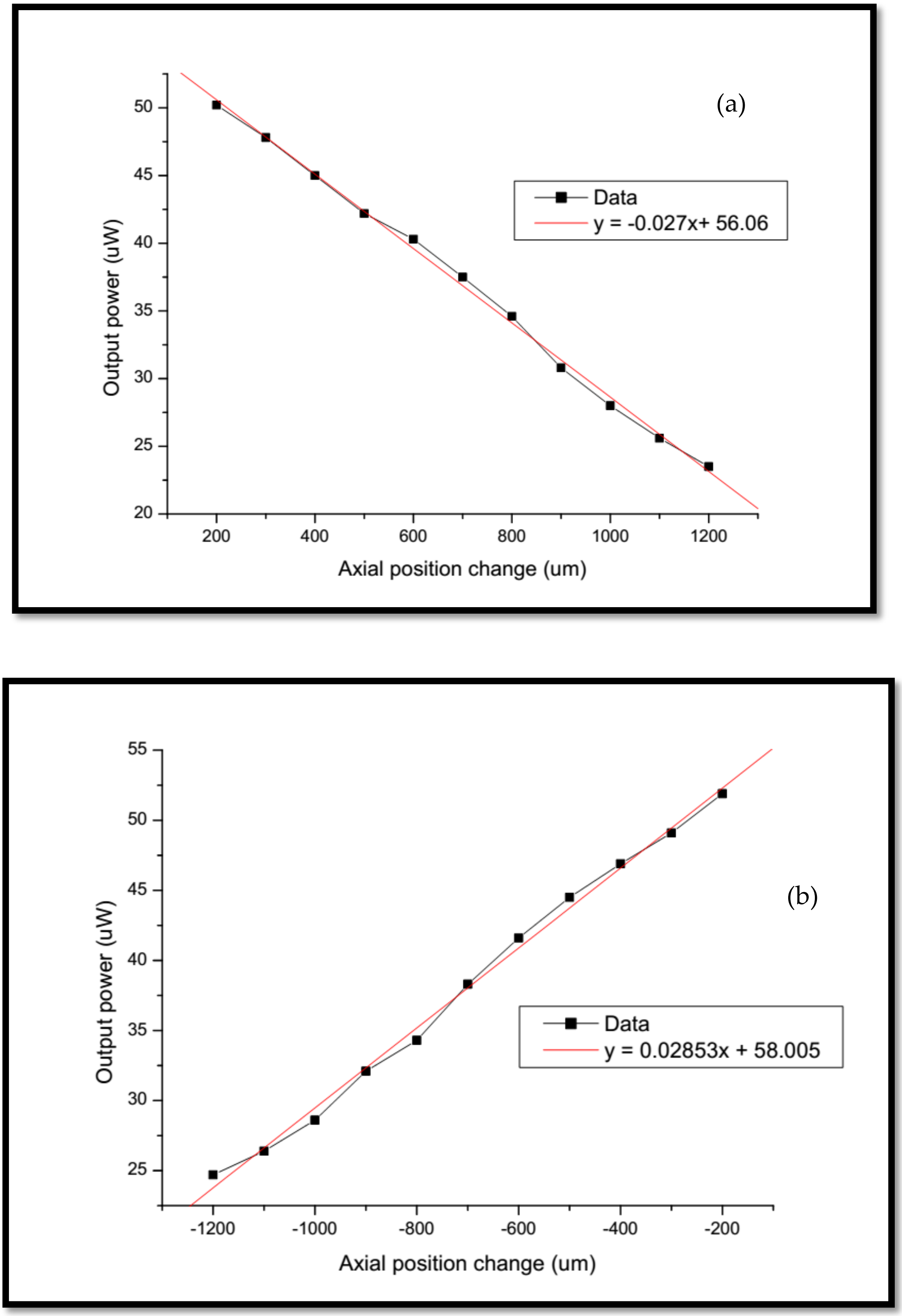

Figure 3.8: Output power vs. axial position change for target of roughness Ra 1.6

(a) far linear region (b) near linear region

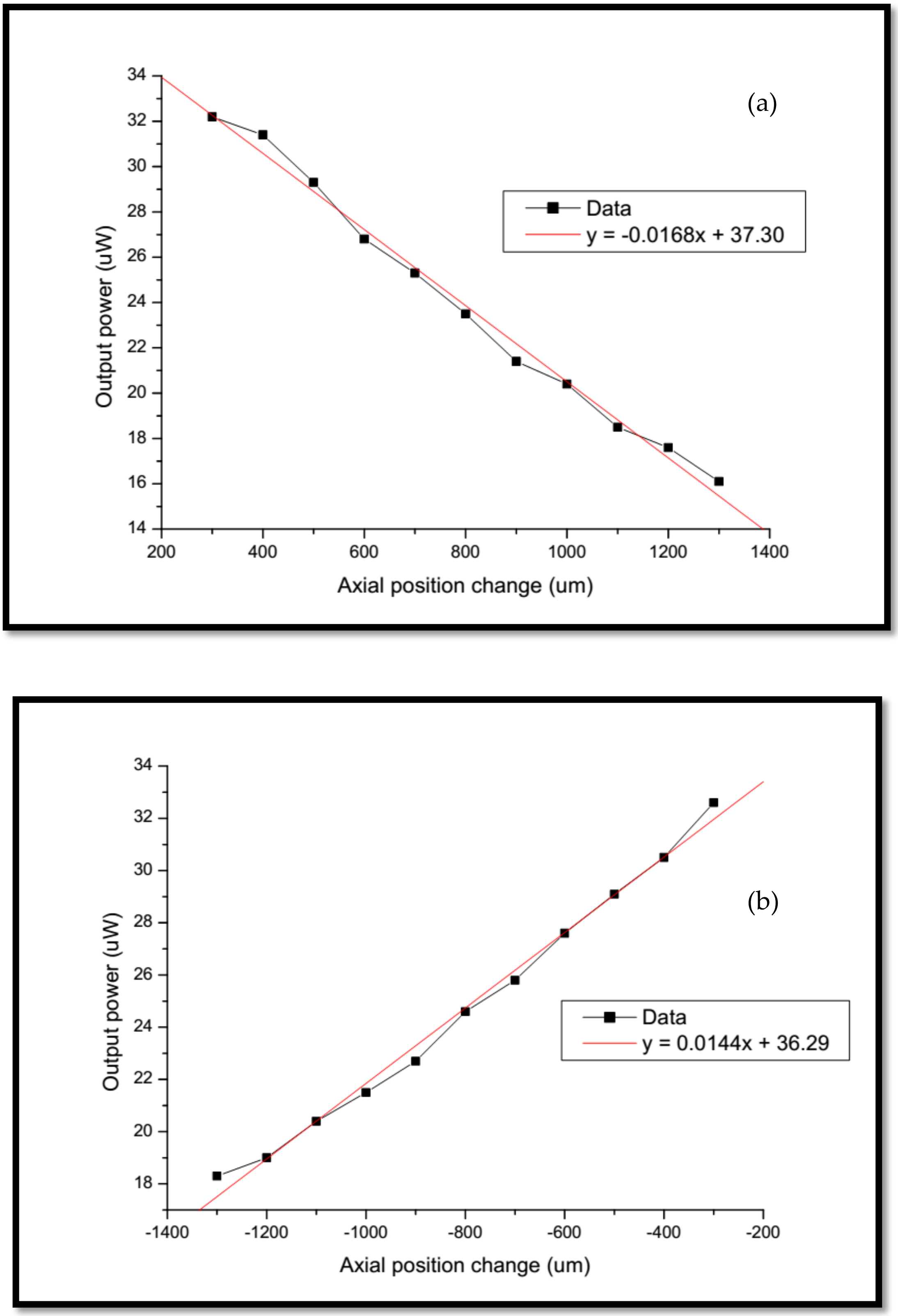

Figure 3.9: Output power vs. axial position change for target of roughness Ra 3.2

(a) far linear region (b) near linear region

From the Figure 3.5 to Figure 3.9, one can conclude that, sensitivity and range varies for different target surfaces. Hence, the system needs to be calibrated for different target surfaces. The slope of the curve explains the direction of the motion of the target. Table 3.1 gives the performance of the position sensor.

Table 3.1: Performance of the Position Sensor

	Near Linear Slope		Far Linear Slope	
Type of Surface	Sensitivity (μW/μm)	Linear Range (μm)	Sensitivity (μW/μm)	Linear Range (μm)
Ra 0.025 μm	0.26	600	-0.243	600
Ra 0.05 μm	0.123	700	-0.125	700
Ra 1.6 μm	0.027	1000	-0.028	1000
Ra 3.2 μm	0.0168	1000	-0.0144	1000
White Surface	0.017	1000	-0.019	1000

From the Table 3.1, it is observed that sensitivity is decreasing with increase in roughness of the target surface. As the output of given sensing technique is expected to be symmetrical about the peak of the curve (for small displacements), both the rising and falling peaks slope should be equal. However, there is small amount of non-linearity seen in the slope of curves. This might be due to the slight angle of target surface from the optical axis of the lens, which leads to an offset in transverse direction of focused reflected light away from the fiber tip.

The measurements were performed in both the dark and ambient light conditions and effect of ambient light on measurement was found to be negligible. This is due to the fact that under the ambient condition (without laser), light coupled from the fiber to detector was found to be in nW and when the laser light is used, the measured values were in orders of tens of μW. The sensor performance depends upon the coupling efficiency between the laser source, optical fiber coupler, lens and detector. Thus, we could achieve a resolution of ~100 μm for targets with different roughness as given in Table 3.1.

By appropriate choice of the optics i.e. the magnification of system and the fiber core diameter, one can control the width of the output response with respect to the target position change to be either sharp or broad. This allows to modify the response according to the specific requirements of a given application, which may require high resolution over a short range of displacements, or conversely, lower resolution over a broader range. The spot diameter on the target should be greater than the surface roughness of the object; otherwise, the reflected signal will be prone to erratic fluctuations according to the surface irregularities.

3.4 CONCLUSION

A single optical fiber based sensor for non-contact axial position measurements is presented and its performance is evaluated. We have achieved resolution of ~100 μm with a range of ~1000 μm. Current state of the art of these sensors includes their application in nano-measurements and as reference sensors in metrological applications as reported by Felix G Balzer et al. [61]. In addition, Shafir et al. [59] have used confocal sensors for position, velocity and displacement measurements. However, range of measurements in case of both these researchers is

100 to 200 μm whereas in our case range is ~1000 μm. The sensor is developed by using Y-optical fiber coupler and lens. The position change is calculated by the variation in the output power received after reflection from the target surface whose position change has to be measured. The effect of target surface roughness is also studied based on the maximum output voltage received at the detector. For low roughness samples, higher light intensity is received and as the target roughness increases, the light intensity decreases at the detector. These sensors have advantages as same probe acts as a transmitting and receiving signal. The range and resolution of the sensor system can be configured by varying the fiber diameter and focal length of lens used. These sensors can be used for position measurement in hazardous regimes for real time applications.

CHAPTER 4: LASER BASED ONE-DIMENSIONAL POSITION SENSOR FOR LONG STANDOFF DISTANCE

In the previous chapter, we have designed an optical fiber based axial position sensor that can measure the position change in one dimension with a range of 1 mm at a standoff distance of 46.36 mm. In this chapter, we design and demonstrate a compact laser based sensor for range ~100 mm at long standoff distance ~1000mm. Therefore, we go for a Laser triangulation based position sensor which is generally used for longer standoff distance. To make the sensor compact, beam-folding technique was used in the path of the converging light from lens, which ultimately falls on the position-sensing detector (PSD). Position resolution of 1 mm at a standoff distance of ∼1000 mm between the target and light collecting lens was achieved for the developed sensor. The calibration of the sensor was done based on the output voltage obtained at PSD with near and far displaced position of the target. The sensor output was found to be linearly varying with the target position. The sensor performance was tested for different target roughness and ± 10° variation in angle between laser and target surface. The effect of temperature on the output of developed sensor was also studied and the error in measurement was found to be within the sensor resolution. The developed sensor has many potential applications in industrial environment for the targets having different surface roughness and variable ambient temperature.

4.1 PRINCIPLE OF OPERATION

The principle of oblique configuration for laser triangulation was used for target position measurement. The configuration was selected as it has high resolution compared to the direct configuration as discussed in chapter 2. When the laser falls on the target, a negligible part of the incident energy gets absorbed and the reflected portion of the light is split into the two components i.e. specularly-reflective light and diffused-reflective light. The specularly reflected light has high intensity as compared to the diffused light. The diffused scattered light from the target surface is used to perform the measurement as it has low intensity (no saturation problem for PSD). Moreover, while using the specularly reflected light based measurement it will be difficult to maintain the laser axis and optical axis of the lens make same angle with the plane of the target for long measurement range. As wavelength of laser (0.65 μm) is more than the roughness of target surface, diffraction induced change in intensity pattern of diffused light is negligible as reported by Inari et al [77]. So, the diffuse light from the target surface will not cause measurement variability in our case. The back scattered light from the target surface is made to focus on the PSD via focusing lens and beam folding as shown in Figure 4.1.

As, the laser always makes an angle of 5° with the normal to the target surface whereas optical axis of lens makes 0° with the normal. This ensures that only diffused light is captured for measurement and at the standoff position of the target, the image of the laser spot is focused at the center of PSD. Thus, the reflected portion of light falls outside the area of lens and only diffused light is being captured from the surface.

As the target position is shifted from the standoff position, the focused spot moves towards the edges of PSD. By measuring the displacement of spot on PSD, target displacement and hence the position can be measured.

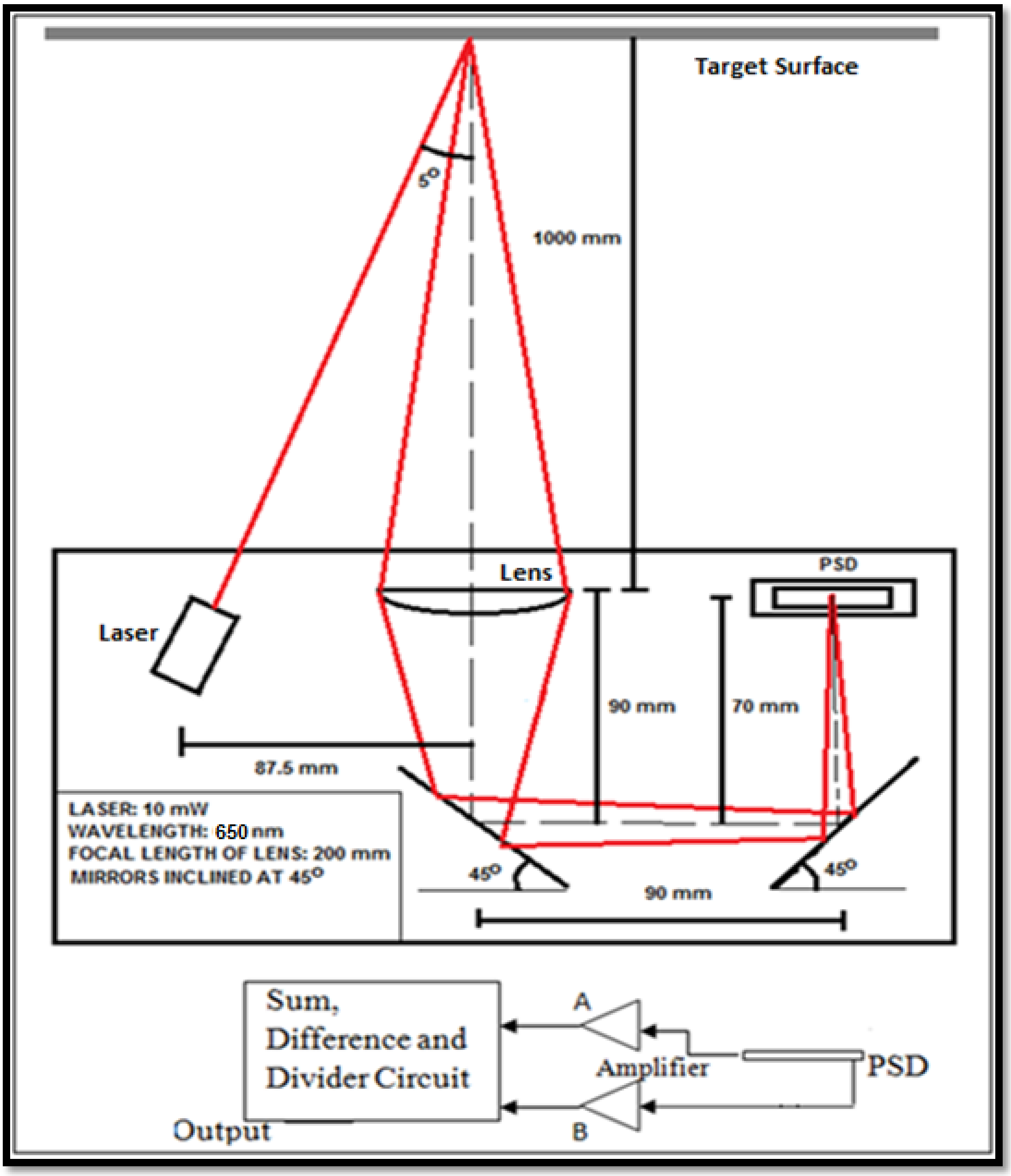

Figure 4.1: Schematic of developed sensor

Using the Eq. (2.57), the relation between the target displacement Δ and the image spot displacement δ at the detector is given as

$$\varDelta = \frac{d_o \delta \, cos\, \theta}{d_i \, sin\, \theta \pm \delta \, cos\, \theta} = \frac{d_o \delta}{d_i \, tan\, \theta \pm \delta} \tag{4.1}$$

In the Eq. (4.1), the measured surface moves down from the reference position, it is "–" in this formula, otherwise, it is "+". Here, d_o is the standoff distance (object distance), d_i is the distance between lens and detector (image distance) and θ is the angle of incidence.

For$\delta \ll \varDelta$, Eq. (4.1) can be written as,

$$\varDelta = \frac{d_o \delta}{d_i \tan\theta} \tag{4.2}$$

$$\delta = \varDelta m \tan\theta \tag{4.3}$$

Where, m is magnification of lens,

$$m = \frac{d_i}{d_o} \tag{4.4}$$

Eq. (4.3) shows that deviation of the beam spot on the PSD is directly proportional to the displacement of the target and magnification m of the lens. For long standoff distance applications, d_o is high which tends to reduce the value of m (or sensitivity). Therefore, to attain higher sensitivity in spite of high d_o, di should be kept high. In order to accommodate high d_i in a compact optical sensor, a beam-folding technique is required. This is why we have used the beam folding technique in the path of converging light coming from the lens.

The position of fixing the PSD at the sensor is determined using the lens formula given by,

$$\frac{1}{f} = \frac{1}{d_o} + \frac{1}{d_i} \tag{4.5}$$

Where, f = focal length of lens, d_o = object distance from lens at standoff distance, d_i = image distance from lens.

4.2 SENSOR DESIGN AND DESCRIPTION

The developed sensor system comprises of a laser diode, a plano-convex lens of 48 mm clear aperture and a position-sensing detector (PSD-SL 15 of M/s UDT, effective length of PSD is 15 mm) having cross sectional area 15 mm^2. The responsivity of detector is 0.4 A/W for 670 nm wavelength. The position detector error is about 15 µm over 80% of length and position detection drift is about 0.1 µm / $^{\circ}$C. The operating temperature range of detector is -10°C to 60°C.Laser diode used in the sensor has an advantage due to their optical characteristics, small size, and ruggedness. Coherence and single wavelength characteristics of laser diodes enable the outputs of these devices to be focused to a diffraction limited spot size. The size of the resultant spot is dependent on the wavelength of the laser - the shorter the wavelength of light, the smaller the size of the spot that can be generated. A continuous wave output diode laser (650 nm, 10 mW output power, Make: World StarTech) is inclined at the angle of 5° from the target surface as shown Figure 4.1. This small angle was selected such that base length of the developed sensor remains small. The diode laser produces a fine spot on the metallic target of ~ 1 mm. The target was at the 1000 mm standoff distance from the lens. The lens of focal length 200 mm is used for the collection of scattered light from the target surface. To minimize the volume of the sensor without sacrificing sensitivity as explained in earlier section, a beam-folding technique has been used to focus the scattered light between the lens and PSD. This beam folding was achieved by the help of the two mirrors inclined at an angle of 45° as shown in Figure 4.1. The positioning of lens, mirrors and detector was done in such a way that when the target is at a standoff distance, then the scattered light from the target is focussed at the centre of PSD.

In our case f = 200 mm, $d_o = 1000$ ± 50 mm, so d_i comes out to be 250 ± 3 mm from Eq. (4.5). However, as PSD is kept at a fixed distance of 250 mm from the lens, any change in the position of the target is going to defocus the image. However, since the change in image distance is much less than the distance between the lens and PSD $[(\frac{3}{250}) X\ 100\ ) = 1.2\ \%]$, we expect negligible defocusing and corresponding error.

As the sensor is developed for diffused light collection, we consider Lambertian model [75] ignoring the diffraction effects. Eq. (4.6) gives the light power received by PSD as signal power Ps.

$$P_s = \frac{P_o \Omega_D \cos\theta}{\pi} \tag{4.6}$$

Where, P_o is the laser transmitting power, Ω_D is the receiving solid angle subtended by the receiving lens aperture, θ is the angle between the laser line and the line joining the point of intersection of the target surface and lens.

When the test surface has a position variation Δ, the receiving solid angle Ω_D is computed as:

$$\Omega_D = \frac{\pi d^2}{4 d_o^2}\left(1 + \frac{2\Delta}{d_o}\cos\theta\right) \tag{4.7}$$

Where, d is the clear aperture diameter of the receiving lens.

Thus, the signal power at the detector can be stated as:

$$P_s = P_o \frac{d^2}{4d_o^2}\left(1 + \frac{2\Delta}{d_o}\cos\theta\right)\cos\theta \tag{4.8}$$

In our case, as the sensor is developed based on the scattered light collection, for 10 mW incident laser power, signal power P_s received at the detector using Eq. (4.8) comes out to be 6 μW and 7.2 μW respectively at the far and near position for the target range. This P_s is the amount of signal power received at PSD. PSD's are continuous single element planar diffused photodiodes with no gaps. They provide direct readout by providing an analog output directly proportional to both the position and intensity of a light spot present on the detector active area. A light spot present on the active area will generate a photocurrent, which flows from the point of incidence through the resistive layer to the contacts. This photocurrent is inversely proportional to the resistance between the incident light spot and the contact. When the input light spot is exactly at the device center, equal current signals are generated. The signal generated at the output of PSD is proportional to the displacement of image spot from its center position of the measurement range. Any displacement of the target leads to shifting in laser spot on the PSD. The two electrodes of the PSD give the current output and the output current of PSD is converted into voltage with the trans-impedance amplifier implementation using OPAMP (OP 27). The value of C_f = 12 pf, R_f = 47 kΩ. The feedback capacitor stabilizes the frequency dependence of the gain. The accuracy of V_A+V_B and V_A-V_B depends upon the bandwidth of the amplifier which in our case was 8 MHz. The two output voltages are normalized using analog multiplier wired as a divider and then reading is processed further via analog to digital conversion to calculate the displacement in a microcontroller. The schematic of the developed PSD circuit is shown in Figure 4.2.

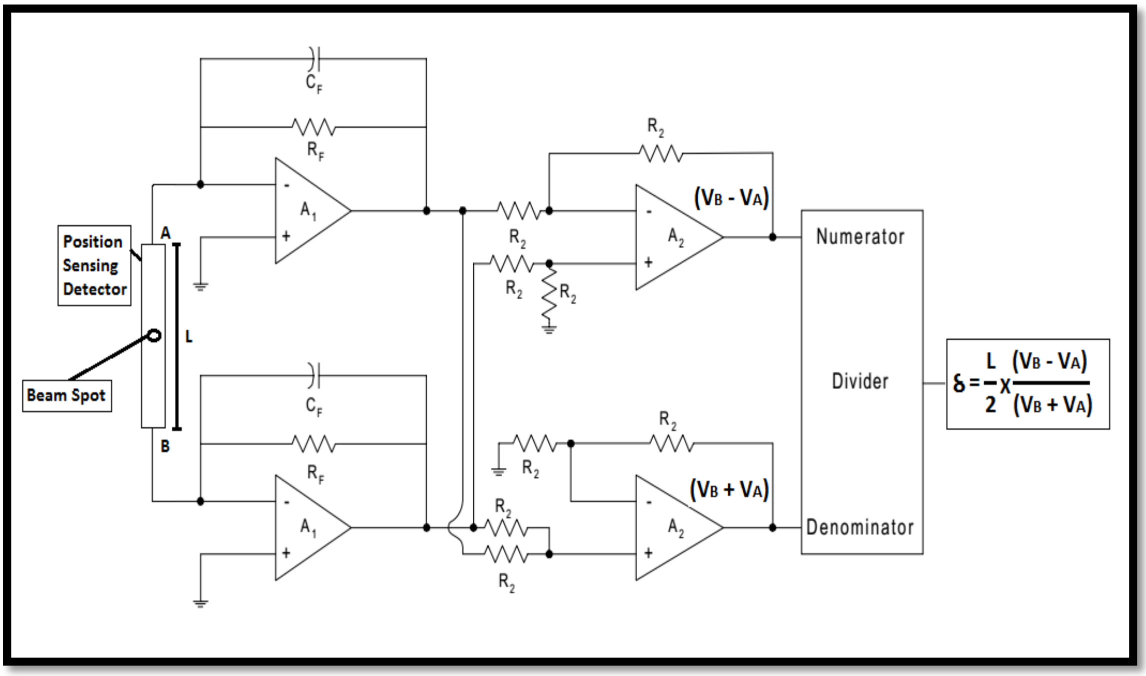

Figure 4.2: Schematic of developed PSD circuit

The spot position on the PSD is calculated by,

$$\text{Spot Position}(\delta) = \frac{L}{2} \times \left(\frac{V_B - V_A}{V_B + V_A}\right) \tag{4.9}$$

Where, V_A and V_B are the two voltage outputs, L is the effective length of PSD. The sum (V_B+V_A) and difference $(V_B\text{-}V_A)$ are determined using Op-Amp based adder and difference circuit. The $(V_B\text{-}V_A)$ output contains the position information and (V_B+V_A) contains the total power of the incident beam.

As the sensor is designed for standoff distance of 1000 mm and diameter of lens used for capturing the back scattered light is of 48 mm, the acceptance angle of lens α is given as:

$$\alpha = \tan^{-1}\frac{d}{2L} = \tan^{-1}\left(\frac{48}{2 \times 1000}\right) = 1.375°$$

Similarly, at 950 mm and 1050 mm target distance, acceptance angle comes out to be: 1.4471 ° and 1.3093 ° respectively. Thus, the spherical aberration is negligible in our case due to the small acceptance angle of lens.

4.3 CALIBRATION OF SENSOR

Calibration of the system is done by recording the location of the image spot position using Eq. (4.9) versus the known object movement through the measurement range. The schematic of calibration procedure of the sensor is done as shown in Figure 4.3. The laser is positioned in a way that the path of the laser and the optical axis form a horizontal plane and point C is the target position of interest. U is the projection of point C on the image plane i.e. on PSD. A and B are two extreme points of the range used in the calibration of the system.

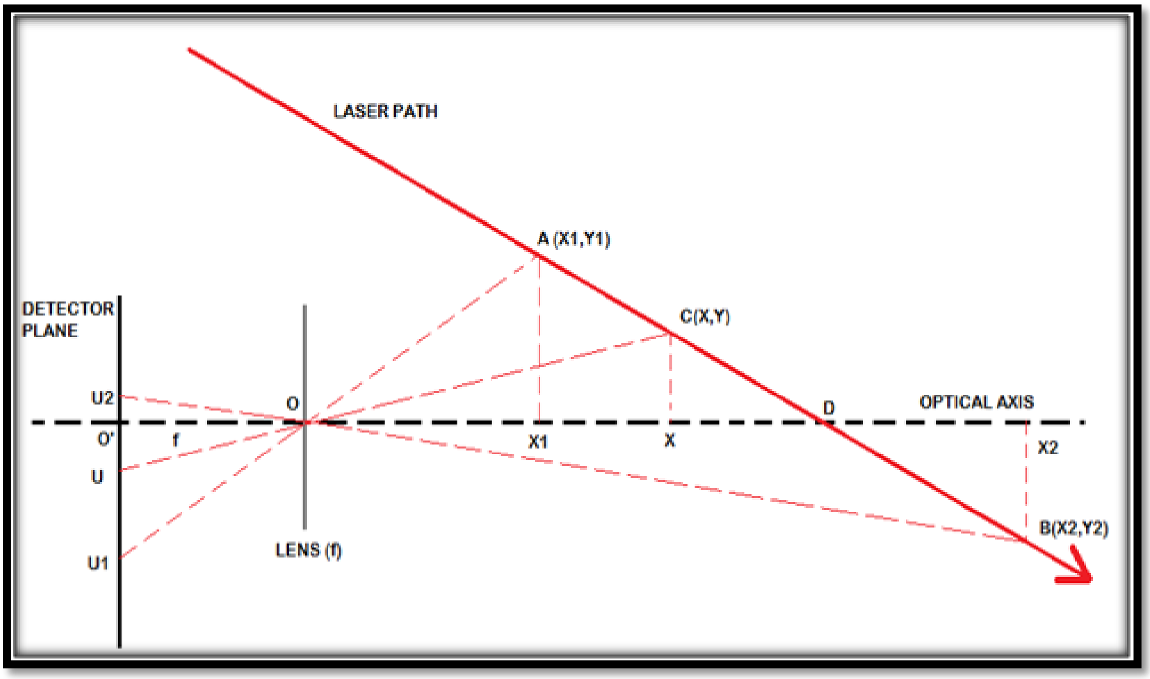

Figure 4.3: Calibration of developed sensor system

D is the point of intersection of laser path and optical axis. Laser is angled in a way that point D is at the center of the range of interest, which is 1000 mm in our case.

Applying similar triangle geometry in ΔAOX_1 and $\Delta OO'U_1$

$$\frac{Y_1}{X_1} = \frac{U_1}{f} \tag{4.10}$$

Similarly,

$$\frac{Y_2}{X_2} = \frac{U_2}{f} \tag{4.11}$$

The origin of the coordinate system at the focal point *O*. The slope *m* of the laser path and the y-intercept *c* are given by

$$m = \frac{Y_2 - Y_1}{X_2 - X_1} \tag{4.12}$$

$$c = Y_2 - mX_2 \tag{4.13}$$

Substituting the values of Y_1 and Y_2 we get,

$$m = \frac{U_2X_2 - U_1X_1}{f(X_2 - X_1)} \tag{4.14}$$

$$c = \frac{U_2X_2 - fmX_2}{f} \tag{4.15}$$

From the Figure 4.3, the line *UC* passing through *O* is represented by:

$$\frac{Y}{X} = \frac{U}{f} \tag{4.16}$$

and the laser path is of the form:

$$Y = mX + c \tag{4.17}$$

Solving for *X*, we get:

$$X = \frac{(U_1 - U_2)X_1X_2}{U(X_2 - X_1) - (U_2X_2 - U_1X_1)} \tag{4.18}$$

Where, X_1 and X_2 are the target distance from the lens, U_1 and U_2 are the output values of the PSD at X_1 and X_2 and X is computed in the given range by Eq. (4.18).

Thus, we can easily compute the displacement in a given range without knowing the baseline separation or angles between the detector and laser source. The above-mentioned relation is used in microcontroller where for the known target distances X_1 and X_2, the corresponding output voltages U_1 and U_2 help in determining the displacement.

4.4 VARIATION IN SPOT SIZE OF LASER AT THE DETECTOR

As discussed in section (c) of 2.5 that oblique triangulation has greater sensitivity towards displacement than the direct one, so here we see how the spot varies at the detector. Considering that Laser is striking the target surface at point P and position I, making angle θ with the optical axes as shown in Figure 4.4, and the scattered light is focused through the converging lens at point O'. When the target is displaced by the distance X towards the sensor, is at position II, the Laser strikes at the point P_1, and is focused at point P_3.

When the target is at the original position I, then the position of spot size at CCD is at I', i.e. the focus point of lens. As the target is displaced the spot size of Laser increases as shown in Figure 4.4. The main aim is to calculate the spot diameter represented as CE.

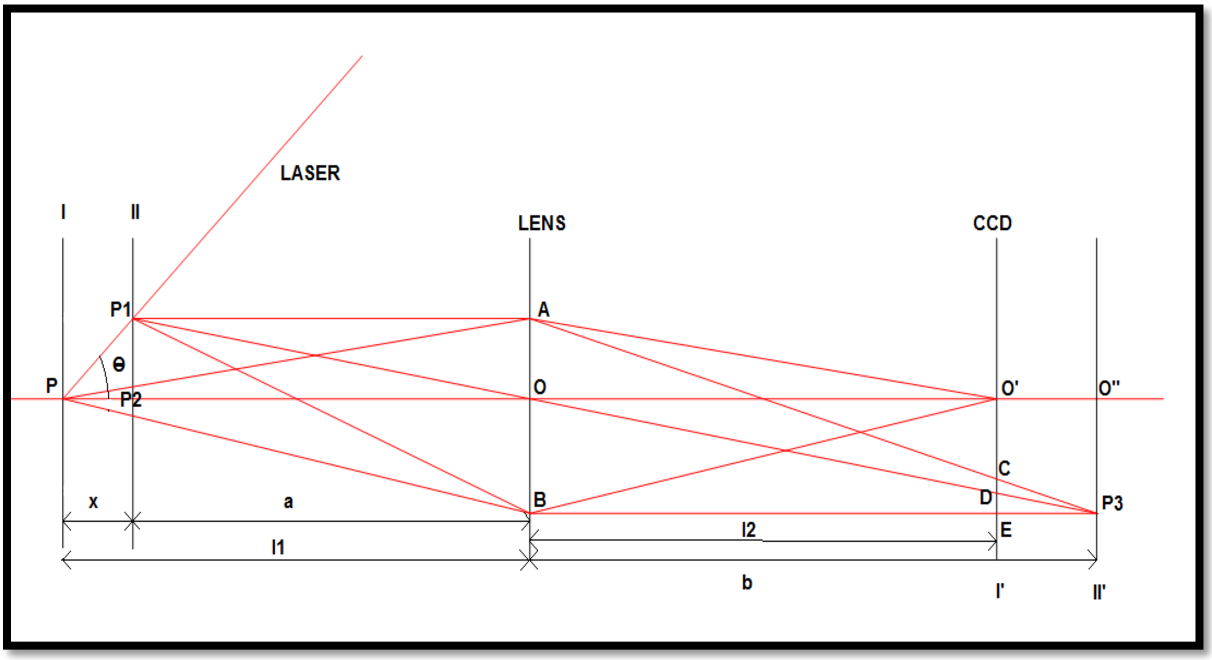

Figure 4.4: Schematic of geometrical ray diagram when target is moved closer to sensor and setup for Laser, Lens and CCD.

According to the optical imaging principle,

Where, a and b are the object distance and image distance, respectively, and f is the focal length of the receiving lens.

$$\frac{1}{f} = \frac{1}{a} + \frac{1}{b} \tag{4.19}$$

Now applying the concept of similar triangles using Figure 4.4;

$\Delta P_1P_2O \sim \Delta OO'D$

$$\frac{P_1P_2}{OP_2} = \frac{O'D}{OO'} \tag{4.20}$$

$$P_1P_2 = x\tan\theta \tag{4.21}$$

As, $P_1P_2 = AO$

So,

$$O'D = \frac{l2 \times xtan\theta}{a} \tag{4.22}$$

$\Delta\ P_1P_2O \sim \Delta OO''P_3$

$$\frac{P_1P_2}{OP_2} = \frac{O''P_3}{OO''} \tag{4.23}$$

So,

$$O''P_3 = \frac{b \times xtan\theta}{a} \tag{4.24}$$

As, $O''P_3 = O'E = OB$

Using above equations, we get, $DE = O'E - O'D$

$$DE = \frac{b \times xtan\theta}{a} - \frac{l2 \times xtan\theta}{a} \tag{4.25}$$

$$DE = (b - l2) \times \frac{xtan\theta}{a} \tag{4.26}$$

$\Delta\ AOP_3 \sim \Delta CDP_3$

$$\frac{AO}{OP_3} = \frac{CD}{DP_3} \tag{4.27}$$

$$OP_3 = \sqrt{(O''P_3)^2 + (OO'')^2} \tag{4.28}$$

$$OP_3 = b \times \sqrt{\left(\frac{xtan\theta}{a}\right)^2 + 1} \tag{4.29}$$

$$DP_3 = \sqrt{(DE)^2 + (EP_3)^2} \tag{4.30}$$

$$DP_3 = (b - l2) \times \sqrt{(\frac{xtan\theta}{a})^2 + 1} \tag{4.31}$$

Now replacing the value of OP_3 and DP_3, we get;

$$\frac{xtan\theta}{b * \sqrt{\left(\frac{xtan\theta}{a}\right)^2 + 1}} = \frac{CD}{(b - l2) \times \sqrt{\left(\frac{xtan\theta}{a}\right)^2 + 1}} \tag{4.32}$$

$$CD = \frac{(b - l2) \times xtan\theta}{b} \tag{4.33}$$

As, $CE = CD + DE$

$$CE = \frac{(b - l2) \times xtan\theta}{b} + (b - l2) \times \frac{xtan\theta}{a} \tag{4.34}$$

$$CE = \frac{(b - l2)}{f} \times xtan\theta \tag{4.35}$$

From the calculation as, $CD \neq DE$, this signifies that the shape of the Gaussian peak is changing as the target is displaced.

The ratio of CD and DE will correspond to the shape change as imaged by CCD camera. So,

$$\frac{CD}{DE} = \frac{a}{b} \tag{4.36}$$

Similarly, when the target is displaced away from the sensor the variation of image spot is given as shown in Figure 4.5.

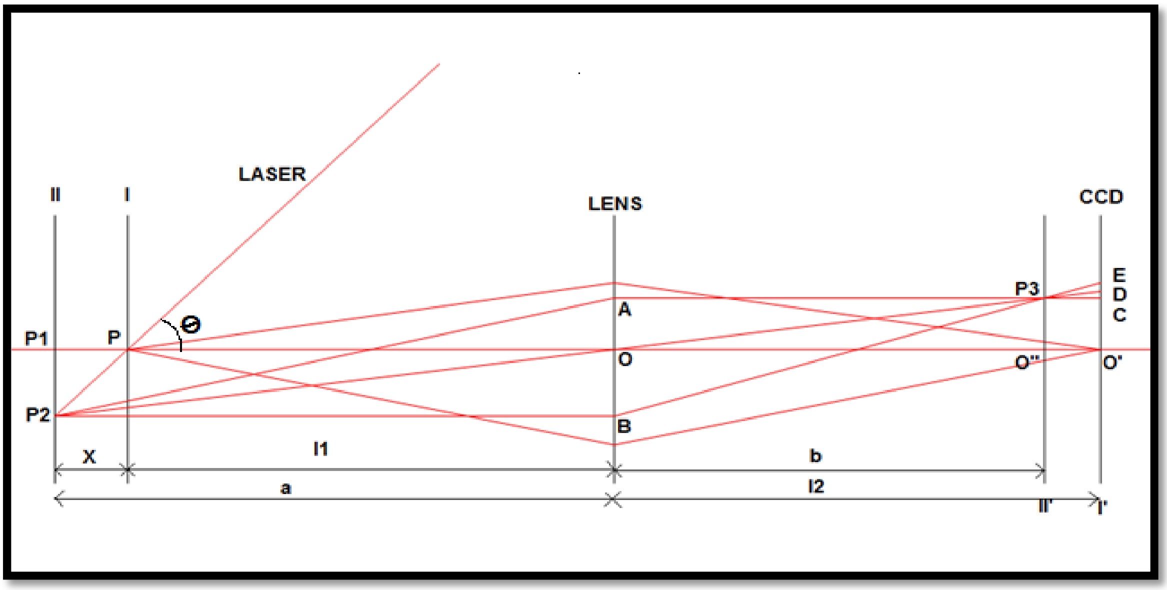

Figure 4.5: Schematic of Geometrical ray diagram when target is moved away from sensor and setup for Laser, Lens and CCD.

Again using the concept of similar triangle, the ratio of CD and DE will correspond to the shape change as imaged by CCD camera as given by:

$$\frac{CD}{DE} = \frac{b}{a} \tag{4.37}$$

Thus, it can be seen that, shape of the Gaussian peak changes with the ratio of object distance to the image distance when the target is displaced toward the detector system and with the ratio of image distance to the object distance when the target is displaced away from the detector system. This case arises when the detector is kept parallel to the lens.

4.5 EXPERIMENT

The experiments were performed using the metallic target as in most of the industries, the shafts, pipes, spindles; fuel rods etc. whose position and alignment need be measured are metallic in nature.The target was fixed on the linear micrometer stage and was kept at the standoff distance of 1000 mm from the developed sensor. The stray light was prevented by encasing the complete detection unit to an aluminium box, as it may change the PSD output current that can generate an error. The target was displaced gradually ± 50 mm from the standoff position and the outputs were measured. A large number of experiments were performed to test the developed sensor. The experimental setup along with the developed sensor is shown in Figure 4.6.

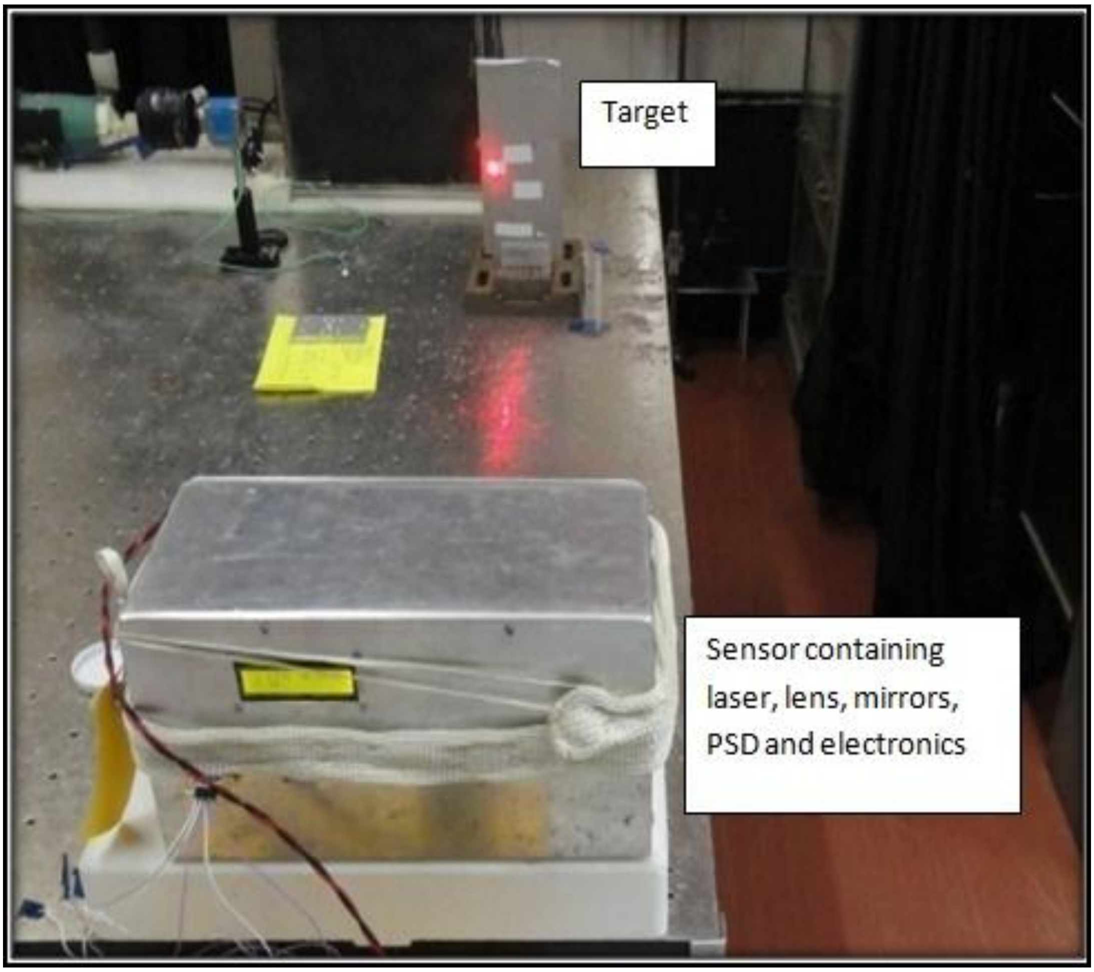

Figure 4.6: Experimental setup and developed sensor

The effect of target inclination (± 10˚) at the output of developed sensor was studied. The developed sensor was also tested with standard surfaces of known roughness values (0.025 μm Ra, 0.05 μm Ra, 0.1 μm Ra, 0.2 μm Ra, 0.4 μm Ra).

Effect of temperature on the sensor readings was also studied. As the developed sensor head comprises of electronic components and aluminium mechanical assembly, there might be drift in the readings due to the change in temperature. In order to check the effect of temperature, the sensor reading was taken initially at room temperature of 25° C. Then it was heated using coiled heater wound for 1 hour 30 minutes and temperature of the sensor was elevated up to 50°C.

4.6 RESULTS AND DISCUSSION

Results obtained are shown in Figure 4.7. It shows the linear relationship between the target displacements from the standoff position and developed sensor readings.

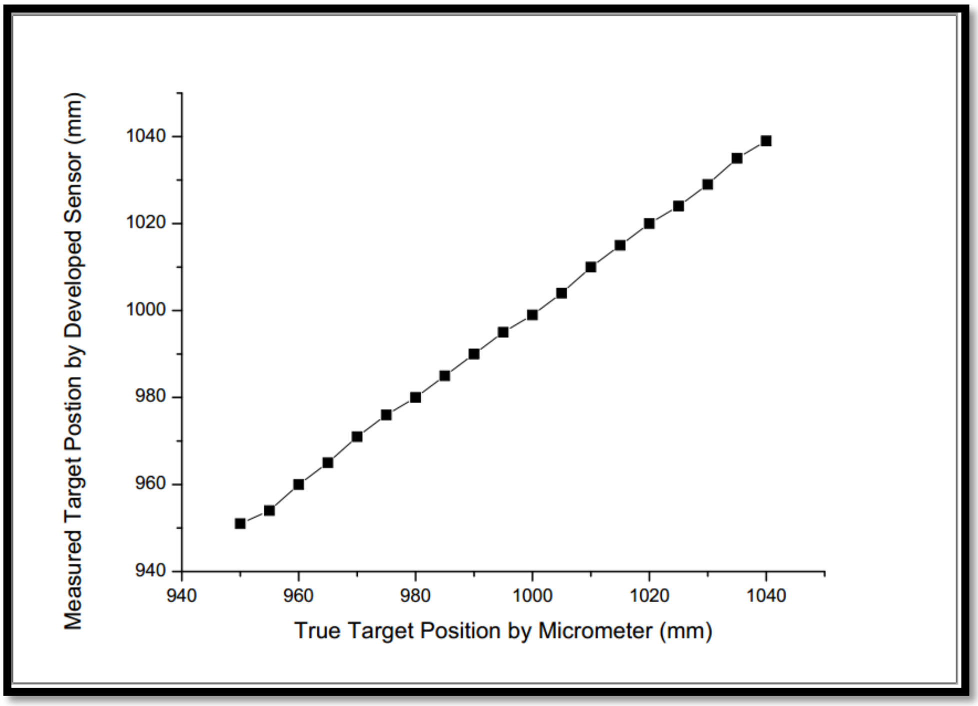

Figure 4.7: Measured target position by developed sensor (mm) vs true target position by micrometer (mm)

The maximum error in position was ± 0.1% (or ± 1 mm at a standoff distance of ~1000 mm). Error plot is presented in Figure 4.8. The major source of error comes from the estimation of image centroid at the PSD as the error in the micrometer is not more than ~10 microns, and rounding off the digits during calibration in microcontroller is also small. For the PSD (SL-15) used, the accuracy is about 15 μm (as per data sheet). Therefore, the uncertainty in measurement calculated using Eq. (4.3) (for δ= 15 μm, m = 0.25 and θ = 5°) comes out to be ~ 0.7 mm which explains the major part of observed error.

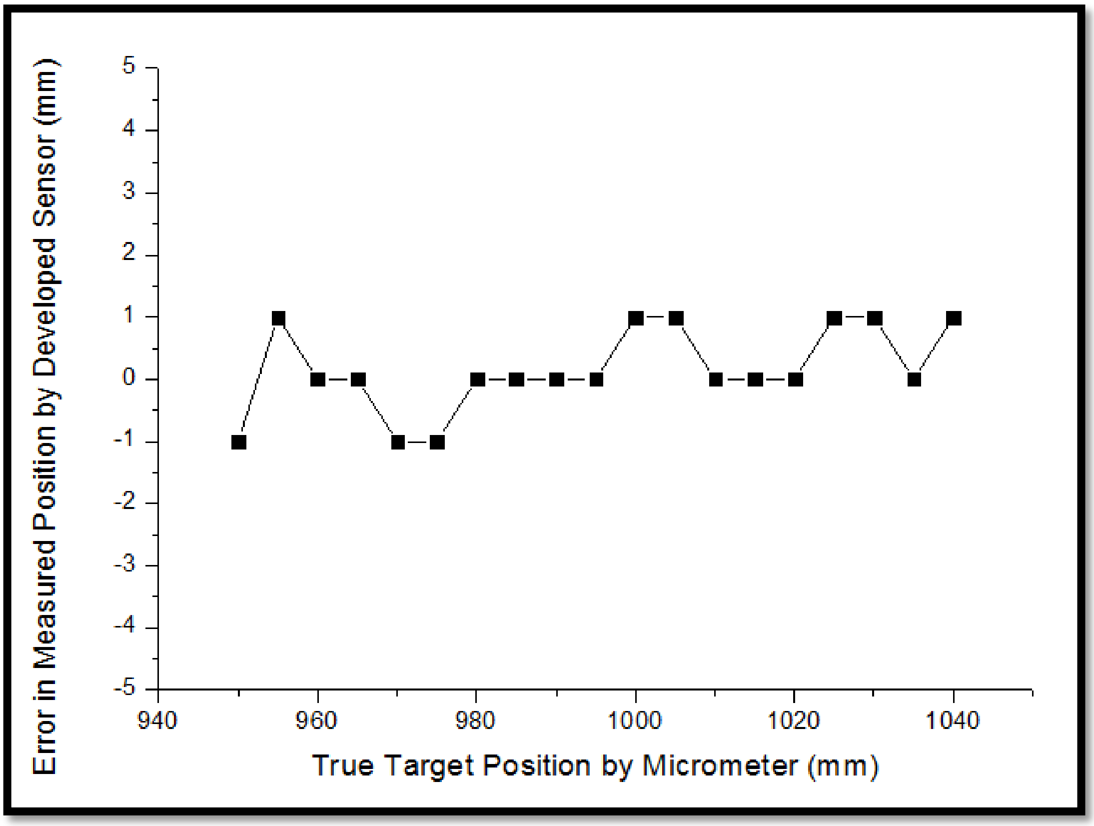

Figure 4.8: Error plot for the developed sensor.

The size of focused laser spot on target at 1000 mm standoff distance is ~1 mm and at the extreme ends of measurement range (950 mm and 1050 mm), size increases to ~1.2 mm. As magnification of our sensor is 0.25, image size at the detector is 0.25 mm at standoff distance and 0.3 mm at the extreme ends. This increase of image size at PSD might be causing the error in measurement to some extent. In general, read-out sensitivity generally depends on the noise floor of the detector and read-out electronics used. However, the output of the detector circuit when no laser light was present, the signal level was about ~10 μV that indicated the order of noise floor of the detector. When the laser is switched on, the output level of the signal is in mV. Thus, Signal to noise ratio is high in our case.

Figure 4.9 describes the output of the displacement sensor corresponding to change in angular position of the target. During this study, distance of the point of intersection of laser and target from lens was kept constant while only the tilt angle of the target surface was varied. The readings were taken by rotating the target by fixing it on a rotating stage at the point of intersection of the laser with the target at distances of 950 mm, 1000 mm and 1050 mm. Position measured by the developed sensor is found to be quite insensitive to the angular position of target surface (for $\theta \leq 10^{\circ}$).

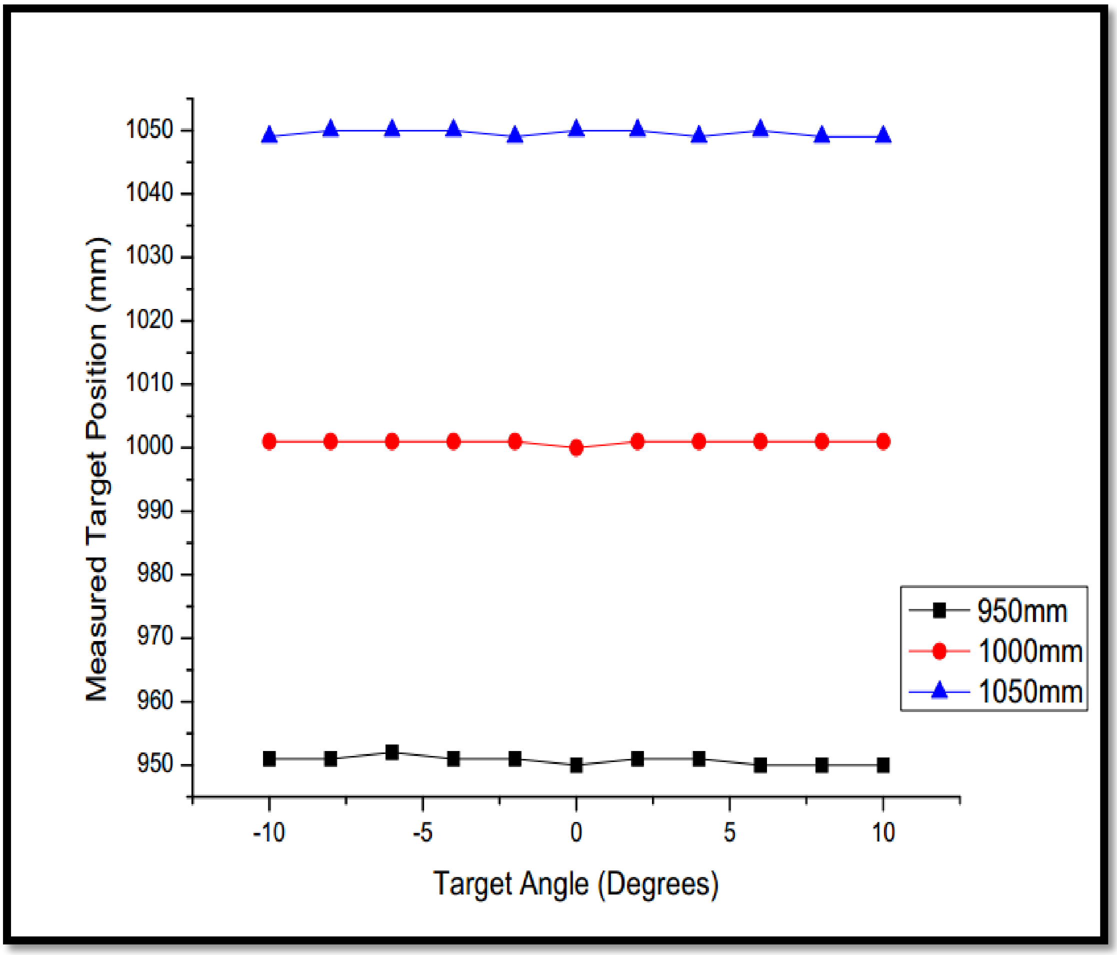

Figure 4.9: Effect of target inclination on the sensor output

Figure 4.10 describes the effects of change in temperature at the sensor output. The sensor was used to measure the target position while keeping it at 25˚C and 50˚C.

Temperature induced error may due to the expansion of aluminum body due to increase in temperature that affects the optical alignment of the setup leading to the change of laser spot position on the PSD. It is well known that dark current of the detector increases in every 5-6˚ C temperature. The sensor current when laser falls on the detector was few microamperes whereas the dark current due to thermal phenomena was less than 300 nA upto 60 ˚C as per data sheet of detector. So, dark noise is not affecting the measurement.

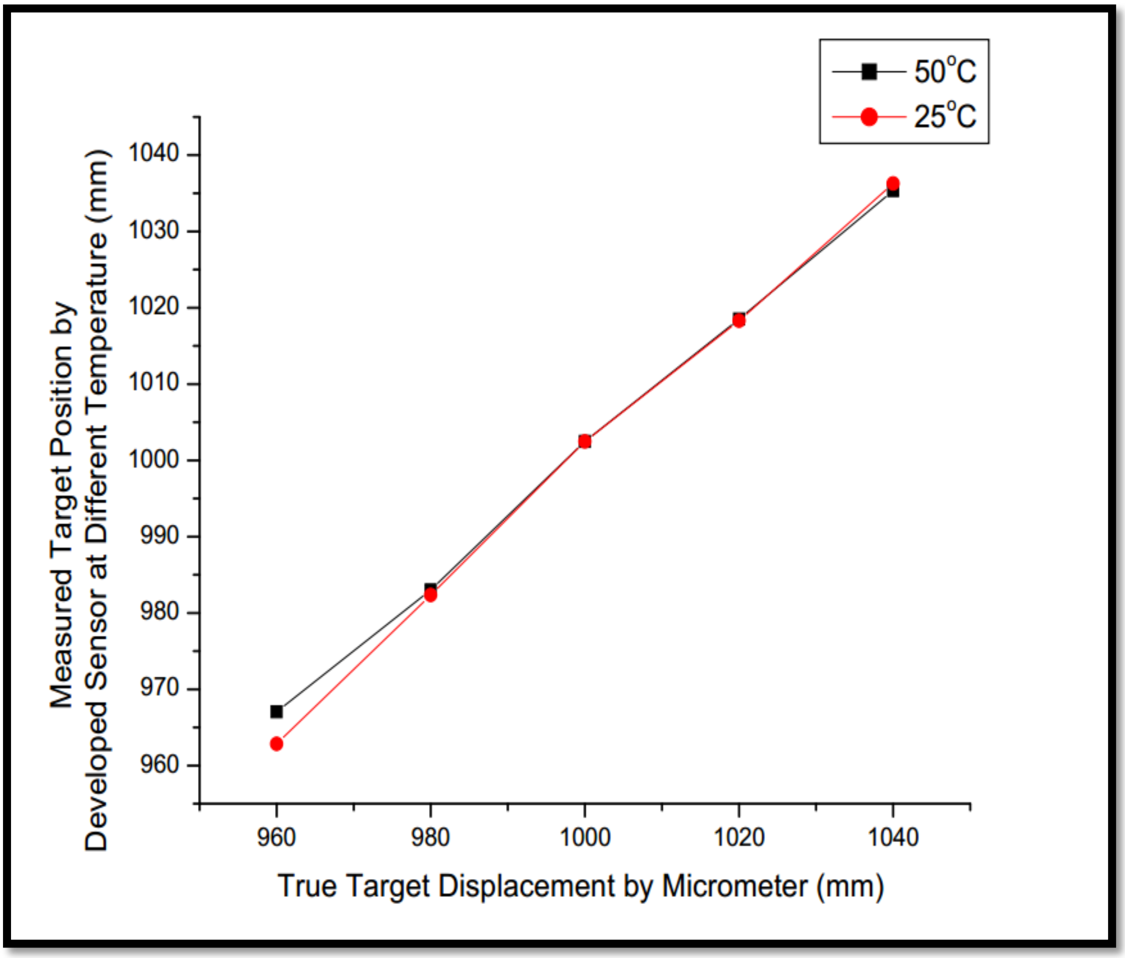

Figure 4.10: Effect of temperature on sensor reading

Finally, the results of position measurement were found to be quite insensitive to the different target surface roughness (0.025 µm Ra, 0.05 µm Ra, 0.1 µm Ra, 0.2 µm Ra, 0.4 µm Ra) as shown in Figure 4.11.

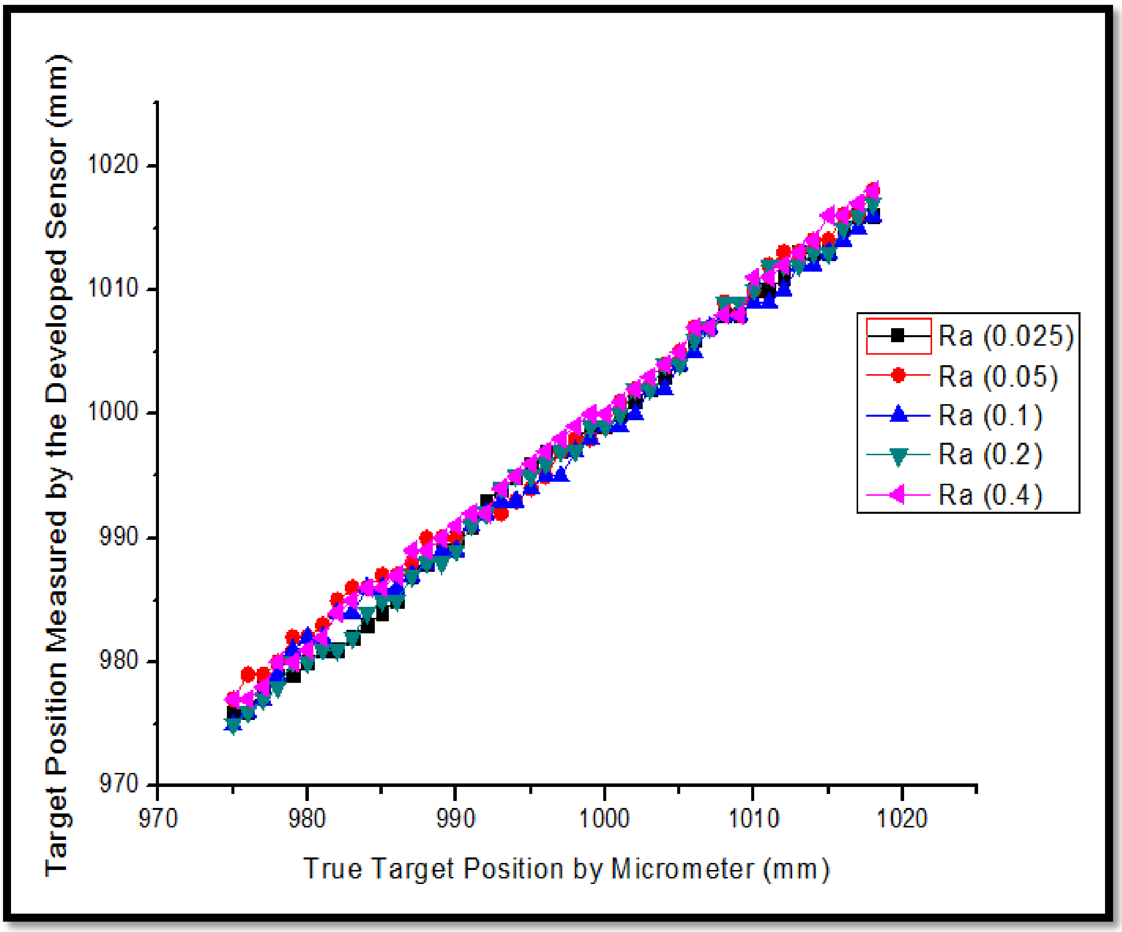

Figure 4.11: Results for position measurement for the target of different roughness samples

4.7 CONCLUSION

In this chapter, laser- based position sensor for long standoff distance is developed to measure the position of the target in the range of ± 50 mm at 1000 mm distance with accuracy of ± 1 mm. The position sensor shows a linear relationship between the output signal and the actual displacement of target to measure the position. Compactness of the sensor without affecting the sensitivity was achieved by incorporating beam-folding technique at the focusing side of the lens. At different angular inclinations of the target surface (±10 degrees from normal), it produced output within ±1 mm error. The sensor was also tested for the different standard surfaces with known roughness and was found to be working effectively. Effect of temperature on the sensor was also studied which was found to be negligible. The developed sensor is compact and can be used for reasonably accurate position measurement at long standoff distance of the target.

CHAPTER 5: DESIGN & DEVELOPMENT OF LINEAR FIBER ARRAY BASED POSITION SENSOR

In the previous chapter, we have described the working principle of oblique laser triangulation sensor for long standoff distance. The position change of the target is measured based on the output voltage received at the PSD. Although the sensor measures accurate position for long standoff distance applications, the presence of electronics in the system is prone to give erratic results or can be damaged in case of radioactive or EMI/EMC environments. Therefore, to apply the technique in the aforesaid environmental conditions, we propose optical fiber based triangulation sensors in this chapter where the electronic components such as CCD camera can be located remotely.

In this chapter, we describe development of linear optical fiber array based non-contact and remote position sensor that uses oblique laser triangulation technique. As discussed in Chapter 2, oblique triangulation method was selected as it has better resolution. In all the optical triangulation techniques reported in literature, scattered or reflected light from the target is collected by the lens and is directly focused onto the CCD or PSD without use of optical fibers, and so these methods are not meant for remote measurement and thus not suitable in the hazardous environments. However, in our technique, instead of imaging directly on CCD camera position information is achieved using linear optical fiber array. This helps in placing the CCD camera remotely at the other end of linear optical fiber array. Determination of target position is done by finding the centroid of laser spot on camera using Fourier series method. Of course, due to oblique incidence of laser, the point of incidence on the target surface gradually changes its location with distance of separation and local surface property can change the intensity pattern on lens ultimately introducing errors in the estimated position. To assess this effect, we have experimentally measured the position of standard surfaces with known roughness using our developed sensor and compared it with the true position measured by micrometer. Factors contributing to the errors are discussed in the chapter.

5.1 DESIGN ASPECTS FOR REMOTE POSITION SENSOR

This section gives the design aspects of remote position sensor comprising of sensor head, linear fiber array, detection unit, and algorithm used for measurement. Sensor head can be mounted near the target whose position is to be sensed and detection unit is placed remotely. The information of position is transmitted continuously from the sensor head to the detection unit via linear optical fiber array.

5.1.1 Sensor head

The sensor head is designed to hold all the optical components with mechanical stability and alignment. The sensor head configured for 100 mm standoff target distance comprises of a diode laser (3 mW, wavelength 638 nm) having spot diameter of 1 mm at target surface, an aspheric lens and a linear optical fiber array for non-contact position measurement. The laser diode provides a compact, efficient, long-lifetime light source for sensor. The working angle i.e. angle between normal of surface and laser line was 30°. An aspheric lens of focal length 25 mm is used to focus the light scattered from the target onto the linear fiber array. The aspheric lens helps in reducing the spherical aberration and distortion. Linear fiber array used in the system was fixed in such a way that at the standoff position of the target, the scattered light from the target is focused by the aspheric lens at the center fiber of linear fiber array. Linear fiber array acquires the scattered light from target and transmits the information to the remotely placed CCD camera as shown in schematic Figure 5.1.

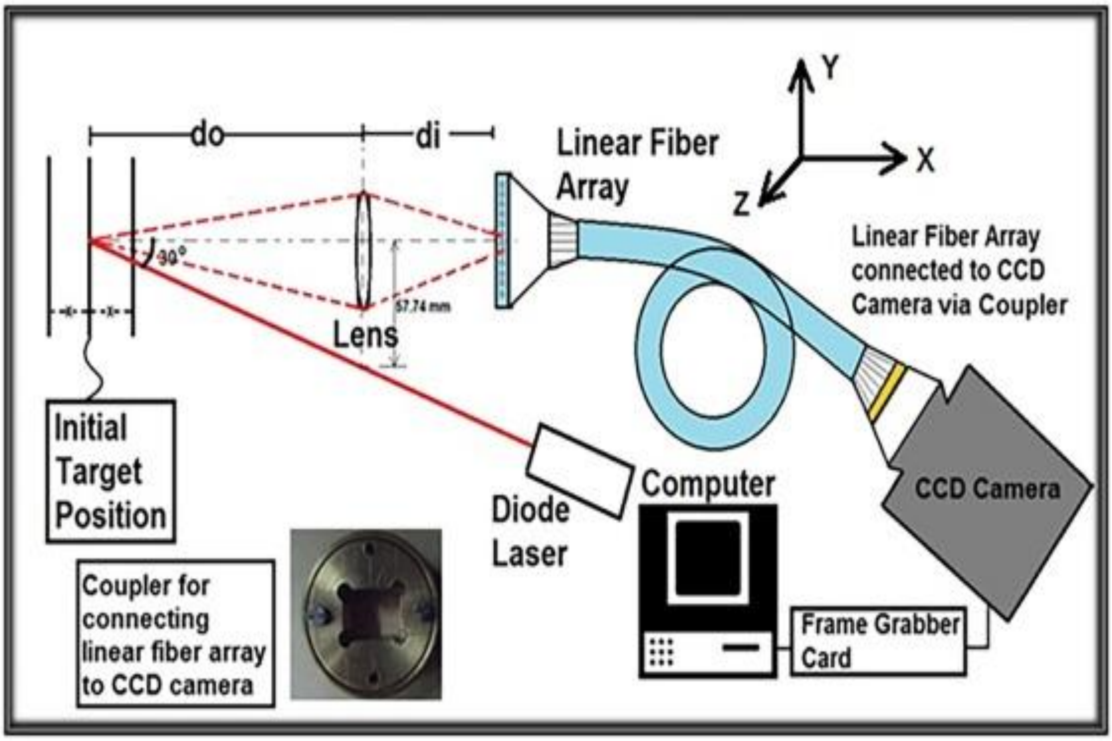

Figure 5.1: Schematic of setup of laser triangulation based position sensor using linear fiber optic array

All the components in the sensor head were mounted such that center of diode laser, aspheric lens and linear fiber array all lie in same plane. The developed sensor head is shown in Figure 5.2 (a). The dimension of sensor head is 12.5 cm × 4.8 cm × 3.2 cm. The schematic of fiber array is as shown in Figure 5.2 (b).

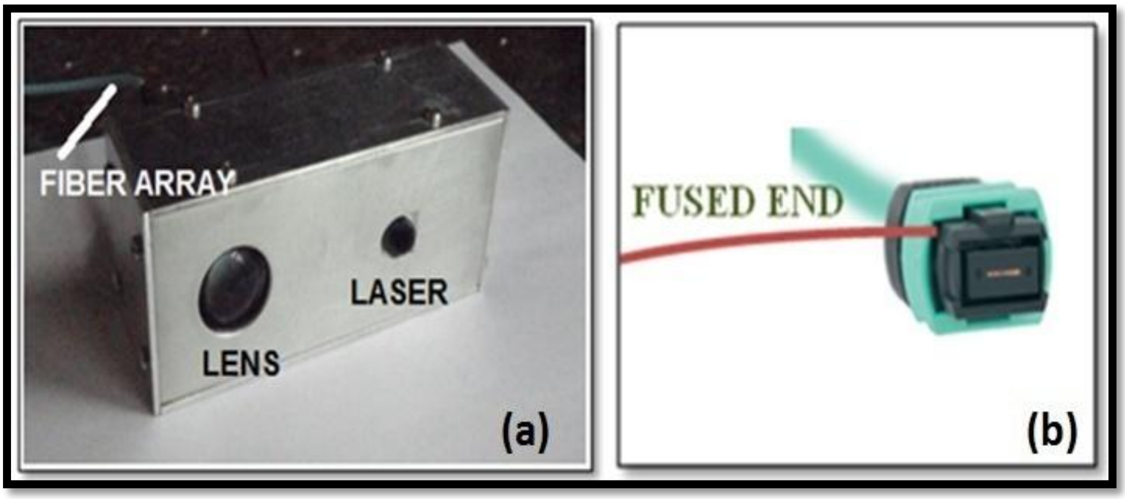

Figure 5.2: (a) Developed sensor head (b) Linear fiber array

5.1.2 Selection of Linear Fiber Array

The resolution of the developed sensor is governed by the diameter of the each individual fiber in linear fiber array and pitch. When the fiber diameter is small, the spatial resolution is more. However, due to the relatively large area of the focused sensing spot on the fiber, the light collection efficiency of individual fiber would be poor. When the fiber diameter is large, the light collection efficiency would be good, but the spatial resolution would be poor. Therefore, the selection of optical fiber size has to be such that a balance between spatial resolution and light collection efficiency is maintained.

The commercially available linear fiber array of 5 m length with 12 multimode fibers is used in our experiment. The core diameter and Numerical Aperture (NA) of each fiber is 50 μm and 0.2 respectively. The pitch of the fiber array was 250 μm. For the standoff distance of 100 mm, by applying the lens formula, the magnification of the optical system is 0.33. Therefore, the image spot on the fiber tip was 330 μm. As the image spot has more diameter than the pitch of fiber array, the image spot is coupled in two fibers for transmission to remotely placed CCD camera.

5.1.3 Detection system

The detection system comprises of analog CCD Camera (area of sensor 640 × 480 pixels with pixel size of 10 µm × 10 µm) placed remotely connected with the light receiving end of linear fiber array. The camera is running in the scan mode and the readout pattern is global shuttering. A CCD is a highly sensitive photon detector, which is divided into a large number of light-sensitive small areas (known as pixels) and is used to build up an image. A photon of light that falls within the area defined by one of the pixels causes flow of electrons and the number of electrons collected is directly proportional to the intensity of the image at each pixel. When the CCD is clocked out, the number of electrons in each pixel is measured and the image can be reconstructed. As position of target changes, the corresponding position of laser spot shifts across the fiber array and finally at the CCD camera. The change in centroid of laser spot determines the change in the position of the target. There are various techniques such as centre of intensity, least square technique and the Fourier method [78-80].

Centre of intensity method is used for calculating the centroid of the image spot. In this method, the intensity values for each pixel are treated as weights and the centroid is calculated as per the following formulas.

$$x = \frac{\iint xI(x,y)dxdy}{\iint I(x,y)dxdy} \tag{5.1}$$

$$y = \frac{\iint yI(x,y)dxdy}{\iint I(x,y)dxdy} \tag{5.2}$$

Direct implementation of the above formulas will give erroneous results if the image obtained is noisy. Also, due to background effect, the centroid value will change. Least square method is computationally expensive and needs lot of time for the processing. Therefore, for precise and speedy centroid measurement in order to calculate the position, technique used in our sensing system for measurement was Fourier method as proposed by [79-81]. We have adopted the Fourier series method as we can remove the asymmetric components and effectively eliminate the noise. The algorithm is based on the detection of the phase shift in the Fourier domain, i.e., the spatial frequency domain. Because the noise has a different frequency spectrum than the image spot and the processing of offset estimation in the Fourier domain can efficiently suppress the noise from pixels. The basic idea of this method is to measure the symmetric and asymmetric proportion of the profile with respect to the coordinate axis. If we are dealing with a symmetrical profile, whose symmetry axis is not the origin, the Fourier expansion is asymmetric. The given technique is used to find a position at which the asymmetric portion of the transform is minimal. The shift in the position is described by Δ x, and gives us the centroid of the beam spot. At 2N discrete points, the Fourier series of the profile *f(x)* is given by:

$$f(x) = \sum_{k=-N}^{k=N} C_k e^{2\pi ikx/N} \tag{5.3}$$

Where, $C_k = a_k + ib_k$ are the Fourier coefficients. The condition $C_k = C^*_{-k}$ results from the Fourier transformation of the measured distribution.

If the function is symmetric about the origin x = 0, imaginary components of C_k disappears. The measure of asymmetry of function f(x) with respect to origin is given as:

$$A(x) = \sum_{k=0}^{N} [IM(C_k)]^2 \quad (5.4)$$

If we consider a function where the origin is shifted by a distance Δx i.e. *f (x-Δx),* the Fourier series of the function is given by:

$$f(x - \Delta x) = \sum_{k=-N}^{k=N} C_k e^{2\pi ik\,(x-\Delta x)/N} \quad (5.5)$$

Measure of asymmetry of function centered at Δx is given by [77],

$$A(\Delta x) = \sum_{k=0}^{N} \left[IM\left(C_k e^{-\frac{2\pi ik\,\Delta x}{N}}\right)\right]^2 \quad (5.6)$$

For an ideal or symmetric profile such as the Gaussian shaped profile of laser spot, the maximum of the fundamental oscillation is the axis of symmetry of the profile and if all the other higher order oscillations are symmetrical about the axis of symmetry, they will not contribute in Eq. (5.7).

In many cases phase of the fundamental frequency is stable, hence only first order Fourier coefficients positions are needed. So, from [79] for fundamental frequency (k=1),

$$IM\left(C_1 e^{-\frac{2\pi i\,\Delta x}{N}}\right) = -a_1 \sin(\frac{2\pi\Delta x}{N}) + b_1 \cos\left(\frac{2\pi\Delta x}{N}\right) = 0 \quad (5.7)$$

Let ∅ represent the phase change between *f(x)* and $f(x - \Delta x)$,

$$\emptyset = angle\big(f(x)\big) - angle\big(f(x - \Delta x)\big) \quad (5.8)$$

$$\emptyset = \frac{-2\pi\Delta x}{N} \quad (5.9)$$

Thus, the shift Δx is given as

$$\Delta x = \frac{N}{2\pi}[\tan^{-1}(\frac{b_1}{a_1}) + \emptyset] \quad (5.10)$$

Where, a_1, b_1 are the coefficients for fundamental frequency, N is no. of pixels, $\emptyset$ represent the phase. Above equations are for one-dimension and can be extended in two-dimensional plane.

Using the above method, an algorithm was developed to find the centroid of the image spot obtained at the CCD.

5.1.4 Algorithm for determination of target position

The target position measurement is determined using the following steps:

(1) Image registration

(2) Define CCD sensor area

(3) Accumulate the intensity vectors along x-axes and y-axes using Eq. (5.7) to find the maximum intensity co-ordinate

(4) Obtain the phase vectors by applying Fourier Transform

(5) Find the shift in the co-ordinates of x and y using Eq. (5.10).

(6) Convert to position using calibration factor.

As, we are using linear optical fiber array and considering that laser diode center, lens and center of linear fiber array are in same plane, the change of pixels in y direction was neglected.

5.2 EXPERIMENTAL SETUP

As described earlier, the diode laser used in sensor was of 3 mW power and standard stainless steel surfaces of known roughness values were used as a target during the experiment. Linear stage carrying the target was fixed on optical table at standoff distance from the sensor head. The target was moved ± 5 mm in steps of 1 mm from the standoff distance 100 mm using manual linear stages. As position of the target changes from the standoff position, the corresponding change in the image spot at the linear fiber array takes place and also at the remotely placed CCD camera. The CCD sensor (640 × 480 pixel) is mapped to 512 × 480 pixels, which is as per the specification of our frame grabber card. This is done by sampling the 512 data points from video signal from each horizontal pixel line of the camera. The exposure time of camera is 20 ms and has a resolution of 12.5 μm × 10 μm in image plane. The exposure time of camera was fixed and was not changed during the course of experiment. Figure 5.3 shows the standard stainless steel surfaces of known roughness values (0.025 μm Ra, 0.4 μm Ra, 0.8 μm Ra, 1.6 μm Ra, 3.2 μm Ra) which were used as target during the experiment and the results were studied.

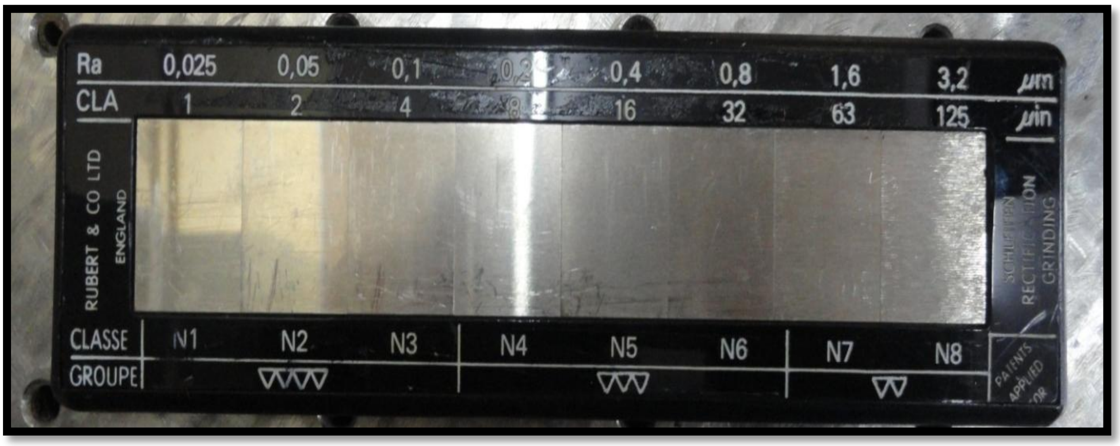

Figure 5.3: Standard stainless steel surfaces of known roughness values used in experiments

5.3 RESULTS & DISCUSSION

From the above experiment discussed in Section 5.2, as the target changes the position from the standoff position the corresponding change in the image spot at the linear fiber array takes place. The CCD camera connected to the other end of linear optical fiber array acquires the image of shifted laser spot. An algorithm based on Fourier series method to calculate the centroid of the laser spot in terms of pixel values was used. Figure 5.4shows the image of laser spot on the camera along with centroid pixel values based on the algorithm.

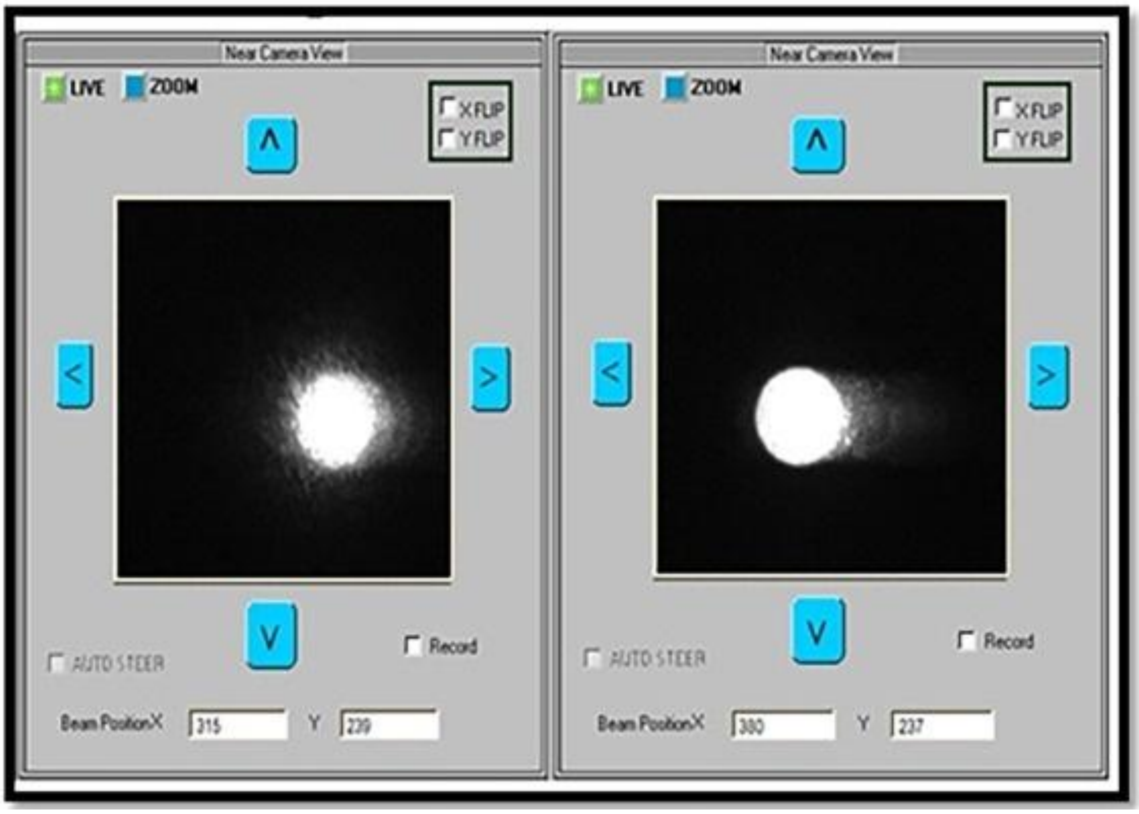

Figure 5.4: Lateral movement of spot captured using CCD camera on the computer.

Theoretically, using Eq. (2.45), 1 mm target displacement corresponds to the shift of 192 µm at the detection. Experimentally, the 1 mm movement of the target resulted in approximately 14 pixels (14 x 12.5 µm = 175 µm) movement of the spot in image plane. The overall 10 mm movement of the target resulted in around 140 pixels (1750 µm) movement. For standard surface of stainless steel of 0.025 µm roughness, variation of the position of centroid of image spot at CCD camera (*y*) with actual position of target (*x*) measured by micrometer is plotted in the Figure 5.5. By linear equation fitting, the fitted equation is:

$$y = 14.054\mathrm{x} - 1096.818 \tag{5.11}$$

Thus, we have experimentally confirmed that movement of the centroid of image spot is linearly dependent on target displacement. Then, similar experiments were conducted with other known roughness specimens and the results obtained are as shown in the Figure 5.6.

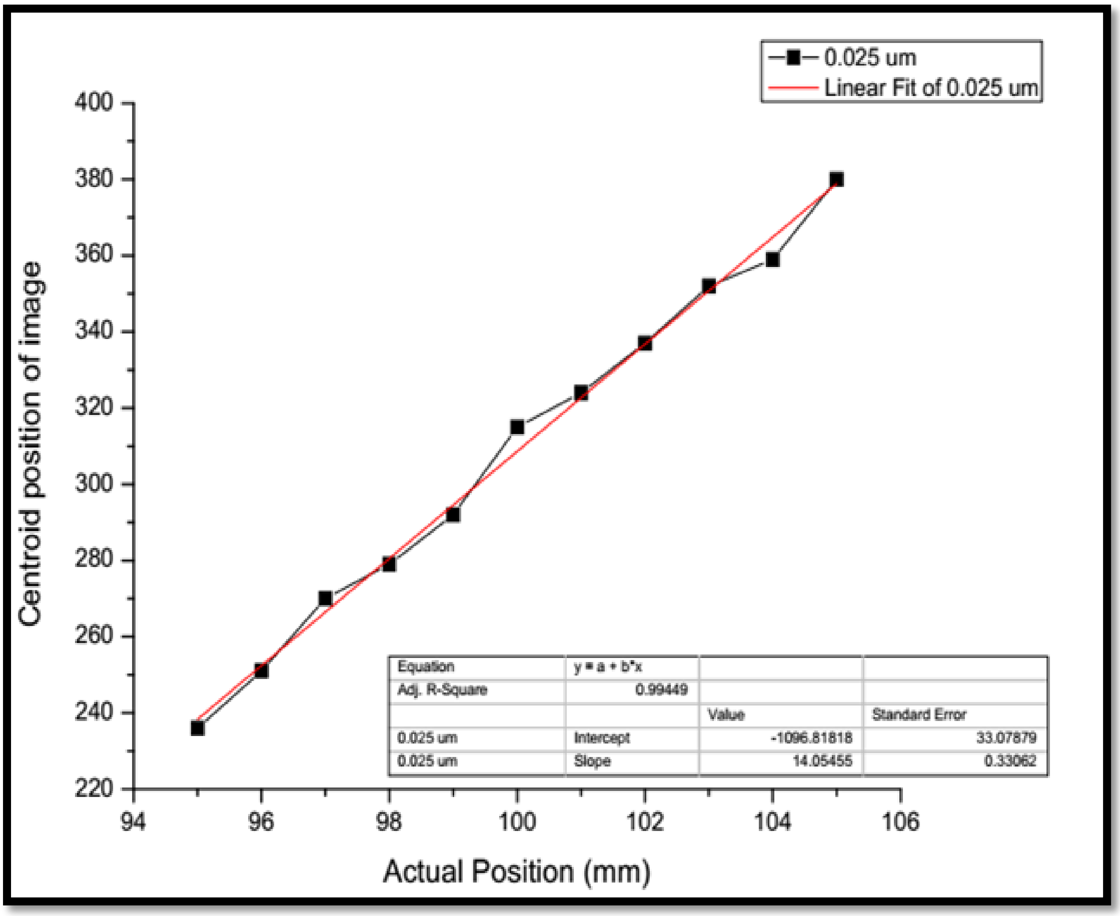

Figure 5.5: Relation between centroid positions on the CCD camera vs actual position (mm)

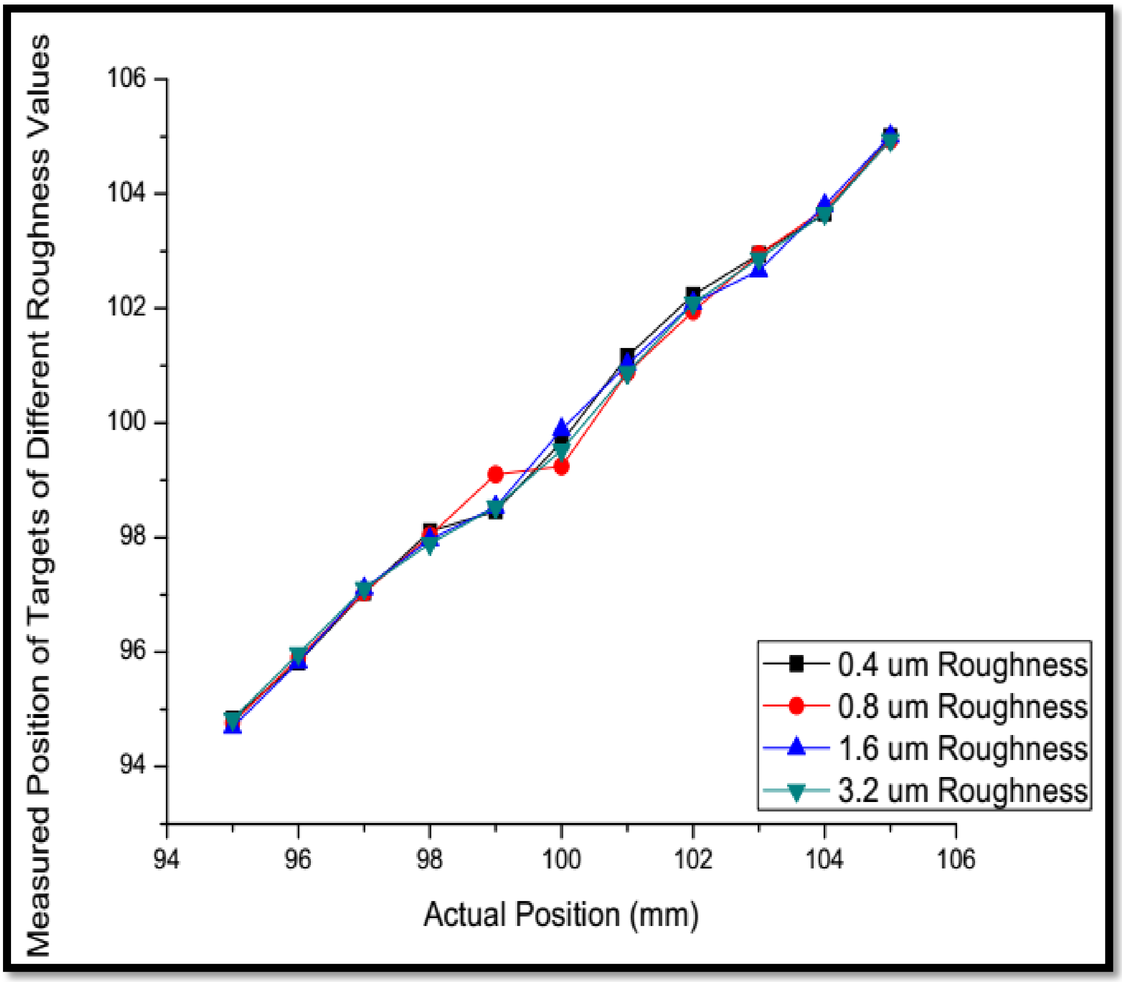

Figure 5.6: Measured position of target of different roughness values (mm) vs actual position (mm)

Figure 5.7gives the comparison of the errors in estimated position of the target relative to true position in case of surfaces with different roughness. It was seen that the error was minimum for target surface with 0.025 µm roughness and it was maximum for surfaces with roughness between 0.4 and 1.6 µm. This might be because the wavelength of laser (0.638 µm) is much larger than the roughness 0.025 µm eliminating the possibility of diffraction effects changing the intensity pattern in this case. However, for surfaces with roughness between 0.4 to 1.6 µm, wavelength of laser (0.638 µm) becomes comparable leading to diffraction and consequent change in intensity pattern as reported by Inari et al [77]. However, the roughness-induced uncertainty in all the cases is less than the resolution ~1%, which is acceptable.

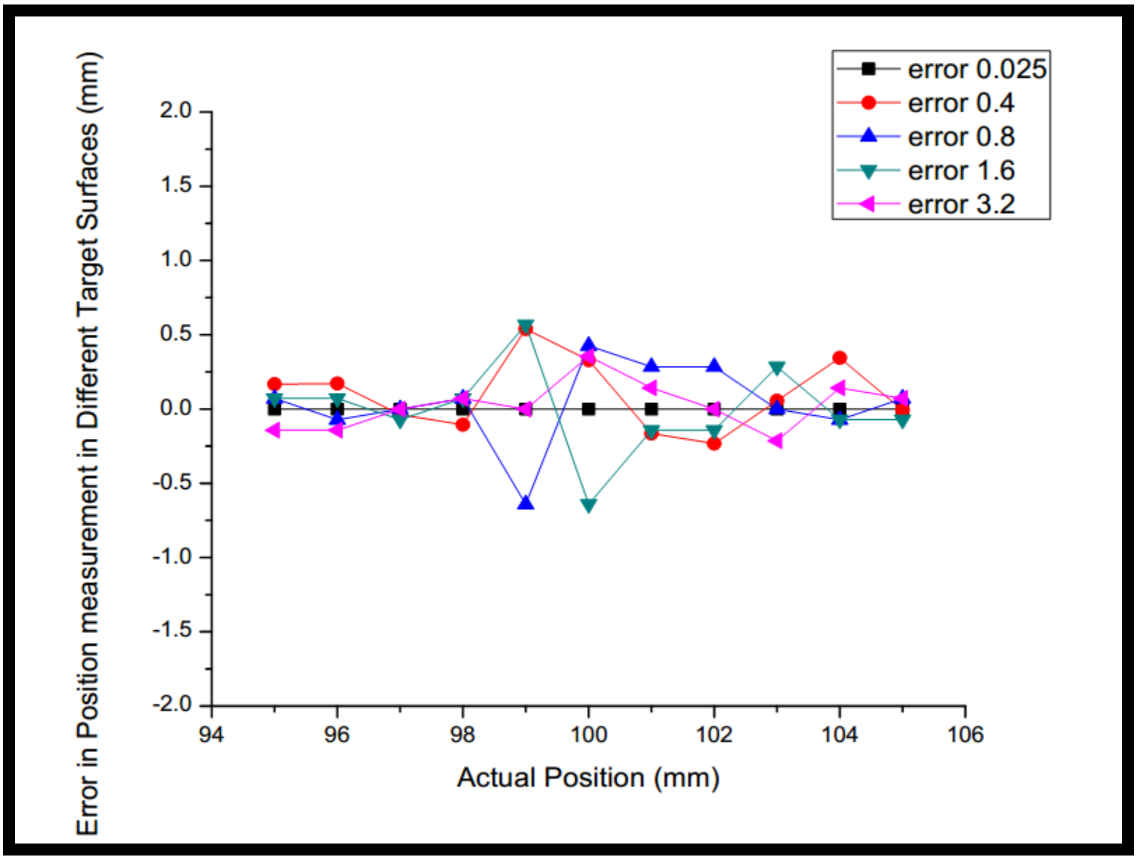

Figure 5.7: Error in position measurement of different target surfaces (mm) vs actual position (mm).

All the above-described experiments were carried out on the isolation optical table so that effect of vibration on the measurement of position of the target can be neglected. Since triangulation based position measurement depends upon the relative intensity distribution, absolute change in laser power is not expected to affect our results. We have used an aspheric lens to avoid optical aberrations. Therefore, the uncertainty observed in our results of Figure 5.7 may be mainly due to surface roughness of the target (when comparable to wavelength of laser), mechanical errors in micrometer, photonic noise and electronic noise of the CCD camera.

5.4 CONCLUSION

We presented the linear optical fiber array based non-contact and remote position measurement system using oblique laser triangulation configuration. Oblique triangulation system was selected due to its higher resolution as compared with the direct configuration. We have used linear array of optical fiber to transmit light to long distance so that CCD camera can be placed remotely and thus the scheme can be suitable for use in special environments containing radioactivity or electromagnetic noise. Application of Fourier series method to find the centroid of displaced image spot to compute the actual position of target is done. The resolution achieved in our system for position measurement was 1 mm at a standoff distance of ~100 mm between target and light collecting lens (this corresponds to accuracy of ~1%). The developed sensor head can be modified based on the resolution requirement, by varying the angle between the incident light axes and imaging optical axis, standoff distance, focal length of lens and the linear fiber array used. For the given sensor head configuration, in order to increase the resolution, one needs to reduce the laser spot size at the target surface and increase the fill factor of the fiber array. In future, a compact sensor using optical fiber both as transmitting and collecting medium for light in oblique triangulation sensor is envisaged.

Since in oblique triangulation technique, the position at which laser strikes the target gets shifted as the target is displaced, changing surface roughness can affect the intensity distribution of scattered light. However, we have experimentally demonstrated that the uncertainty in measured position due to variation in roughness is less than the resolution of our setup. It was also established that uncertainty in position measurement was maximum when the roughness is comparable to wavelength of the laser used due to diffraction effects at the target surface that ultimately alters the intensity pattern of scattered light.

CHAPTER 6: LASER TRIANGULATION BASED TWO-DIMENSIONAL POSITION MEASUREMENT OF A CYLINDRICAL OBJECT

All the previous chapters describe the techniques for position measurement along one dimension. However, in reality, most of the displacements of object happen in a two-dimensional (2-D) plane. So, in this chapter, we present a method for online measurement of position of cylindrical objects in a 2-D plane using linear optical fiber array based laser triangulation sensor. There are various applications where measurement of 2-D position change is required such as power transmission shafts in industries, rollers in rolling mills, 2-D rotor vibration measurement, positioning of fuel channels in nuclear reactors and movement of tools in a plane in Coordinate Measurement Machines (CMM). Vallance et al [82] have studied the 2-D position of spherical targets using capacitive sensors. However, their sensing range was less than 0.1 mm. Nonaka et al [83] have used the principle of ultrasonic 2-D position measurement by phase difference where either transmitter or receiver have to be mounted on the target. Eddy current sensors [84] are in general used to measure position along one dimension only.

During the assembly of the cylindrical objects (shafts, pipes etc.) in heavy machines, change in position and alignment of these from a particular co-ordinate system or from its aligning counterpart needs to be measured accurately to prolong life of machinery and to avoid accidents. By measuring the two-dimensional positions at two different planes perpendicular to the axis of shaft, the alignment/tilt of the cylindrical shaft can be inferred. At first, a mathematical model is developed in order to deduce the 2-D position of target axis from two perpendicularly placed sensors taking into account the curvature of target surface on measurements. Then, using the formulae derived and our recorded experimental data, the measurement of change in 2-D position of cylindrical object with both sensors placed remotely at 100 mm standoff distance is done.

6.1 THEORY FOR MEASUREMENT OF 2D POSITION AND ALIGNMENT OF CYLINDRICAL TARGET

Figure 6.1 shows the schematic of two laser triangulation sensors used for measurement of 2-D position of cylindrical target. It is clear from Figure 6.1 that the change in position of the point of incidence of laser on cylindrical target surface whose image is captured by the sensor depends upon the radius of the curved surface and displacement along both the perpendicular axes X and Y respectively. Therefore, we formulate the relation between shift in image spot on the linear fiber array and 2-D displacement of cylindrical target.

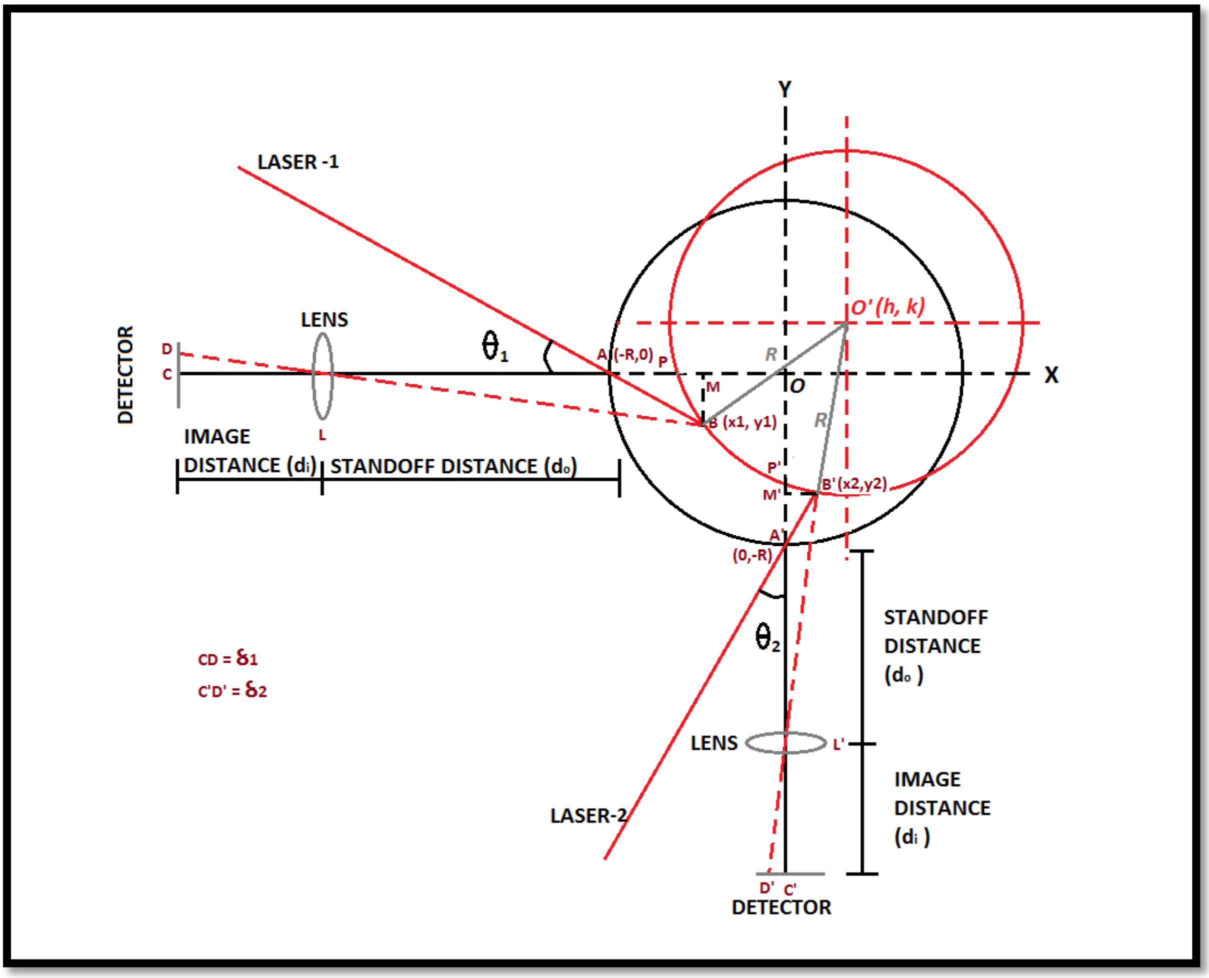

Figure 6.1: Two-sensor configuration for monitoring the two-dimension position of cylindrical target in a plane (Black circle shows the actual position of target in a plane and red circle shows the displaced position of target)

Both the sensors are placed on the same plane in such a way that cylindrical target is at equal standoff distance from both sensors. Initially the cylindrical target is consideredhaving centre at O (*0*, *0*), as the target changes its position or gets misaligned from its actual position, new centre position of cylinder is given as O′ (*h*, *k*). Let δ_1 is the change in position of image point as measured by sensor-1 and δ_2 is the change in position of image point as measured by sensor-2. However, the actual changes in positions of axis of cylinder on same plane as the sensors are *h* and *k* along

X and Y axes respectively. Let the point of incidence of the laser-1 with displaced target surface is (x_1, y_1) and that of laser-2 is (x_2, y_2). Both these points satisfy the equation of circle described by the new target position as,

$$(x_1 - h)^2 + (y_1 - k)^2 = R^2 \tag{6.1}$$

$$(x_2 - h)^2 + (y_2 - k)^2 = R^2 \tag{6.2}$$

Since, the point (x_1, y_1) must also satisfy the equation of line described by laser-1 and using similarity of triangles ΔLCD and ΔLMB, we get

$$y_1 = -(x_1 + R) \times \tan\theta_1 \tag{6.3}$$

$$y_1 = -\left(\frac{\delta_1}{d_i}\right) \times (d_0 + R + x_1) \tag{6.4}$$

Simplifying above two equations, we get

$$x_1 = \frac{\delta_1(d_o + R) - Rd_i \tan\theta_1}{d_i \tan\theta_1 - \delta_1} \tag{6.5}$$

$$y_1 = \frac{\delta_1 d_o \tan\theta_1}{\delta_1 - d_i \tan\theta_1} \tag{6.6}$$

As laser-2 and its sensor are just rotated by 90˚, its expressions will also be similar to Eq. (6.5) and Eq. (6.6) except that x_1 will be replaced by y_2 and y_1 will be replaced by $-x_2$. So, point (x_2, y_2) for the second sensor,

$$x_2 = \frac{\delta_2 d_o \tan\theta_2}{d_i \tan\theta_2 - \delta_2} \tag{6.7}$$

$$y_2 = \frac{\delta_2(d_o + R) - Rd_i \tan\theta_2}{d_i \tan\theta_2 - \delta_2} \tag{6.8}$$

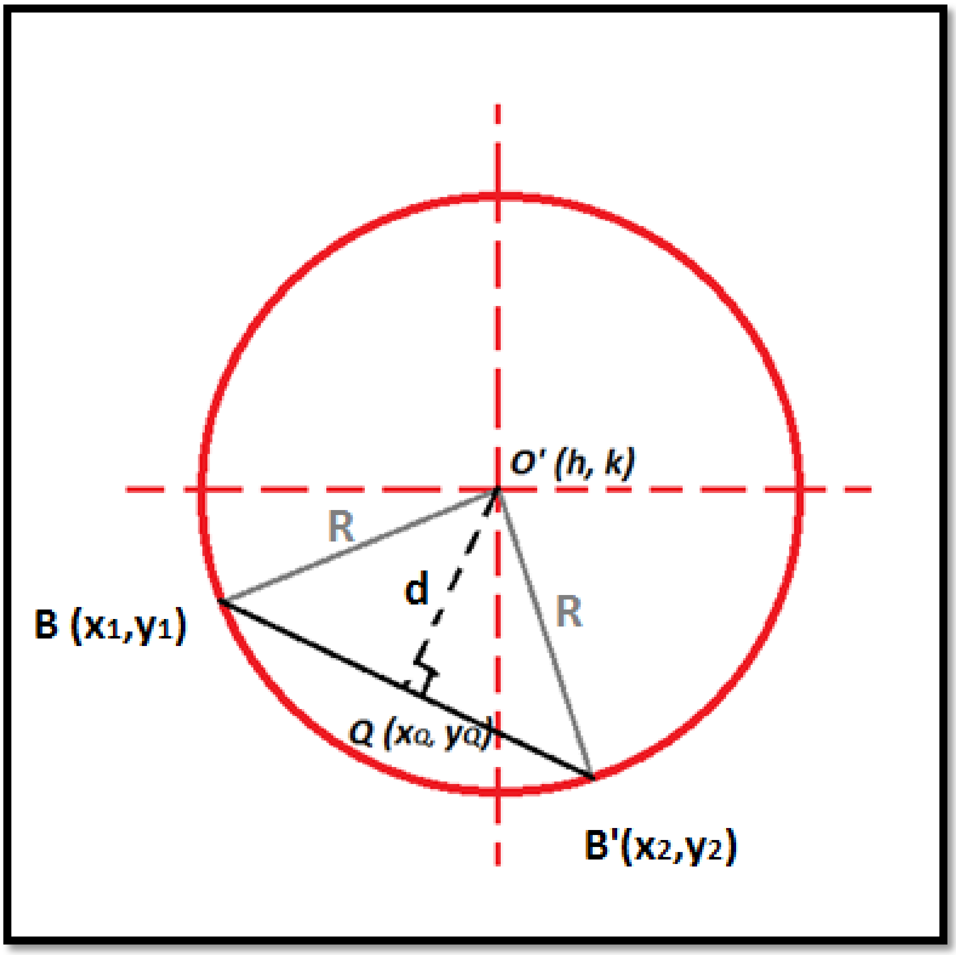

Figure 6.2: Schematic to determine the centre of displaced cylinder position in a plane

From Figure 6.2, as *O′ (h, k)* is equidistant from *B* and *B′*. Therefore, *O′* must lie on the perpendicular bisector of line connecting *B* (x_1, y_1) and *B′* (x_2, y_2) through its midpoint. Let *Q* be the midpoint of *BB′* so,

$$Q = \left(\frac{x_1 + x_2}{2}, \frac{y_1 + y_2}{2}\right) = (x_Q, y_Q) \tag{6.9}$$

Slope of line *BB′* is given as,

$$m_1 = \frac{y_2 - y_1}{x_2 - x_1} \tag{6.10}$$

As *O′Q* is perpendicular to *BB′*, slope of line *O′Q* is

$$m_2 = \frac{-1}{\frac{y_2-y_1}{x_2-x_1}} = -\frac{x_2-x_1}{y_2-y_1} \tag{6.11}$$

If slope m_2 is represented by $\tan\beta$,

$$\beta = -\tan^{-1}\left(\frac{x_2-x_1}{y_2-y_1}\right) \tag{6.12}$$

Considering $\Delta O'QB'$

As, $O'B'$= R, and let QB'= F =$\sqrt{(x_Q-x_2)^2+(y_Q-y_2)^2}$

$O'Q$ = d = $\sqrt{R^2-F^2}$

From Eq. (6.11) as the slope of $O'Q$ is known, and co-ordinates of point Q is also known so, one can easily compute $O'(h, k)$ by

$$h = x_Q + d\cos\beta \tag{6.13}$$

$$k = y_Q + d\sin\beta \tag{6.14}$$

Thus, new centre of displaced cylindrical target can be measured from Eq. (6.13) and Eq. (6.14).

In order to measure the tilt angle of shaft axis, two sensors configuration can be used at two different planes. At first plane, set of two sensors can measure the position of tilted circular shaft as point P_1 (h_1, k_1). Similarly, at another plane at a distance L along axis position of point P_2 (h_2, k_2) can be measured. After knowing the centre points, one can calculate the tilt of the axis using the formulae,

$$\tan\alpha = \frac{\sqrt{(h_2-h_1)^2+(k_2-k_1)^2}}{L} \tag{6.15}$$

Where, α is the angle of tilt along the axes.

6.2 DESIGN OF INSTRUMENT AND EXPERIMENTAL METHOD

As described in Chapter 5, we have used the two sensors of similar configuration earlier, oblique configuration for laser triangulation technique was selected for development of sensors heads. The sensor head comprises of a laser diode, imaging lens and linear fiber array. The scattered light from the target surface is collected by the imaging lens and is focused to the input end of step index linear fiber array. Lens used in our sensor is an aspheric lens; it is selected as it creates a single focal point and allows clearer, sharper vision and reduced peripheral distortion. The output of linear fiber array is collected at the CCD camera. As the position of target changes, corresponding image spot across the fiber also changes. This linear fiber array transmits the position information to the CCD camera. The centroid of image spot formed at the CCD camera helps in determining the actual target position. The centroid of image spot was measured using Fourier series method. The parameters of components used for deigning the sensor head is shown in Table 5.1.

All the components in the sensor head were mounted in the aluminium box such that center of diode laser, imaging lens and linear fiber array all lie in same plane with mechanical stability. All the experiments were conducted on the vibration isolation table so that effect of vibration on the measurement can be neglected.

Table 5.1: Parameters of components used for design of sensor head.

Laser Source	Laser Diode (2.3V, 30 mA)
Beam Wavelength	650 nm (Red color)
Design angle (θ) of sensors	32° and 30° for sensor 1 and sensor 2
Imaging Lens	25 mm focal length (Aspheric), 25 mm diameter
Standoff Distance (Object Distance)	100 mm
Detector	12 fiber linear array coupled to CCD
CCD Camera	Area of sensor 640 × 480 pixels with pixel size of (10 µm × 10 µm).
Optical Fiber Array	Step Index Fiber, Core = 50 µm, Clad = 125 µm, Pitch = 250 µm, N.A. = 0.22, Length = 5 m.

To measure the position of the cylindrical target in a two-dimensional plane, both the sensors were placed perpendicular to each other in a same plane at the standoff distance of 100 mm from target as shown in Figure 6.3.

The cylindrical target of stainless steel material having 150 mm diameter is used for experiments.

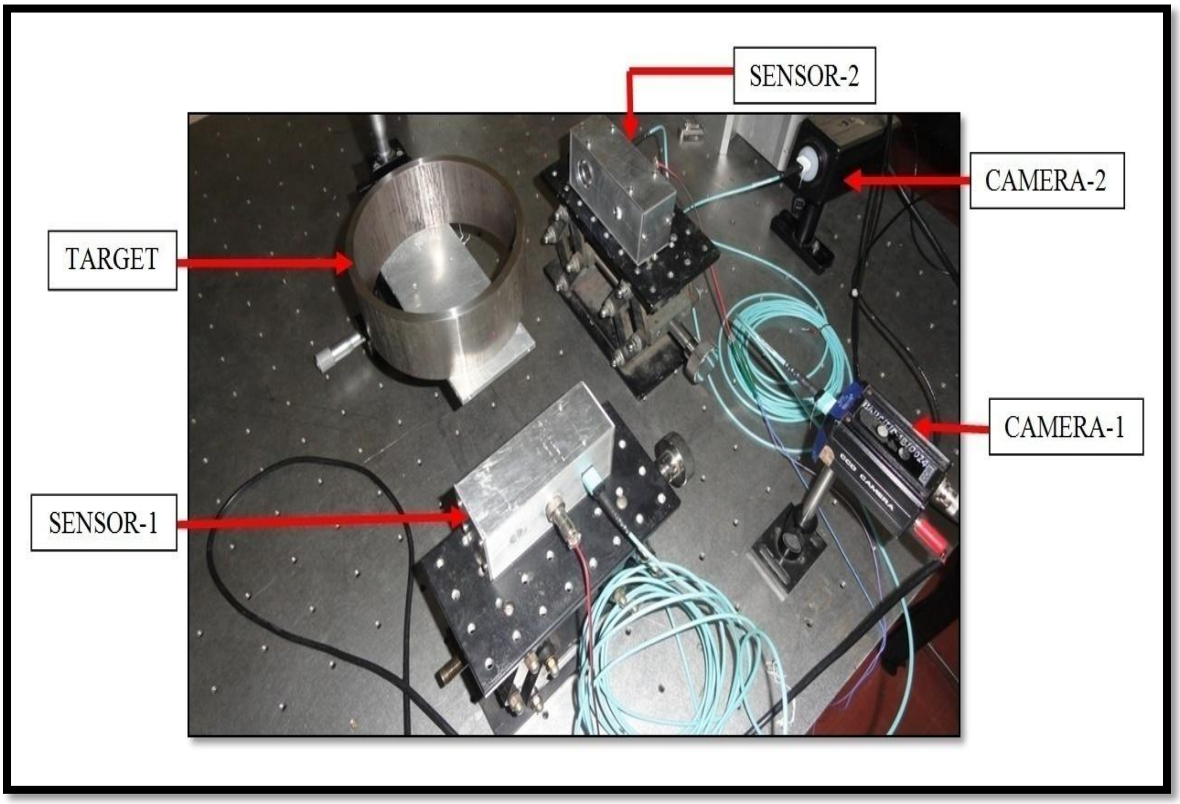

Figure 6.3: Experimental setup of the sensors placed in perpendicular configuration

The cylindrical target was moved ± 5 mm in steps of 1mm from the standoff distance of both sensors using 2-D manual linear stages. As the target changes the position from the standoff, the corresponding change in the image spot is measured using CCD camera at remote location. The centroid of the image spot formed at the CCD is measured using Fourier series method. From the measured displacements of centroid of image (δ_1, δ_2) in both the sensors, new position of the axis of cylindrical object (h, k) was found out by solving the Eq. (6.13) and Eq. (6.14). During the course of experiment, the camera exposure time was kept constant. Figure 6.4shows the typical output image spots at different positions of both sensors.

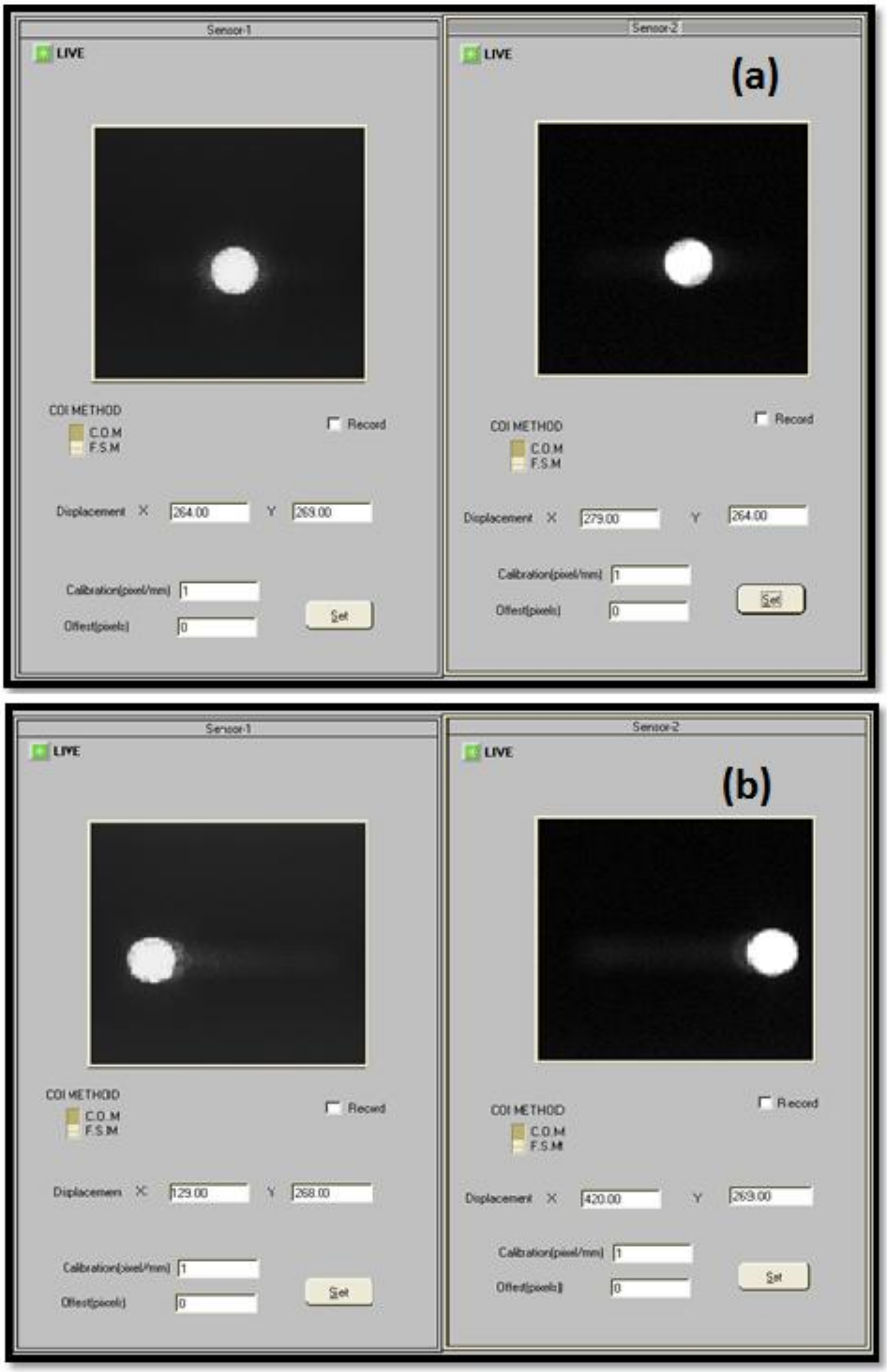

Figure 6.4: (a) Output at CCD when the target is at standoff distance for Sensor 1 and Sensor 2 (b) Output of Sensor 1 and Sensor 2 at extreme ends

As our main objective was to have a more sensitive position measurement and we had concluded that oblique laser triangulation sensors are more sensitive than the normal type, we have used the former one. However, to avoid cross coupling of scattered light from one sensor to other, we have limited the range to ± 5 mm. The non-linear nature of the sensor output due to curvature of surface and oblique incidence on the calculated displacement of target is exactly taken into account by the theory developed in section 6.2.

6.3 RESULTS AND DISCUSSION

As discussed in Section 6.2, the cylindrical target was displaced in all the four quadrants of X-Y plane using a two-dimensional micrometer stage and the output of both the sensors was monitored. Micrometer was given incremental displacement of ±1 mm along both the axes. The output of both the sensors gives the displacement of the image spot across the fiber at CCD in terms of pixel values. These pixels values were normalized to give the displacement of image spot in terms of mm. Figure 6.5 gives the position of centre of target in 2-D plane calculated from sensor outputs verses actual position of the target. It was found that the 2-D position of the cylindrical target measured by our optical technique agreed well with the true position of the target.

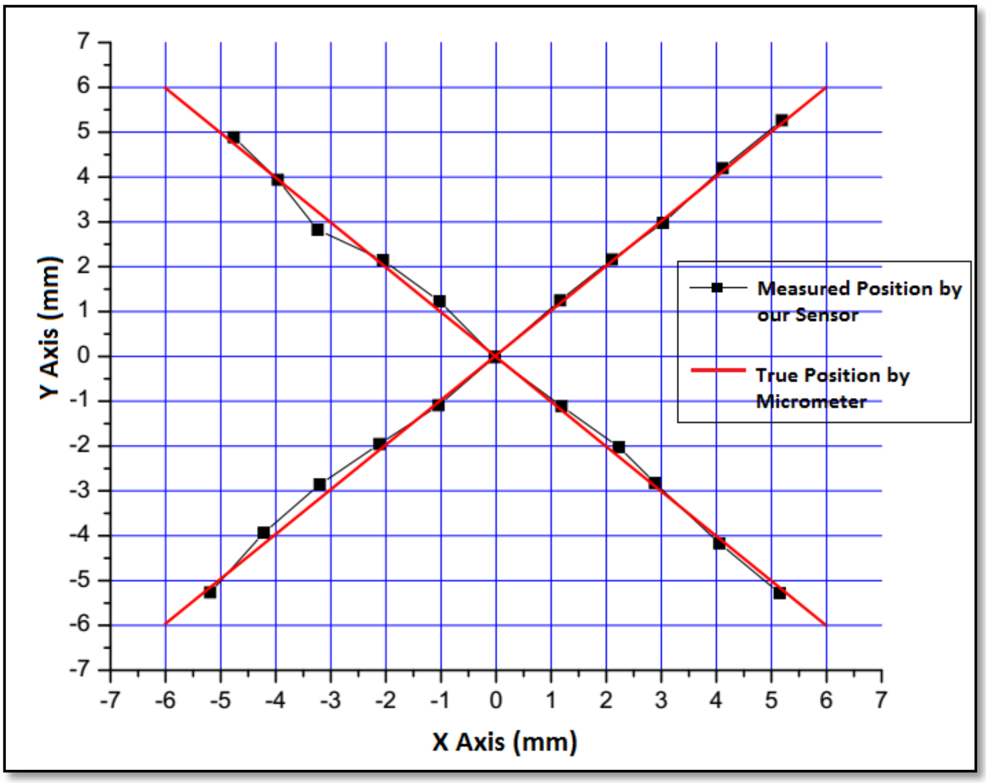

Figure 6.5: Coordinates of centre of cylindrical target as measured by sensors (mm) when the target is moved compared with the true position

Towards the end of the measurement range, there is deviation in measured value of the centre co-ordinates with the actual center co-ordinates. This might be due to the curvature of the target, which leads to the increase in the asymmetry in the elliptical laser spot at the target. The given sensor is limited for the ±5 mm measurement range of operation for 100 mm standoff distance of the cylindrical target. This is because of the limited area of fiber array and field of view of lens that prevents the image to form on CCD beyond this range. The other factors for deviation in the measured value to that of actual value may be due to:

a) Effect of image spot size: As the size of image spot increases, number of fibers collecting the image spot increases, thus leading to the error in the centroid finding. This effect generally occurs at the extreme ends of the measurement.

b) Electronic noise of CCD camera also leads to some uncertainty in measurement.

c) Temperature: The dimensions of sensors case and optical components might change due to the change in temperature. This leads to the change of optical alignments leading to the measurement uncertainty.

In some applications, cylindrical parts tilt in addition to the change in 2-D position in a plane. In such a case the cross section of the target at the plane containing both the sensors will be slightly elliptical whereas our theory is based on circular cross section and hence some error will creep into the measurement. However, in our case, for small tilt angles (upto ~5°), we have observed that the maximum error in the position of center of the target was less than the resolution of the sensor (1 mm).

6.4 CONCLUSION

In this work, we have developed the theory and experimentally demonstrated an optical fiber array based laser triangulation sensor for measurement of change in position and alignment of cylindrical components. Two sensors placed perpendicularly to the cylindrical target can easily determine the position change and can continuously monitor the alignment. The developed position sensor can be used in environments such as EMI and radiation and has the advantage over existing measurement techniques for being a non-contact online technique. The sensor can be helpful in determining the wobble effect in cylinders. Further, the given technique can be extremely useful for fuel channel alignment in Nuclear Reactors where one has to monitor the alignment remotely. The future work might involve improvement of precision by using low pitch fiber optic array and by decreasing the spot size on the cylindrical surface. The use of fiber-coupled laser as the transmitting source instead of diode laser will help the sensor head to become completely isolated from any of the electronic components.

CHAPTER 7: OPTICAL FIBER BASED TWO-DIMENSIONAL POSITION SENSOR

In chapter 6, we have used the two in house developed laser triangulation sensors for the position change measurement of the cylindrical target in a plane from a given reference axis. However, sometimes it becomes difficult to place the sensors across the target due to space constraints. So in order to overcome this, in this chapter, we describe a transmission configuration based two-dimensional fiber optic position sensor that utilizes the simultaneous measurement of the change in intensity and centroid of image on CCD camera. Here the transmitting fiber can be placed on the moving object and the receiving fiber array on the reference target about which the alignment has to be done. Both axial and lateral position change can be measured by using this technique. Axial position change is inferred by the change in peak intensity at the CCD camera and lateral position change is measured by the change in centroid of image spot at CCD camera. The given sensing system is small, and adds very negligible weight when fixed on the aligning components of machines. These sensors have wide applications due to its simplicity, high accuracy and immunity to EMI. In the measurement technique, the pitch of the fiber array determines the resolution of lateral position and the sensitivity of axial position is decided by the diameter of optical fiber. This system can be used for position measurement and alignment monitoring in a 2-D plane for structural health monitoring, alignment monitoring of shafts etc. where the non-contact measurement is needed.

7.1 SENSOR SYSTEM SETUP AND MODEL

The single fiber-to-fiber light transmission based axial measurement technique for position measurement is explained in Chapter 2. In this type of configuration, a moveable and fixed fiber is involved; optical power is transmitted from the moveable fiber and is received by the fixed fiber. A change in position of the moveable fiber will cause a change in the received power to an extent dependent on the movement. Here the system is modified by using the single fiber as the transmitting fiber and linear fiber array as the receiving fiber. The schematic of the sensor system setup is shown in Figure 7.1. Both the axial and lateral translation position change of the transmitting fiber with respect to the receiving fiber array can be detected by the intensity variation and the centroid change across the receiving fiber arrayusing the CCD camera. As the distance x between the transmitting and receiving fiber array increases, due to the movement along X-axis, the peak intensity in the image recorded by the camera changes which indicates the displacement along the X-axis. Any movement along the Y-axis results in the change in position of the centroid on CCD Camera. The position of the centroid of the image is linearly dependent on the position of transmitting fiber along Y-axis. In other words,

$$y = a \times y_c + b \tag{7.1}$$

Where, y is the position of the transmitting fiber along Y-axis, y_c is the position of centroid of the image spot and a, b are the constants.

Eq. (7.1) is needs to be calibrated before using the sensor to know the values of a and b.

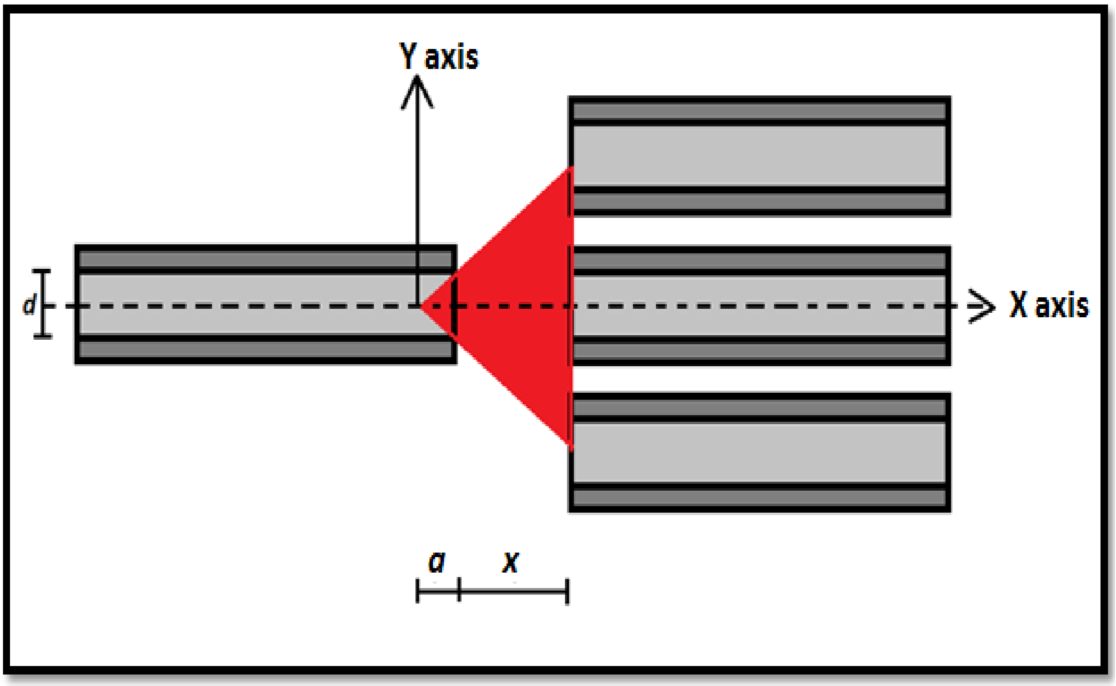

Figure 7.1:Schematic of the optical sensor arranged in transmission mode

7.2 EXPERIMENTAL SETUP & SYSTEM DESCRIPTION

Figure 7.2 shows the schematic of the two-dimensional position sensor used in our experimental setup. The sensor works by light coupling between the transmitting fiber and the individual fibers of receiving linear fiber array. The CCD does the detection of the image spot from the cores of linear fiber array at the other end. The experimental study is done to study the position change along X-direction i.e. axial and Y-direction i.e. lateral.

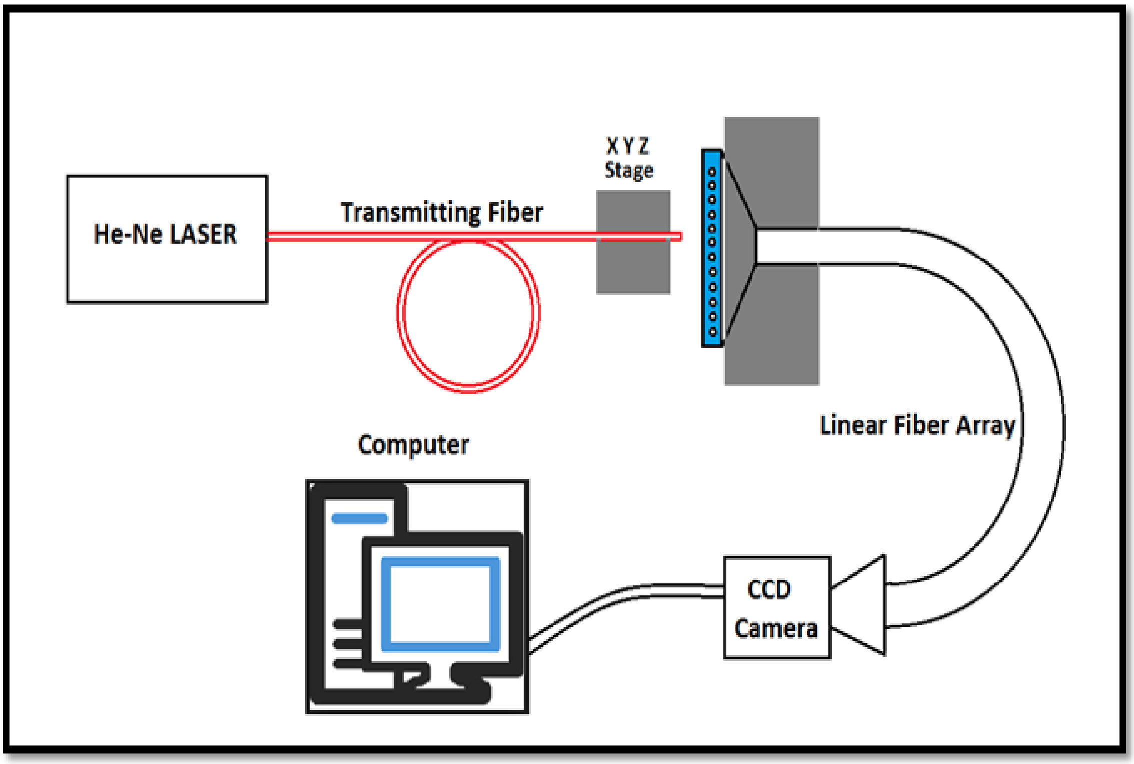

Figure 7.2: Schematic of the working principle of optical sensor for position measurement

The system consists of following components: a light source, a transmitting fiber, a linear fiber array, CCD camera and computer for data analysis. The setup was made on the vibration isolation table in order to minimize the effect of the vibration of the surrounding on the measurement.

7.2.1 Light Source and Transmitting Fiber

The light source used in the experiment is He-Ne Laser (λ = 633 nm and 5 mW power). The laser is coupled to the transmitting multimode fiber of 1 m length having core and cladding diameter 62.5 μm and 125 μm and NA of 0.22. The other end of the optical fiber is fixed on the X-Y-Z stage leaving the fiber end about 1mm. The output power coupled across the length of fiber is 0.08 mW.

7.2.2 Receiving Fiber Bundle

The fiber bundle used is a 5 m long linear fiber array having 12 fibers. The fiber has a typical core and cladding diameter of 62.5 μm and 125 μm respectively. The pitch of fiber array is 250 μm. The width of fiber array is 3 mm. The one end of fiber array is mounted on a linear stage and the other end is coupled to the camera.

7.2.3 CCD Camera

The CCD camera used is 512 x 480 pixels having pixel size of 10 μm x 10 μm. The camera is used to capture the image from the other end of fiber array. The camera used in the sensor setup is 8-bit camera. There is C mount connected to the camera that is used for fixing the receiving end of fiber array to the camera. This helps in determining and fixing the working region of CCD camera.

7.2.4 Peak and Centroid Measurement Algorithm

Peak intensity of the image recorded by the CCD camera can be easily observed which is directly related to the X-position of the target. For Y-position, centroid of the image is to be found out. As already discussed in Chapter 5, Fourier technique is used for the measurement of centroid.

During the experiment, it was ensured that angular alignment between the two fiber probes was zero prior to the actual measurements.

7.3 CALIBRATION

Before the use of sensor for position measurement in a 2-D plane, it needs to be calibrated. The transmitting fiber holder was fixed onto a X-Y-Z translation stage, and the receiving linear fiber array holder was mounted on a fixed stage. Further, the X-Y-Z position of transmitting fiber was adjusted for maximum transmitted power, and it was recorded at CCD. The intensity was maintained in a way that the CCD camera is not saturated.

After the proper alignment, receiving fiber is moved axially along the X-axis and the peak value of the power output of linear fiber array as recorded by CCD (after Gaussian Fitting) was plotted with the displacement. Initial intensity profile during the displacement was maintained in such a way that the output was not saturated. As target was displaced axially, the peak of the output profile goes on decreasing as expected. The peak value at the individual displacement points acts as a calibration curve to infer position change along the X-axis from the change in peak value of intensity. Figure 7.3 gives the calibration curve for the axial displacement.

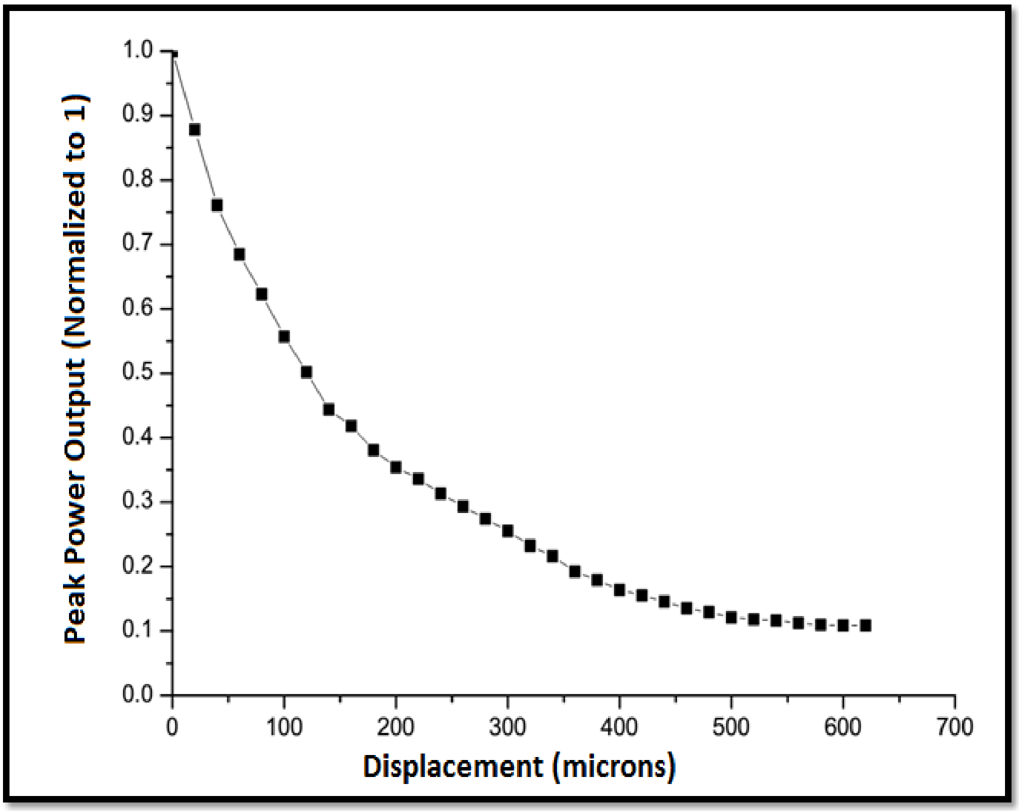

Figure 7.3: Calibration curve for peak intensity in image on CCD for position change in X direction

After the calibration was done along X axis, the position of transmitting fiber was changed laterally (along Y-axis), the corresponding change in the image spot position at the linear fiber array took place. The CCD camera connected to the other end of linear optical fiber array acquires the image of shifted laser spot. An algorithm based on Fourier series method to calculate the centroid of the laser spot in terms of pixel values was used.

Variation of the position of centroid of image spot at CCD camera (y) with actual position of target measured by micrometer is plotted in the Figure 7.4. By linear equation fitting, the fitted equation is:

$$y = 433.44 - 0.11x \tag{7.2}$$

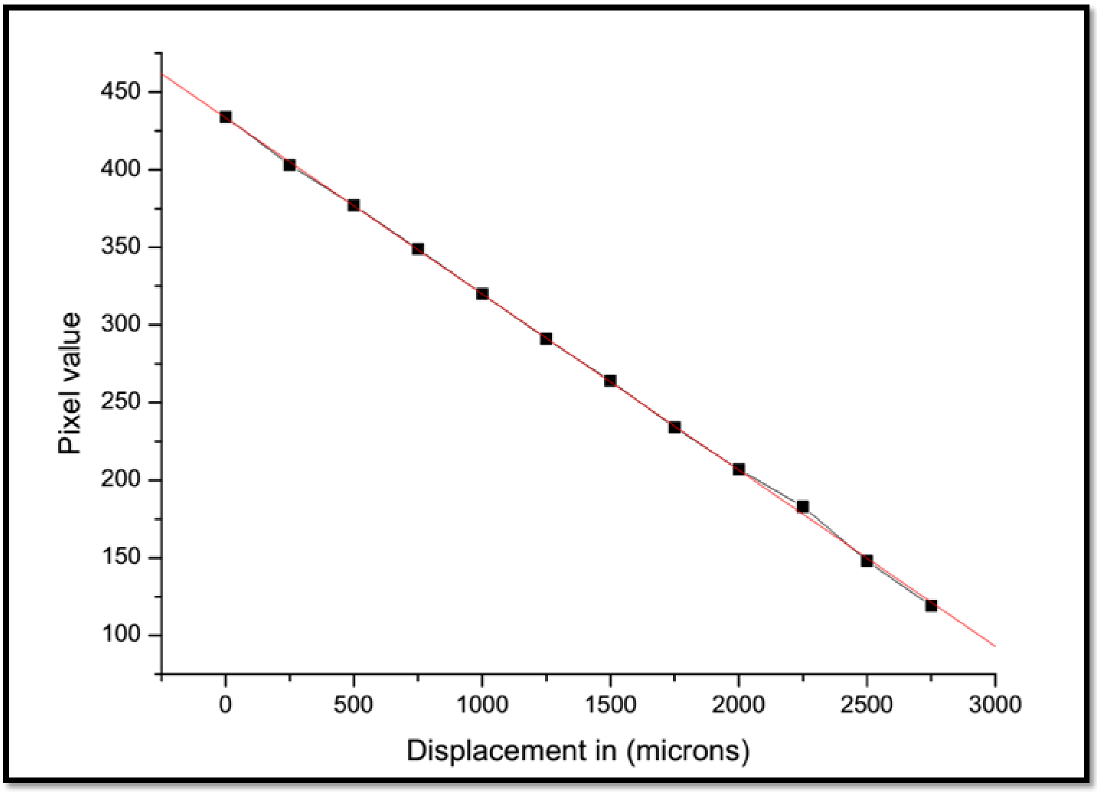

Figure 7.4: Output in terms of pixel values vs. transmitting fiber position change in Y direction

Thus, we have experimentally confirmed from Eq. (7.2) that movement of the centroid of image spot is linearly dependent on transmitting fiber displacement. Using the Figure 7.4as the calibration curve, one can easily calculate the lateral shift across the receiving fiber array.

7.4 EXPERIMENT

After calibration, experiment was conducted to study the change of position in two-dimensional plane. The transmitting fiber was displaced in both the X direction and Y direction with (50 μm, 50 μm; 50 μm, 100 μm) resolution respectively for the given range and output of image spot in terms of peak intensity and centroid were recorded.

Then by using the previously described calibration curves, X and Y position were inferred. Comparison of 2-D position of target (transmitting fiber) as estimated by our sensor with that measured by the micrometer is plotted in Figure 7.5.

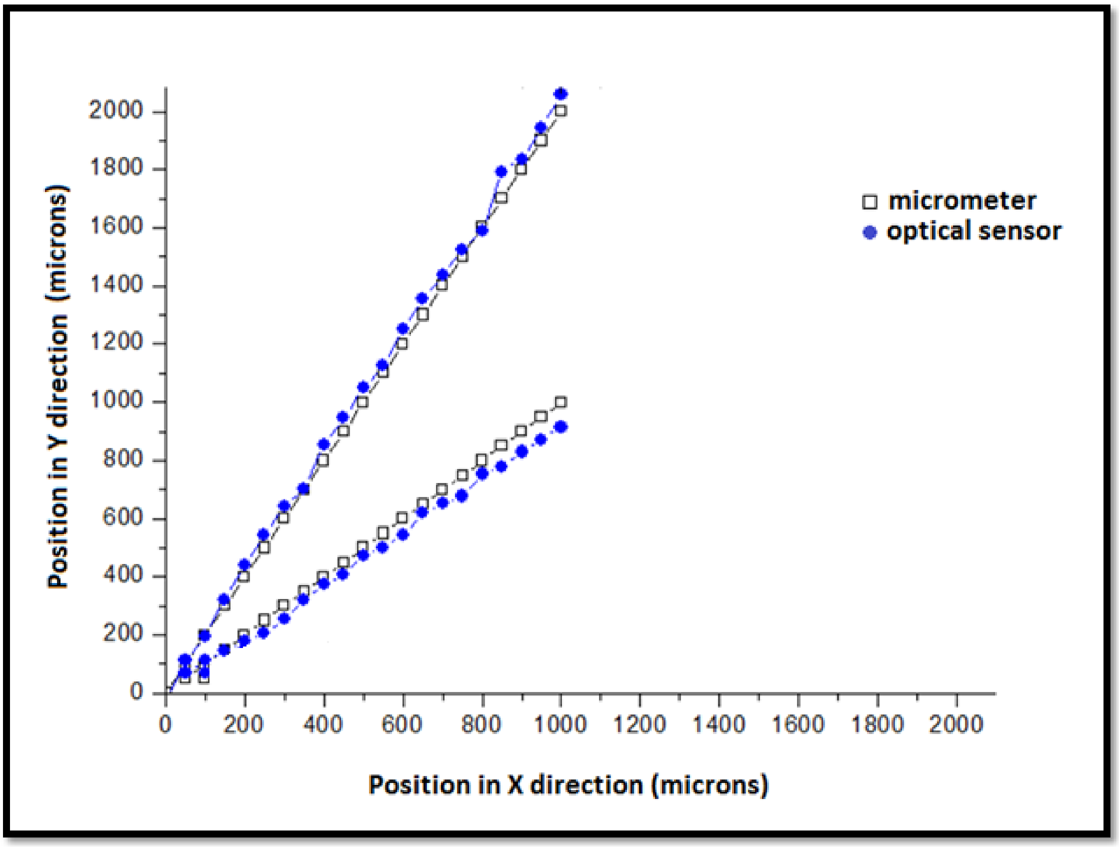

Figure 7.5: Comparison of position by our optical sensor and by micrometer in X-Y plane

The position measurement data produced by our sensor was found to be reasonably matching with the value measured by the micrometer. The maximum error was 6% of the measurement range. The error might be due to the mechanical errors in micrometer or photonic noise and electronic noise of the CCD camera in optical sensor. The pixel value uncertainty that arises due to the noise in CCD camera was minimized by keeping the camera gain low. In order to study this effect, online monitoring of the centroid for continuous operation of four hours was done. The effect of this uncertainty on the centroid position was found to be below the resolution of our sensor.

7.5 CONCLUSION

In this chapter, we have experimentally demonstrated a fiber optic 2-D position sensor by the coupling of light between transmitting optical fiber and a receiving linear fiber array connected with a CCD based readout system. The experiment shows that lateral position information can be attained by finding the centroid of the image obtained at the CCD. Axial translation motion can be determined by the change in the peak intensity of the image recorded by CCD. The resolution and range of the sensor can be improved by decreasing the pitch across the linear fiber array and by increasing the number of fibers in the array. The given sensing system can be used for various applications including the alignment of shafts, vibration measurement and in the environment that needs non-contact 2-D position measurement. The three-dimension position can be measured by replacing the linear fiber array with the 2-D area fiber array.

CHAPTER 8: CONCLUSION & FUTURE SCOPE

8.1 CONCLUSION

This thesis contributes to the studies of different optical techniques that can be used in various industries for position measurement and alignment monitoring. Different optical techniques for position measurement and alignment such as intensity based fiber optic sensors, time of flight sensors, interferometers, confocal sensors and laser triangulation sensors have been discussed. Optical sensors were designed and developed to measure both the one-dimension and two-dimension position changes. Initially, confocal based fiber optic sensors were designed to study the axial position change of the target. The output profile shows the Gaussian fingerprint and the slope on the either side of the peak intensity gives the direction of the position change. Being a single probe like system, the given system can be easily employed in the industries.

The design and performance study of laser triangulation sensors for long standoff distances were done. Generally, the laser triangulation sensors are reported for small standoff distances. But here we have developed the sensor suitable for the target placed at 1000 mm distance. Moreover, in order to make the sensor head compact, we have used the beam folding technique. The PSD based circuit gives the voltage output that is converted into the target displacement based on the calibration. The sensor can be used in variable temperature environment upto 50 ˚C and thus suitable for industrial environments.

Then the modification of laser triangulation sensors was done using the linear fiber array for collecting and transmitting the collected light to the CCD camera. The variation of target position is represented as the change in the image spot at the Fiber array tip and correspondingly to the CCD camera. By calculating the centroid of the image spot the target position change is inferred. Using the fiber array for the measurement helped the system for remote measurement especially for hazardous environments. Target surfaces of different roughness values were considered during the experimentation and were found to have negligible effects on the measurement data. The given system can be used in the Nuclear reactors where high radiation may affect the electronics.

Application of the developed linear fiber array based triangulation sensors is done to measure the position change of a cylindrical target in a two-dimensional plane. At first the mathematical model was developed in order to deduce the two-dimensional position of target axis taking into account the curvature of the target surface on measurements. The experimental results were confirmed with the predictions of the mathematical model. Presently, it is being planned to use such a linear fiber array based 2-D position sensor for the X-Y tilt measurement of the fuel channel with respect to the snout assembly in nuclear reactors.

Due to the space constraints in the industrial environments, sometimes it becomes difficult to place multiple sensors around the components whose position has to be measured for alignment. So, to overcome this problem, we have experimentally demonstrated a single fiber optic based 2-D position sensor by coupling light between transmitting optical fiber and a receiving linear fiber array connected with a CCD based readout system. The experiment shows that lateral position information can be attained by finding the centroid of the image and axial translational motion can be determined from change in peak intensity of the image recorded by CCD.

8.2 FUTURE SCOPE

The given thesis contributes towards the studies of different optical techniques that can be used for position and alignment monitoring of the machines. The different types of sensors were designed and developed for the position change studies in one and two-dimensions. However, there are various other challenges that can be addressed further with the understanding developed with the work and the techniques employed in this thesis. The following are the key challenges that can be addressed further with the developed understanding and employed techniques:

a) All the studies done in the thesis is for one and two dimensional position change of the target. Next level is to study the position change across the three dimensions.

b) Selection and testing of the optical components that can be used in the radioactive environments. Accuracy and life of sensor can be studied under these conditions.

c) Improvement of range and resolution can be done based on the selection of components used in the designing of the sensor.

d) Factors leading to uncertainty in the measurement are mentioned in the thesis. But, how the individual factors and combined factors lead to the uncertainty in measurement can be further studied in details.

REFERENCES

[1] J. Giannone, Laser-optical shaft alignment cuts energy costs, World Pumps, 1995, pages 22-24.

[2] A. Simm, Q. Wang, S. Huang and W.Zhao, Laser based measurement for the monitoring of shaft misalignment, Measurement, vol. 87,2016, pages 104-116.

[3] G. Williams, E.Chalupa and S. Rahhal, Automated Positioning and Alignment Systems, Society of Automotive Engineers, 2000, (white paper).

[4] W. Gao et al, Measurement technologies for precision positioning, CIRP Annals, vol. 64(2), 2015, pages 773-796.

[5] A. A. Potdar, S. Fletcher and A.P. Longstaff, Performance characterisation of a new photo-microsensor based sensing head for displacement measurement, Sensors and Actuators A: Physical, vol. 238, 2016, pages 60-70.

[6] A. J. Fleming, A review of nanometer resolution position sensors: Operation and performance, Sensors and Actuators A: Physical, vol. 190,2013, pages 106-126.

[7] D.S. Nyce, Linear Position Sensors. Theory and Application, John Wiley and Sons, Hoboken, New Jersey (2004)

[8] M. C. Amann, T. M. Bosch, M. Lescure, R. A. Myllylae and M. Rioux, Laser ranging: a critical review of usual techniques for distance measurement, Optical Engineering, vol. 40, No. 1, 2001, pages 10-19.

[9] G. Berkovicand E. Shafir, Optical methods for distance and displacement measurements, Adv. Opt. Photonics, vol. 4, 2012, pages 441-471.

[10] J. M. Senior, Optical fibre communications: principles and practice, Prentice Hall. Ch 2, Ch 7, 1992.

[11] D. Marcuse, Principles of optical fibre measurements Academic Press. Ch. 1, 1981.

[12] R. C. Hochberg, Fibre-optic sensors, IEEE Trans on Instru. Meas., 35, 1986, pages 447-450.

[13] C. K. Kao, Optical fibre systems: technology, design, and applications, McGraw-Hill, Ch 8, 1986.

[14] C. M. Davis: Fibre optic sensors: an overview, Opt. Engg. 24, 1985, pages 347-351.

[15] E. Udd and W. B. Spillman Jr, Fiber optic sensors: an introduction for engineers and scientists, Ch 6, John-Wiley & Sons, 2011.

[16] M. Sumathi and R. Pratheep, Intensity based fiber optic deflection sensor, ICOP-2009 International Conference on Optics and Photonics, 2009.

[17] P. V. Rao, K. Srimannarayana, M. Sai Shankar, P. Kishore, D. Sengupta, and P. Saidi Reddy, A diaphragm based low-cost fiber optic pressure sensor, Microwave and Optical Technology Letters, vol. 54 (10), 2012, pages 2229-2231.

[18] A.L. Chaudhari and A. D. Shaligram, Fiber optic sensor for the measurement of concentration and refractive index of liquids based on intensity modulation, International Journal of Modern Physics: Conference Series, vol. 6, 2012, pages 589-593.

[19] E. Ollier, P. Labeye and P. Mottier, Integrated micro-optomechanical vibration sensor connected to optical fibers, Electron. Lett., vol.33, 1997, pages 525-526.

[20] J.M. López-Higuera et al, New low-cost fiber optic accelerometer system for stator winding monitoring of hydroelectric generating machines, Proc. SPIE, 2868, 1996, pages 510-515.

[21] M. Kimura and K. Toshima, A new type optical fiber vibration-sensor, transducers '97 International Conference on Solid State Sensors and Actuators, Chicago, IL, 1997, pages 1225-1228.

[22] V. Svyryd, N. N Solis Osorno and Salazar, An analysis of a displacement sensor based on optical fibers, Rev. mex.fis. [online], vol.52, suppl.2, 2006, pages 61-63.

[23] Y. Libo, P. Jian, Y.Tao and H. Guochen, Analysis of the compensation mechanism of fiber-optic displacement sensor, Sensors and Actuators A, vol. 36, 1993, pages 177-182.

[24] J. Jason, H. Nilsson, B. Arvidsson, and A. Larsson, Robustness analysis of an intensity modulated fiber-optic position sensor with an image sensor readout system, Appl. Opt. vol. 52, 2013, pages 3876-3883.

[25] J. Jason, H. Nilsson, B. Arvidsson, and A. Larsson, Experimental study of an intensity modulated fiber-optic position sensor with a novel read out system, IEEE Sensors, vol. 8(7), 2008, pages 1105-1113.

[26] M. Abdullah, N Bidin, G. Krishnan, M.F.S. Ahmad and M. Yasin, Fiber optic radial displacement sensor-based a beam through technique, IEEE Sensors Journal, vol. 16, No. 2, 2016, pages 306-311.

[27] J. B. Faria, A theoretical analysis of the bifurcated fiber bundle displacement sensor, IEEE Trans. Instrum. Meas. 47, 1998, pages 742–747.

[28] H. Golnabi, P. Azimi, Design and operation of a double-fiber displacement sensor, Opt. Commun. 281, 2008, pages 614–620.

[29] M.Yasin, S.W. Harun, Kusminarto and H. Ahmad, Simple design of optical fiber displacement sensor using a multimode fiber coupler, Laser Phys. 19, 2009, pages 1446–1449.

[30] L. Bergougnoux, J. Misguich-Ripault and J. L. Firpo, Characterization of an optical fiber bundle sensor, Rev. Sci. Instrum., 69, 1998, pages 1985– 1990.

[31] A. Shimamoto and K. Tanaka, Geometrical analysis of an optical fiber bundle displacement sensor, Appl. Optics 35 (34), 1994, pages 6767–6774.

[32] X. D. Zhang and L. Yang, Research on displacement sensor of two circle reflective coaxial fiber bundle, International conference on advanced intelligent mechatronics, 2008.

[33] P. B. Buchade and A. D. Shaligram, Simulation and experimental studies of inclined two fiber displacement sensor, Sens. Actuators, A, vol. 128, 2006, pages 312–316.

[34] J. M. S. Sakamoto, R. T. Higuti, G. M. Pacheco and C. Kitano, Overlap integral factor applied to reflective fiber optic displacement sensor: theory and experiment, Submitted to XXX Encontro Nacional de Física da Matéria Condensada, São Lourenço, MG, 2007.

[35] H. Z. Yang, S.W. Harun and H. Ahmad, Displacement sensing with two asymmetrical inclined fibers, Microw. Opt. Technol. Lett. 52(6), 2010, pages 1271–1274.

[36] P. B. Buchade and A. D. Shaligram, Influence of fiber geometry on the performance of two-fiber displacement sensor, Sens. Actuators- A 136, 2007, pages 199–204.

[37] F. E. Utou, J. Gryzagoridis and B. Sun, Parameters affecting the performance of fiber optic displacement sensors, Smart Mater. Struct. 15, 2006, pages 154–157.

[38] H. Z. Yang, S.W. Harun and H. Ahmad, Fiber optic displacement and liquid refractive index sensors with two asymmetrical inclined fibers, Sens. Transducer 108, 2009, pages 80–88.

[39] M. Yasin, S. W. Harun, H. A. Abdul Rashid, Kusminarto, KaryonoandH. Ahmad, The performance of a fiber optic displacement sensor for different types of probes and targets, Laser Phys. Lett. 5, 2008, pages 55–58.

[40] M. Johnson and C. Goodman, One- and two-dimensional, differential, reflective fiber displacement sensors, Appl. Opt. 24, 1985, pages 2369–2372.

[41] Z.Q. Zhao, W.S. Lau, C. Choi Albert and Y. Y. Shan, Modulation function of a reflective fiber sensor with random fiber arrangement based on a pair model, Opt. Eng. 34 (10), 1995, pages 3055–3061.

[42] H.M. Cao, Y. P, Z.D. Zhou and G. Zhang, Theoretical and experimental study on the optical fiber bundle displacement sensors, Sens. Actuators, A 136, 2007, pages 580–587.

[43] H.Y. Huang and U. Tata, Simulation, implementation, and analysis of an optical fiber bundle distance sensor with single mode illumination, Appl. Optics 47 (9), 2008, pages 1302–1309.

[44] P.J. Muephy and T.P. Coursolle, Fiber optic displacement sensor employing a graded index lens, Appl. Opt. 29, 1990, pages 544–547.

[45] K.S. Lim, S.W. Harun, H.Z. Yang, K. Dimyati and H. Ahmad, Analytical and experimental studies on asymmetric bundle fiber displacement sensors, J. Mod. Optic 56, 2009, pages 1838–1842.

[46] H. A. Rahman, A.I.C. Ani, S. W. Harun, M. Yasin, R. Apsari and H. Ahmad, Feasibility of fiber optic displacement sensor scanning system for imaging of dental cavity, J. Biomed. Opt. 17, 7, 2012, 071308.

[47] S.W. Harun, H.Z. Yang, M. Yasin and H. Ahmad, Theoretical and experimental study on the fiber optic displacement sensor with two receiving fibers, Microw. Opt. Technol. Lett., 52, 2009, pages 373–375.

[48] P. Giacomo, News from BIPM, Metrologia, 20, 1, 1984, pages 25-30.

[49] B. E. A. Saleh and M. C. Teich, Fundamentals of Photonics, Wiley, 1991.

[50] C. K. Kirkendall and A. Dandridge, Overview of high performance fibre optic sensing, J. Phys. D: Appl. Phys. 37, 2004, pages 197-216.

[51] Shao-Kang Humg, En-TeHwu and Mei Yung Chun, Design and Experiment of Range Extended Fiber Fabry-Perot Interferometer Utilizing the second Harmonic Displacement Modulation, proceedings of the 2005 IEE/ASME, 2005.

[52] S. Pullteap, Development of a fiber based interferometric sensor for non-contact displacement measurement, World Academy of Science, Engineering and Technology, vol. 4, 2010, pages 923-927.

[53] H. J. Jordan, M. Wegner, and H. Tiziani, Highly accurate non-contact characterization of engineering surfaces using confocal microscopy, Meas. Sci. Technol. 9(7), 1998, pages 1142–1151.

[54] L. Yang, G. Wang, J. Wang, and Z. Xu, Surface profilometry with a fibre optical confocal scanning microscope, Meas. Sci. Technol. 11(12), 2000, pages 1786–1791.

[55] H. J. Tiziani and H. M. Uhde, Three-dimensional image sensing by chromatic confocal microscopy, Appl. Opt. 33(10), 1994, pages 1838–1843.

[56] J. Cohen-Sabban, J. Gaillard-Groleas and P. J. Crepin, Extended-field confocal imaging for 3D surface sensing, Proc. SPIE 5252, 2004, pages 366–371.

[57] J. R. Garzon, J. Meneses, G. Tribillion, T. Gharbi and A. Plata, Chromatic confocal microscopy by means of continuum light generated through a standard single mode fiber, J. Opt. A, Pure Appl. Opt. 6 (6), 2004, pages 544–548.

[58] T. Dabbs and M. Glass, Fiber-optic confocal microscope: FOCON, Appl. Opt. 31(16), 1992, pages 3030–3035.

[59] E. Shafir and G. Berkovic, Expanding the realm of fiber optic confocal sensing for probing position, displacement, and velocity, Appl. Opt. 45(30), 2006, pages 7772–7777.

[60] E. Shafir and G. Berkovic, Multi-wavelength fiber optic displacement sensing, Proc. SPIE 5952, 59520X (2005).

[61] F. G. Balzer et al Fibre –coupled monochromatic zero point sensor for precision positioning systems using laser interferometers. Measurement Science & technology, Vol 23(7), 2012, 074008.

[62] Z. Ji and M. C. Leu, Design of optical triangulation devices. Optics & Laser Technology, vol. 21(5), 1989, pages 339–341.

[63] B. H. Zhuang, J. H. Zhang, C. Jiang, Z. Li and W. Zhang, Precision laser triangulation range sensor with double detectors for measurement of CMMs, SPIE vol. 2349, Industrial Optical Sensors for Metrology and Inspection; 1995, pages 44-52.

[64] H. X. Song, X. D. Wang, L. Q. Ma, M. Z. Cai and T. Z. Cao, Design and Performance Analysis of Laser Displacement Sensor Based on Position Sensitive Detector (PSD), Journal of Physics: Conference Series 48, 2006, pages 217–222.

[65] D. J. Park, G. J. Park, T. S. Aum, J. H. Yi, J. H. Kwon, Measurement of displacement and vibration by using oblique ray method, Applied Optics, Vol. 45, No. 16, 2006, pages 3728-3732.

[66] J. K. Jung, S. G. Kang, J. S. Nam and K. H. Park, Intensity control of triangulation based PSD sensor independent of object color variation, IEEE Sensors Journal, vol. 11 (12), 2011, page 3311-3315.

[67] C. Dong et al A regression model for analysing the non-linearity of laser triangulation probes, International Journal of Advanced Manufacturing Technology, 59(5-8), 2012, pages 691-695.

[68] J. L. Vilaça, J. C. Fonseca and A M Pinho , Non-contact 3d acquisition system based on stereo vision and laser triangulation. Machine Vision and Applications, vol. 21 (3), 2010, pages 341-350.

[69] M. F. M. Costa, Optical Triangulation-Based Microtopographic Inspection of Surfaces, Sensors, 12, 2012, pages 4399-4420.

[70] C. Miao and Y. Qinghua, Design of a Miniaturization Laser Triangulation Probe. International Journal of Control and Automation, Vol. 8 (2), 2015, pages 291-298.

[71] Fang-Jung Shiou and Min-Xin Liu, Development of a novel scattered triangulation laser probe with six linear charge-coupled devices (CCDs), Optics and Lasers in Engineering, 47 , 2009, pages 7–18.

[72] D. Cheng, X. Lou, Q. Liu and M. Dong, Structure parameters optimization and system simulation of a double-triangulation probe, Proc. SPIE 8916, Sixth International Symposium on Precision Mechanical Measurements, 891616, 2013.

[73] B. Muralikrishnan, W. Ren, D. Everett, E. Stanfield and T. Doiron, Performance evaluation experiments on a laser spot triangulation probe, Measurement, 45, 2012, pages 333-343.

[74] G. Guidi, M. Russo, G. Magrassi and M. Bordegoni, Performance evaluation of triangulation based range sensors, Sensors, 10, 2010, pages 7192–7215.

[75] M. Buzinski, A. Levine and W. H. Stevenson, Performance characteristics of range sensors utilizing optical triangulation, IEEE 1992 National Aerospace and Electronics Conference, pages 1230–1236.

[76] B. Li, F. Li, H. Liu, X. Mao and F. Peng, A measurement strategy and an error compensation model for the on-machine laser measurement of large-scale free-form surfaces, Meas. Sci. Technol., vol. 25, 2014, 015204.

[77] T. Inari and N. Aoki, Measurement of Surface States by Optical Patterns Produced by Laser Scattering and Diffraction, Progress in Electromagnetic Research Symposium, Pisa, Italy, March 28 – 31, 2004, pages 289-292.

[78] K. Liu, Q. Wang, Y. Wang and C. Liu, Research on Image processing in laser triangulation system, Journal of Physics: Conference Series 276, 2011.

[79] R. Isaac, Evaluation of a compact CCD-based high-resolution autocollimator for use as a slope sensor.(www.physics.berea.edu/KAS/Rohan2012.pdf).

[80] B. F. Alexander, Elimination of systematic error in subpixel accuracy centroid estimation, Optical Engineering, vol. 30, no. 9, 1991, pages 1320-1332.

[81] J. P. Fillard, Subpixel accuracy location estimation from digital signals, optical engineering, vol. 31(11), 1992, pages 2465-2471.

[82] R. R. Vallance, E. R. Marsh and P. T. Smith “Effects of spherical targets on capacitive displacement measurements”, ASME. J. Manuf. Sci. Eng.vol. 126(4), 2005, pages 822-829.

[83] H. Nonaka and T. Da-te “Ultrasonic position measurement and its applications to human interface”, IEEE Trans. Inst. & Meas. vol. 44(3), 1995, pages 771-774.

[84] S. Fericean and R. Droxler “New Non contacting Inductive Analog Proximity and Inductive Linear Displacement Sensors for Industrial Automation” IEEE Sensors Journal, vol.**7** (11), 2007, pages 1538-1545.